ANL/RERTR/TM-12-30

Technical Basis in Support of the Conversion of the University of Missouri Research Reactor (MURR) Core from Highly-Enriched to Low-Enriched Uranium – Core Neutron Physics

Nuclear Engineering Division

About Argonne National Laboratory

Argonne is a U.S. Department of Energy laboratory managed by UChicago Argonne, LLC under contract DE-AC02-06CH11357. The Laboratory's main facility is outside Chicago, at 9700 South Cass Avenue, Argonne, Illinois 60439. For information about Argonne and its pioneering science and technology programs, see www.anl.gov.

Availability of This Report

This report is available, at no cost, at http://www.osti.gov/bridge. It is also available on paper to the U.S. Department of Energy and its contractors, for a processing fee, from:

U.S. Department of Energy
Office of Scientific and Technical Information
P.O. Box 62
Oak Ridge, TN 37831-0062
phone (865) 576-8401
fax (865) 576-5728
reports@adonis.osti.gov

Disclaimer

This report was prepared as an account of work sponsored by an agency of the United States Government. Neither the United States Government nor any agency thereof, nor UChicago Argonne, LLC, nor any of their employees or officers, makes any warranty, express or implied, or assumes any legal liability or responsibility for the accuracy, completeness, or usefulness of any information, apparatus, product, or process disclosed, or represents that its use would not infringe privately owned rights. Reference herein to any specific commercial product, process, or service by trade name, trademark, manufacturer, or otherwise, does not necessarily constitute or imply its endorsement, recommendation, or favoring by the United States Government or any agency thereof. The views and opinions of document authors expressed herein do not necessarily state or reflect those of the United States Government or any agency thereof, Argonne National Laboratory, or UChicago Argonne, LLC.

ANL/RERTR/TM-12-30

Technical Basis in Support of the Conversion of the University of Missouri Research Reactor (MURR) Core from Highly-Enriched to Low-Enriched Uranium – Core Neutron Physics

by
J. Stillman[1], coordinating author
E. Feldman[1], L. Foyto[2], K. Kutikkad[2], J.C. McKibben[2], N. Peters[2], and J. Stevens[1]
[1]GTRI Reactor Conversion Program, Nuclear Engineering Division, Argonne National Laboratory
[2]University of Missouri-Columbia Research Reactor

September 2012

(This page intentionally left blank.)

EXECUTIVE SUMMARY

This report contains the results of reactor design and performance for conversion of the University of Missouri Research Reactor (MURR) from the use of highly-enriched uranium (HEU) fuel to the use of low-enriched uranium (LEU) fuel. The analyses were performed by staff members of the Global Threat Reduction Initiative (GTRI) Reactor Conversion Program at the Argonne National Laboratory (ANL) and the MURR Facility. The core conversion to LEU is being performed with financial support of the U. S. government.

The objective of this work was to provide and document the technical basis for the neutron physics characteristics of the MURR operating with LEU fuel, under a set of manufacturing assumptions. The goal was to design a MURR LEU fuel element that could safely replace the current MURR HEU fuel element and maintain performance while requiring minimal, if any, changes to the control blades and control blade drive mechanisms as well as the instrumentation and control system. Steady-state thermal-hydraulic safety analyses for the MURR with the LEU fuel are the topic of a companion report.

Documents that were reviewed by ANL as bases for the design and safety evaluations were the MURR design drawings and historic analyses of the facility. All of the information and data needed to construct the reactor models and perform the analyses were provided by MURR. The methods and codes that were utilized have been qualified by extensive conversion analysis experience and international benchmark.

The current HEU fuel element has 24 plates that are 50 mil thick (0.050 inches), with fuel meat being 20 mil thick in each plate. The fuel meat is aluminide fuel containing uranium with a ^{235}U enrichment of 93%. The Al-6061 aluminum cladding thickness of the HEU plates is 15 mil.

The proposed LEU fuel elements have the same overall design and exterior dimensions as the current HEU fuel elements, except for reducing the number of fuel plates from 24 to 23, and reducing the thickness of the fuel plates. Furthermore, the proposed LEU fuel element has fuel meat thicknesses varying from 9 mil to 20 mil thick and consists of U-10Mo monolithic foils containing uranium with a ^{235}U enrichment of 19.75% clad with Al-6061 aluminum. There is also a 1 mil layer of zirconium between the fuel foil and aluminum. The thinnest nominal combined zirconium and aluminum thickness on the fuel plates is 12 mil; the clad thickness is based on feedback from the Fuel Development (FD) and Fuel Fabrication Capability (FFC) pillars of the GTRI Reduced Enrichment for Research and Test Reactors (RERTR) program to reliably manufacture the fuel plates. The overall thickness of the plates is 44 mil, except for exterior plate 23 (the plate that is furthest from the center flux trap), which is 49 mil thick. The LEU U-10Mo monolithic fuel is not yet qualified as driver fuel in research reactors, but is under intense development under the auspices of the GTRI FD and FFC programs.

To design the proposed MURR LEU element, optimization analyses were performed to limit power peaking factors to ensure that acceptable shutdown and safety margins will still exist with the LEU fuel, as well as maintain the fuel cycle and experimental performance for the current HEU core. Experimental performance evaluations showed that a power up-rate to approximately 12 MW is needed to maintain fluxes and reaction rates at the mission critical irradiation locations. Consequently, all safety margins should be evaluated at the uprated power of 12 MW.

TABLE OF CONTENTS

EXECUTIVE SUMMARY ..... **i**

TABLE OF CONTENTS ..... **iii**

List of Figures ..... **iv**

List of Tables ..... **v**

1.0 INTRODUCTION **1**

1.1 Description of Facility 1

1.2 LEU Fuel Element Design Development 3

2.0 COMPUTATIONAL METHODOLOGY AND MODELS **5**

2.1 Description of Neutron Physics Codes 5

2.2 Credibility of Neutron Physics Models 7

2.2.1 MCNP and DIF3D models – Comparisons with 1971 HEU Fresh Core Measurements *7*

2.2.2 Description of Changes to HEU Core Models (1971 to 2008 Core Configuration) *9*

2.2.3 Development of Fuel Cycle Model *15*

2.2.4 Credibility of the Mixed-Burnup Core Model *20*

2.2.5 Azimuthal Discretization of Fuel Plates for Detailed Power Distribution Analysis *25*

3.0 DEVELOPMENT OF LEU FUEL ELEMENT DESIGN **29**

3.1 Preliminary Studies in LEU Fuel Element Design 29

3.2 LEU Fuel Element Design Optimization 30

4.0 NEUTRON PHYSICS FOR HEU AND LEU FUELED CORES **36**

4.1 Selection of HEU and LEU Reference Cores 37

4.2 Power Distributions for Steady State Safety Margin Evaluations 38

4.3 Fuel Cycle Performance 49

4.4 Control System Reactivity Worth 51

4.5 Reactivity Coefficients 54

4.6 Experimental Performance 57

5.0 CONCLUSIONS **65**

REFERENCES **66**

Appendix A: Material Properties and Composition Data in MURR Core Models **67**

List of Figures

Figure 1.1. Cross-Sectional View of MURR. 1
Figure 1.2. MURR Fuel Element. 2
Figure 1.3. MURR Core Layout with Control Blades Identified. 2
Figure 2.1. Suite of Neutron Physics Codes Used for MURR Analyses. 6
Figure 2.2. MCNP Model of 1971 MURR Core. 7
Figure 2.3. MCNP Model of 2008 MURR Core. 9
Figure 2.4. Identification of Graphite Reflector Wedges and Flux Trap 10
Figure 2.5. Axial Heat Flux Profile in MURR Element X1 for Feasibility Study Design. 12
Figure 2.6. MCNP Modeling of Sample Loading in MURR Flux Trap. 14
Figure 2.7. MURR Core Layout. 16
Figure 2.8. Weekly Core k-effective for MURR HEU Fuel Cycle Simulation. 17
Figure 2.9. MURR Core k_{eff} vs. Burnup – Straight Rundown without Shuffling. 18
Figure 2.10. Weekly Core k-effective for MURR LEU Fuel Cycle Simulation. 19
Figure 2.11. ECP Deviation from Critical vs. Blade History. 22
Figure 2.12. Critical Withdrawl of Shim Blades vs. Blade History. 22
Figure 2.13. Effect of Residence Time on B-10 Atom Density in MURR Control Blades. 23
Figure 2.14. ECP Deviation From Critical With ("CB Burnup") and Without ("no CB Burn") Modeled Control Blade History. 24
Figure 2.15. Azimuthal Striping Detail with Equal-Angle Stripes at Edge of Fuel Meat. 25
Figure 2.16. Azimuthal Peaking Factor For Representative Core Loaded with LEU-FSD. 26
Figure 2.17. Simulated Geometry in CFD Analysis of MURR Hot Channel. 27
Figure 2.18. Azimuthal Heat Flux Distribution for MURR Hot Channel. 28
Figure 3.1. Comparison of Core k_{eff} vs. Burnup for FSD and Non-Optimized Element. 30
Figure 3.2. Hot-Stripe Heat Flux by Plate for Candidate LEU Element Designs in All Fresh Core. 33
Figure 4.1. MURR Core Layout with Typical BOC Burnups. 37
Figure 4.2. Normalized Radial Power Factors in Fresh Element in LEU Reference Core. 40
Figure 4.3. Hot-Stripe Heat Flux Radial Peaking Factor in Fresh Element in LEU Cores. 40
Figure 4.4. Average Heat Flux in Each Plate of Each Element in Case 8A2. 46
Figure 4.5. Azimuthal Peaking Factors for Each Plate of Each Element in Case 8A2. 47
Figure 4.6. Azimuthal Peaking Factors by Plate Averaged for All Elements in Core. 48
Figure 4.7. Hot-Stripe Heat Flux for Each Plate of Each Element in Case 8A2. 48
Figure 4.8. Heat Flux Profile in Plate 23 in LEU Reference Mixed Burnup Core. 50
Figure 4.9. Fission Density by Plate in Discharged HEU Fuel. 52
Figure 4.10. Fission Density by Plate in Discharged LEU Fuel. 53
Figure 4.11. Comparison of LEU and HEU Beam Tube E Outbound Current at Day 0. 62
Figure 4.12. Comparison of LEU and HEU Beam Tube E Outbound Current at Day 2. 62
Figure 4.13. Comparisons of LEU 10 MW to HEU 10 MW at Day 0. 63
Figure 4.14. Comparisons of LEU 12 MW to HEU 10 MW at Day 0. 63
Figure 4.15. Comparisons of LEU 10 MW to HEU 10 MW at Day 2. 64
Figure 4.16. Comparisons of LEU 12 MW to HEU 10 MW at Day 2. 64

List of Tables

Table 1.1. LEU Fuel Element Design Parameters. 4
Table 2.1. Critical State Evaluations for 1971 All Fresh HEU Core. 8
Table 2.2. Comparison of MCNP and DIF3D k-effectives for Fresh HEU 1971 Core. 9
Table 2.3. Reactivity Worths of Typical Samples in Graphite Reflector and Flux Trap for 2008 HEU Core. 11
Table 2.4. Reactivity Worths of Typical Samples in Graphite Reflector and Flux Trap for LEU Fueled Core. 15
Table 2.5. MURR Fuel Cycle Simulation Results for Pseudo-Equilibrium Cycle. 19
Table 2.6. Comparison of MCNP and DIF3D Core k-effective for HEU and LEU Cores. 20
Table 2.7. Summary of Critical States Evaluated for Partially Burned Cores. 21
Table 2.8. %Δk/k Deviation for Estimated Critical Positions for Fresh Blades and Depleted Blades for Partially Burned Cores. 24
Table 3.1. Design Parameters for LEU Fuel Element Optimization Study. 32
Table 3.2. Nominal HEU and LEU Fuel Plate Dimensions. 35
Table 4.1. Summary of Reactor Physics Parameters Calculated by MCNP for MURR. 36
Table 4.2. Summary of Power Distribution Evaluations – HEU Cores. 42
Table 4.3. Summary of Power Distribution Evaluations –LEU Cores. 43
Table 4.4. Summary of Key Hot-Stripe and Local Heat Fluxes Evaluated for HEU Cores. 44
Table 4.5. Summary of Key Hot-Stripe and Local Heat Fluxes Evaluated for LEU Cores. 45
Table 4.6. Current and Proposed MURR Fuel Cycle Operating Characteristics. 51
Table 4.7. Plate Discharge Fission Density for HEU Fuel. 52
Table 4.8. Plate Discharge Fission Density for LEU Fuel. 53
Table 4.9. Control System Worth Calculations. 54
Table 4.10. Coolant Void Coefficient Experiment Performed During Low-Power Testing. 55
Table 4.11. Simulation of Coolant Void Coefficient Experiment in MCNP. 56
Table 4.12. Coolant Void Coefficient Calculated by Density Reduction Method. 56
Table 4.13. Kinetics Parameters and Reactivity Coefficients. 57
Table 4.14. Comparison of Day 0 LEU Fluxes and Reaction Rates to HEU. 60
Table 4.15. Comparison of Day 2 LEU Fluxes and Reaction Rates to HEU. 61
Table A.1. Water Properties. 67
Table A.2. Fuel Properties. 67
Table A.3. Fresh HEU Fuel Meat Composition in 1971 Criticals Models. 68
Table A.4. Fresh HEU Fuel Meat Composition (U-Al_x) in Fuel Cycle Simulation Models. 68
Table A.5. Fresh LEU Fuel Meat Composition (U-10Mo) in Fuel Cycle Simulation Models. 68
Table A.6. Al-6061 Aluminum Composition: MCNP Model. 69
Table A.7. Al-6061 Aluminum Composition: DIF3D Model. 69
Table A.8. Fresh Shim Blade Dimensions and Compositions. 70
Table A.9. Graphite Reflector Composition. 71
Table A.10. Beryllium Reflector Composition. 72

1.0 INTRODUCTION

The University of Missouri is working in conjunction with the Global Threat Reduction Initiative (GTRI) Reactor Conversion Program at Argonne National Laboratory (ANL) to perform fuel element design, fuel cycle performance, and steady state-safety analyses to support conversion of the Missouri University Research Reactor (MURR) from highly-enriched uranium (HEU) to low-enriched uranium (LEU) fuel. The goals of the conversion are to ensure acceptable shutdown and safety margins, as well as maintain the existing experimental performance of the facility. The purpose of this report is to document the neutron physics analyses that have been completed to confirm that these goals are met with a proposed LEU fuel element design.

1.1 Description of Facility

The MURR is a multi-disciplinary research and education facility providing a broad range of analytical and irradiation services to the research community and the commercial sector. The MURR has six types of experimental facilities designed to support these services and research programs: the Center Test Hole (Flux Trap); the Pneumatic Tube System; the Graphite Reflector Region; the Bulk Pool Area; the (six) Beamports; and the Thermal Column. The first four types provide areas for the placement of sample holders or carriers in different regions of the reactor core assembly for the purposes of material irradiation. The six beamports channel neutron radiation from the reactor core to experimental equipment which is used primarily to determine the structure of solids and liquids through neutron scattering. The graphite thermal column is designed for the purpose of performing neutron radiographs and large sample irradiations. Cross-sectional views of the reactor and experimental facilities are shown in Figure 1.1.

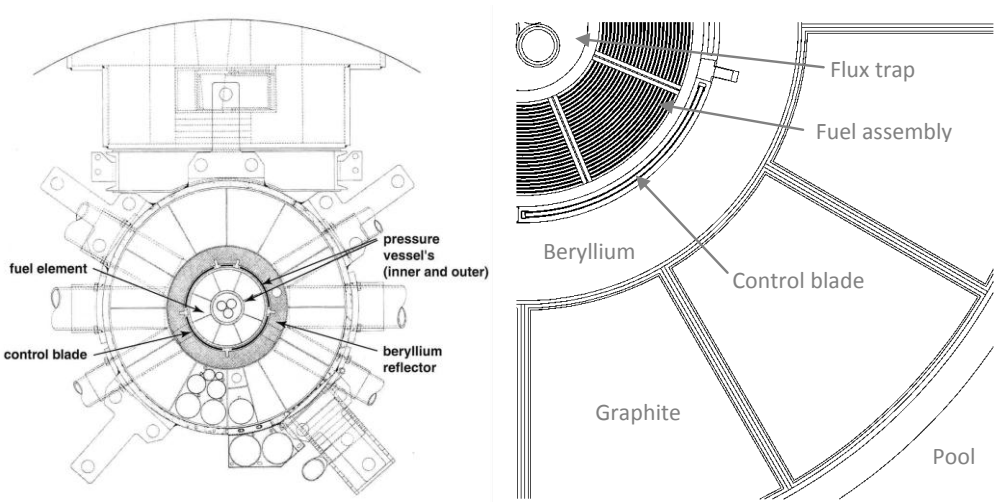

Figure 1.1. Cross-Sectional View of MURR.

The source of neutrons for the experimental facilities of the MURR is a fuel region which has a fixed geometry consisting of eight fuel elements, each having identical physical dimensions. The fuel elements are placed vertically around an annulus between the two cylindrical aluminum reactor pressure vessels. The MURR is currently fueled with HEU fuel.

Each HEU fuel element has 24 curved plates that form a 45-degree arc. Drawings of the MURR fuel element (pictorial and cross sectional views) are shown in Figure 1.2. The HEU fuel plates are 50 mil thick (0.050 inches). The fuel meat is 20 mil thick in each plate and consists of aluminide fuel containing uranium with a ^{235}U enrichment of 93%. The HEU plates are clad with 15 mil of Al-6061 aluminum. The overall length of the elements is 32.5 inches, with an active fuel meat region 24 inches long.

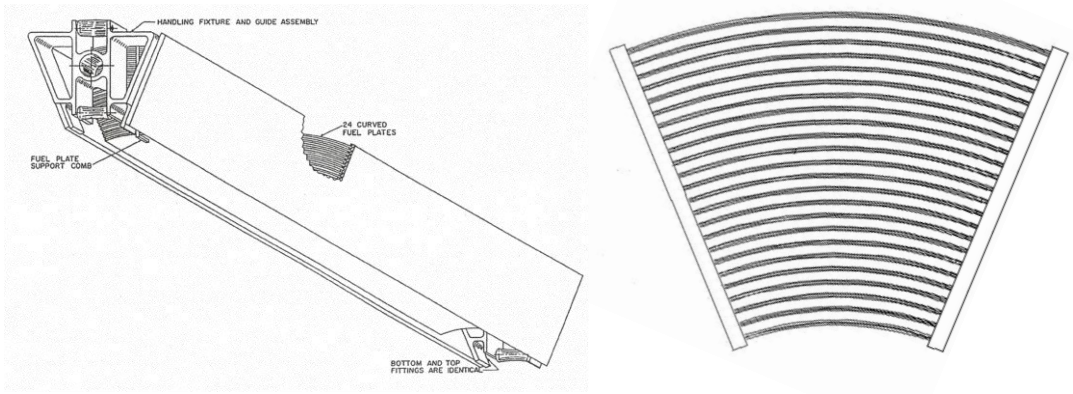

Figure 1.2. MURR Fuel Element.

The reactor is controlled by control blades that move vertically in an annular gap between the outer pressure vessel and the beryllium reflector, as shown in Figure 1.1, and in close-up detail in Figure 1.3. The control blades are curved to follow the contour of the gap. The blades control the reactivity by varying neutron reflection from the beryllium reflector. Four of the control blades are constructed of Boral (shim blades), and one is stainless steel (regulating blade). The shim blades were modeled as 101 mil (0.101 inches) thickness of Boral, clad with 37 mil of Al-6061 aluminum, for a total thickness of 175 mil. The poison section of the shim blades is 34 inches long. The stainless steel regulating blade is 188 mil thick.

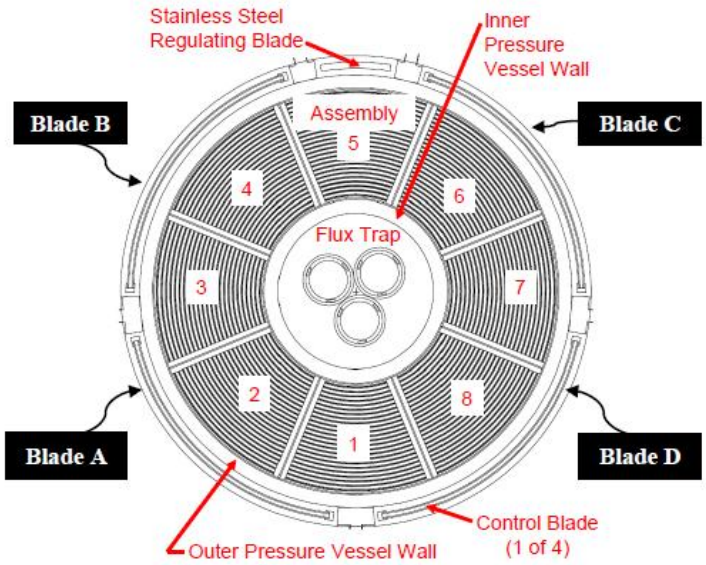

Figure 1.3. MURR Core Layout with Control Blades Identified.

The MURR is currently licensed for a maximum core power of 10 MW. This power level provides neutron flux levels in the center flux trap and irradiation positions in the graphite reflector to enable MURR to fulfill its mission of providing experimental and irradiation services. The MURR operates continuously with the exception of a weekly scheduled shutdown. Over the past 35 years of operation, the MURR has averaged approximately 6.3 days/week at full power. The weekly shutdown provides an opportunity to access samples in the center test hole, to perform surveillance tests and maintenance, and to replace all eight fuel elements in the core. Replacing the fuel elements provides a xenon free core for restart and the chance to remix or shuffle the elements that will be used in the core. The active fuel cycle

typically consists of 32 fuel elements; corresponding to sixteen pairs of elements. A core loading will always consist of four different pairs of elements, with the two elements of each pair loaded opposite of each other in the core.

The compact core volume limits excess reactivity and causes the control blades to be fully withdrawn when the HEU core, with equilibrium xenon, achieves approximately 640 MWd. This results in an HEU fuel element reaching a maximum burnup of 150 MWd, which in turn corresponds to a calculated hot spot burnup of less than 1.6×10^{21} fissions/cm^3. This ensures that the Technical Specification limit of 2.3×10^{21} fissions/cm^3 for the UAl_x dispersion fuel is not approached or exceeded. Cores are usually loaded such that the average power history of the fuel elements is approximately 75 MWd. Typically a fuel element will be used in 18 to 20 different core loadings before being retired from the fuel cycle. A core with fuel elements approaching the burnup limit will also include a corresponding number of elements with a very low burnup history. This maximizes the number of MWd obtainable per fuel element. This same approach is also planned for the LEU fuel cycle.

1.2 LEU Fuel Element Design Development

The compact core design of the MURR requires a much higher loading density of ^{235}U than available in currently qualified LEU fuel forms. However, in a previous report [1] the feasibility of meeting the conversion goals with a monolithic U-10Mo fuel form was shown. The fuel element design developed in the Feasibility Study was constructed similar to the HEU fuel element, with 24 fuel plates, but with thinner fuel foil thicknesses for the plates near the flux trap and the beryllium reflector to flatten the radial heat flux profile. The study showed that the "FSD" (Feasibility Study design) fuel element met the thermal-hydraulic safety and shutdown margins for the MURR, maintained the experimental performance of the facility – provided the reactor power level could be uprated from 10 to 12 MW, and yielded a decrease in the number of fuel elements needed per year to maintain the reactor's weekly operating schedule.

Following the release of the Feasibility Study and the Preliminary Safety Analysis Report [2], experience gained by the Fuel Development (FD) and Fuel Fabrication Capability (FFC) pillars of the GTRI's Reduced Enrichment for Research and Test Reactors (RERTR) Program revealed that initial assumptions regarding design constraints on the LEU plates needed to be adjusted. In particular, the Al-6061 aluminum clad surrounding the fuel foils in the FSD was designed as thin as 10 mil (nominal) based on these initial assumptions. While HEU fuel plates with nominal 10 mil clad have been routinely fabricated for research reactors such as HIFR, experience has shown that in order to reliably fabricate the fuel plates with U-10 Mo fuel foils, the nominal clad thickness should be no thinner than 12 mil.

The Reactor Conversion (RC) pillar has responded to this feedback by redesigning the LEU fuel element to meet this constraint. An extensive series of "contingency designs" were evaluated through scoping studies, followed by optimization of a design that meets the conversion goals. The newly designed fuel element that is now proposed has been labeled "CD35," and is constructed with 23 fuel plates (instead of 24 plates as in the FSD and HEU elements). The element still uses graded foil thicknesses to flatten the radial heat flux profile, but the thinnest nominal clad is 12 mil (versus 10 mil in the FSD) and the thinnest total plate thickness is 44 mil (versus 38 mil in the FSD). The fuel cladding consists of Al-6061 aluminum and a thin (1 mil) zirconium layer at the fuel-aluminum interface. A summary comparison of the fabrication parameters for the FSD and CD35 fuel element designs is provided in Table 1.1. A detailed description of the scoping studies and redesign process is provided in Section 3 of this report.

Table 1.1. LEU Fuel Element Design Parameters.

FSD 24 Fuel Plates 4 Unique foil/plate combinations 10 mil thinnest nominal clad 38 mil minimum plate 1439 g U-235/element				
Channel or Plate	Meat thickness (mil)	Clad thickness (mil)	Plate thickness (mil)	Channel thickness (mil)
1	9	20	49	95
2	12	13	38	92
3	18	10	38	92
4	18	10	38	92
5	18	10	38	92
6	18	10	38	92
7	18	10	38	92
8	18	10	38	92
9	18	10	38	92
10	18	10	38	92
11	18	10	38	92
12	18	10	38	92
13	18	10	38	92
14	18	10	38	92
15	18	10	38	92
16	18	10	38	92
17	18	10	38	92
18	18	10	38	92
19	18	10	38	92
20	18	10	38	92
21	18	10	38	92
22	18	10	38	92
23	18	10	38	92
24	17	16	49	92
25				95

CD35 23 Fuel Plates 5 Unique foil/plate combinations 12 mil thinnest nominal clad 44 mil minimum plate 1507 g U-235/element				
Channel or Plate	Meat thickness (mil)	Clad thickness (mil)	Plate thickness (mil)	Channel thickness (mil)
1	9	17.5	44	95.5
2	12	16	44	93
3	16	14	44	93
4	20	12	44	93
5	20	12	44	93
6	20	12	44	92
7	20	12	44	92
8	20	12	44	92
9	20	12	44	92
10	20	12	44	92
11	20	12	44	92
12	20	12	44	92
13	20	12	44	92
14	20	12	44	92
15	20	12	44	92
16	20	12	44	92
17	20	12	44	92
18	20	12	44	92
19	20	12	44	92
20	20	12	44	93
21	20	12	44	93
22	20	12	44	93
23	17	16	49	93
24				95.5

The proposed LEU fuel element is based on the presumption that the U-10Mo fuel foils will become qualified as a fuel form for reactors regulated by the U. S. Nuclear Regulatory Commission (USNRC). Active work in the FD and FFC pillars is validating the in-reactor performance of the monolithic U-10Mo fuel foils and the hydro-mechanical stability of the fuel plates in the proposed design.

In the remainder of this report, the technical basis for the steady-state neutron physics of the MURR operating with the proposed LEU fuel element will be described. The technical basis for the steady-state thermal-hydraulics safety analyses will be described in a companion report [3]. In Section 2, the computational methodology and models used for the neutron physics analyses will be described and validated. Section 3 will discuss the development of the proposed LEU fuel element design that was evaluated to ensure the goals of acceptable shutdown and safety margins, as well as maintaining existing experimental performance of the facility, are achieved. Lastly, a summary of neutron physics performance parameters for the current HEU and proposed LEU fuel element design will be compared in Section 4. Conclusions will be summarized in Section 5.

2.0 COMPUTATIONAL METHODOLOGY AND MODELS

The design and evaluation of the MURR LEU fuel element design requires accurate calculations of the core k-effective, control blade position, and detailed power distribution and experimental fluxes/reaction rates. In order to perform these calculations, it was necessary to assemble a suite of analysis codes, develop models of the MURR with both HEU and LEU fuel, and then evaluate the credibility of the models.

2.1 Description of Neutron Physics Codes

Historically, the neutron physics modeling and analyses of MURR have been performed with several multi-group and multi-dimensional neutron diffusion theory codes: PDQ, EXTERMINATOR-II, and BOLD VENTURE-IV. The BOLD VENTURE model was benchmarked against the destructive analysis of an HEU element that had been burned to 82.5 MWd (a little over half of the current discharge burnup of the HEU fuel). The analytical results showed very good agreement with the experimental data.

To perform the neutronics calculations of a compact core such as MURR, it is preferable to use a transport theory code to capture the rapidly changing spectra across the various regions. Therefore, the MCNP [4] continuous energy Monte Carlo code was used for all calculations of the core k-effective, control blade position, and detailed power distribution and experimental fluxes/reaction rates.

Since realistic experimental flux and reaction rate performance must be evaluated for typical weekly cycles rather than for an all-fresh core, a detailed set of compositions for partially burned fuel elements is needed. In order to obtain these compositions, a neutronics analysis code suite utilizing WIMS-ANL [5], REBUS-DIF3D [6], MCNP [4], and REBUS-MCNP [7] was assembled. Each component of the suite and its function is described below. Figure 2.1 illustrates the linkage of the codes in the analysis suite.

WIMS-ANL. WIMS-ANL is a one-dimensional lattice physics code used to generate burnup dependent, multi-group cross sections. The code utilizes either 69- or 172-group libraries of cross-section data for 123 isotopes generated from ENDF-6. The 69-group library is typically used for research reactor analysis. A customized 10-group structure was developed based on the neutron spectrum that exists in the MURR core. [8] Cross-section data for actinides, structural materials, explicit fission products, and a lumped fission product were collapsed to the 10-group structure and stored in a library to be used by the REBUS-DIF3D code. The collapsed data were saved for several color sets within the fuel plates, as well as different structural regions. WIMS-ANL was also used to generate a 69-group lumped fission product library that represents fission products not explicitly represented in the MCNP libraries [9]. This multi-group data can be used in MCNP and REBUS-MCNP analyses of depleted cores.

REBUS-DIF3D. DIF3D is a multi-dimensional, multi-group neutron diffusion code that can model systems in a number of geometries. REBUS is a depletion code that utilizes neutron fluxes from a neutronics solver and cross-section data to solve isotopic transmutation calculations. A detailed Theta-R-Z diffusion model was developed for DIF3D. The details of the DIF3D model were developed iteratively to assure fidelity of the diffusion calculations with MCNP and experiments. A REBUS model was created to perform an extended single-cycle depletion (a “straight rundown”) of an all-fresh core, as well as a highly detailed simulation of the typical weekly operations in MURR with fuel shuffling between in-core and ex-core locations. The depleted core characteristics (plate by plate and axially-segmented atom densities) can be saved and passed on to MCNP for more detailed neutronics analyses.

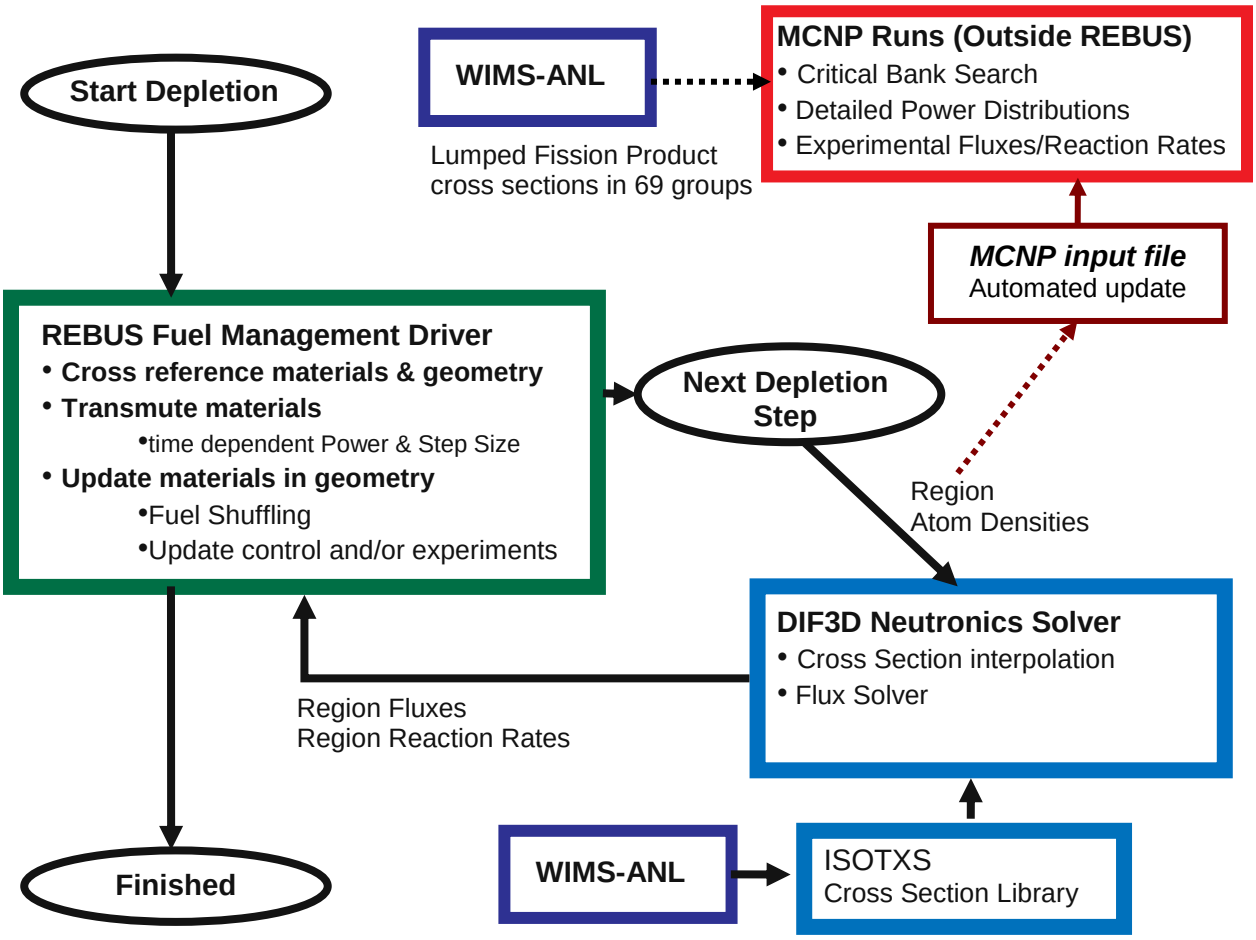

Figure 2.1. Suite of Neutron Physics Codes Used for MURR Analyses.

MCNP. MCNP is a continuous energy Monte Carlo neutron transport code. MCNP is capable of modeling the heterogeneous details of the MURR fuel elements, core structures, and experimental facilities while capturing the rapidly changing spectra across these various regions. Using the 69-group lumped fission product library generated by WIMS-ANL, the code can be used to model cores of depleted and fresh elements. MCNP will be used for all detailed calculations of core k-effective; critical control blade positions and control blade worths; detailed power distributions; and experimental fluxes and reaction rates.

REBUS-MCNP. Like REBUS-DIF3D, REBUS-MCNP is capable of performing depletion analyses, but using the MCNP code to calculate detailed flux profiles and collapse continuous energy cross section data to one-group for use by the REBUS depletion module. The hundreds of state points required to model the complex fuel cycle of MURR made REBUS-MCNP intractable for the full fuel cycle simulation. However, REBUS-MCNP models were still developed for a "straight rundown" of the reactor beginning with a fresh core to benchmark the REBUS-DIF3D models.

2.2 Credibility of Neutron Physics Models

Extensive work was performed to validate the neutron physics codes and models for application to the MURR. Experimental data for HEU fueled cores are available from two sources. The MCNP and DIF3D models were benchmarked against these reference data.

1. In 1971, a report of startup physics tests was compiled by Caudle Julian for a core loaded with 8 fresh HEU elements [10]. The report provided critical blade positions with several different flux trap configurations.

2. Additionally, measured "criticals" for the core loaded with mixed-burnup HEU elements in the current reactor configuration are also available. These critical measurements can be used to validate the models for cores with various total core fuel burnup and history of the shim blades.

In the following sections, the credibility of the all-fresh fuel core model will be assessed first. Then, prior to assessing the credibility of the mixed-burnup core models, the development of the model for the typical conditions of the current reflector and flux trap loading will be described. Also, the development of a fuel cycle simulation model that was used to obtain the detailed compositions of the partially-burned elements will also be described. This will be followed by a comparison of the mixed-burnup core calculations against the critical experiment measurements, as well as a summary of work performed to model the depletion of the shim blade poison based on operating history. Lastly, a discussion of the azimuthal discretization of the MCNP model for power distribution calculations that provide a conservative estimate of the elevated heat conduction into the coolant channels at the edge of the fuel plates will be provided.

2.2.1 MCNP and DIF3D Models – Comparisons with 1971 HEU Fresh Core Measurements

An MCNP model was developed to match the conditions that existed in the MURR in 1971. This corresponds to the core configuration during the initial critical and physics tests performed on the first MURR aluminide 775 g U-235 HEU core, which is still the current fuel element design. A cross-sectional view of the model is shown in Figure 2.2. Since around 1980, MURR has not been able to have a full core of unirradiated fuel elements to perform any clean critical. The startup campaign of the 1971 all fresh core provided an experimental basis for model benchmarking.

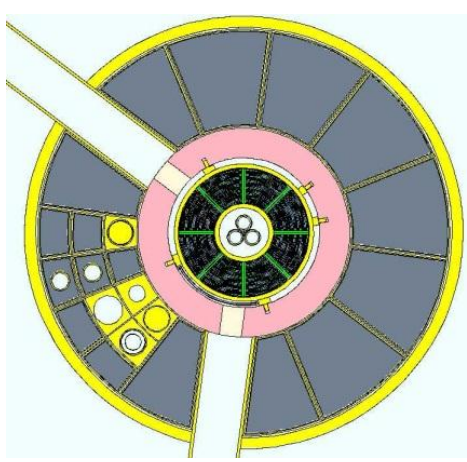

Figure 2.2. MCNP Model of 1971 MURR Core.

The benchmarking effort also demonstrated that a high level of detail is needed in the models to accurately predict the compact, high-flux MURR reactor. These modeling choices were made to the

models to improve agreement with measurements from the low-power startup physics testing compiled by Julian [10]. Many details of the improvements were described in RERTR International Meeting papers in 2007 and 2008 [8, 11, 12]. It proved particularly important to treat the explicit geometry of the reflectors and control blades well. Various tables of composition data and material properties used in the models are provided in Appendix A.

Table 2.1 summarizes the critical states calculated by MCNP for the all-fresh HEU core. The RMS deviation from critical for the five cases is -0.584% ± 0.075% Δk/k. While the bias for the 1971 HEU fresh core remains fairly large, there were details of materials not completely specified in the 1971 data. The compact nature of the MURR core, with both graphite and beryllium reflectors and complex experimental channels is difficult to model. Notably, the best prediction was for Case 1 with all control blades banked, which is the mode for normal MURR operations. Furthermore, the small standard deviation of the reactivity bias despite the skewed blade patterns indicates that comparisons of HEU and LEU burnup performance should be sound.

Table 2.1. Critical State Evaluations for 1971 All Fresh HEU Core.

	Blade Position (inches withdrawn)						MCNP		
Case[1]	A	B	C	D	Regulating Blade	Flux Trap State	k_{eff}	σ (pcm)	Deviation from Critical[3] (%Δk/k)
1	11.93	11.92	11.92	11.92	26.00	Empty	0.99520	12	-0.482
2	11.93	11.92	11.92	12.63	6.00	Empty	0.99485	11	-0.518
3	11.93	11.92	11.92	10.50	11.24	3 Tubes[2]	0.99377	11	-0.627
3A	11.93	11.92	11.92	10.91	6.00	3 Tubes	0.99378	11	-0.626
3B	11.93	11.92	11.92	10.21	26.00	3 Tubes	0.99357	12	-0.647

[1] Julian report Case Number for startup physics testing of HEU UAl_x core.
[2] 3 empty tubes in flux trap indicates sample holder in place, but filled with pool water.
[3] Deviation from critical is (k-1)/k.

The 1971 core configuration was also used as a basis to develop the adequate level of approximations in DIF3D and helped develop the WIMS-ANL methodology. WIMS-ANL and DIF3D model changes were methodological, in addition to the geometry and material updates. Proper generation of cross-sections in WIMS-ANL and appropriate geometric discretization in the DIF3D model were both key to fidelity.

Table 2.2 shows the close agreement achieved for DIF3D vs. MCNP for a variety of core states. The DIF3D model predicts a slightly higher k-effective relative to the MCNP model; the largest difference observed between the two models is 0.137% Δk/k (137 pcm). The bias of the DIF3D model for the critical case is -0.49% Δk/k, compared with a -0.63% Δk/k bias for the MCNP model for the same critical. Comparing Cases 1 and 2, the MCNP model calculates a sample holder worth of 0.344% Δk/k, while DIF3D calculates a worth of 0.394% Δk/k. The measured worth of the sample holder in the HEU MURR core was 0.36% Δk/k, which is comparable to the results of both of these calculations.

Table 2.2. Comparison of MCNP and DIF3D k-effectives for Fresh HEU 1971 Core.

Case	MCNP	DIF3D	Deviation (DIF3D vs. MCNP) (% Δk/k)	Sample Holder Worth (% Δk/k)		
				Measured	MCNP	DIF3D
1. No sample holder ARO (blades out)	1.10209 (±11 pcm)	1.10298	+0.073			
2. Empty sample holder ARO (blades out)	1.10629 (±11 pcm)	1.10779	+0.123	+0.36	+0.344	+0.394
3. Empty sample holder Blades at measured critical[1]	0.99377 (±11 pcm)	0.99512	+0.137			

[1] The control blades are modeled at the recorded heights from a 1971 critical measurements.

2.2.2 Description of Changes to HEU Core Models (1971 to 2008 Core Configuration)

The irradiation positions and typical sample loadings in the graphite reflector and flux trap have changed since the tests performed in 1971. In order to properly model the current reflector and flux trap configurations, it was necessary to modify the MCNP and DIF3D models. Material composition data are tabulated in Appendix A.

The key changes between the 1971 and 2008 reactor configurations were:

- Different control blades are in use, with changes in dimension and composition.
- Most graphite reflector blocks have been replaced, and the associated experimental positions have been markedly changed. One of the most significant features of the current graphite reflector is the presence of large cadmium-lined irradiation positions in the L and N wedges, adjacent to fuel element position 5.
- The beryllium reflector no longer has voids at the entrance of Beam Ports A and E.

A cross-sectional view of the MCNP model of the 2008 reactor configuration is shown in Figure 2.3.

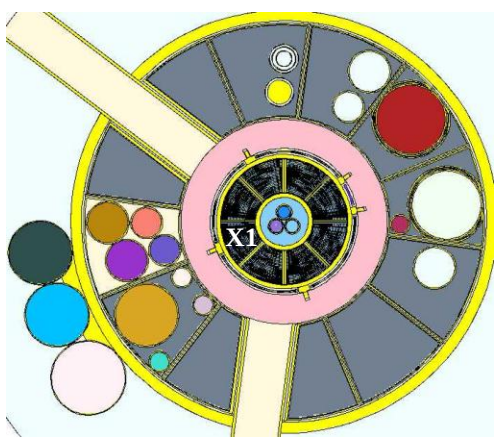

Figure 2.3. MCNP Model of 2008 MURR Core.

To compare HEU and LEU performance relative to the current mission of the facility, typical sample loadings were modeled for reflector and flux trap positions. The reflector irradiation positions and flux trap contents are explicitly modeled in MCNP, but the Theta-R-Z geometry of the DIF3D model does not allow an exact representation of the reflector and flux trap components. Instead, modeling

approximations were tested to determine the most effective way of representing the irradiation positions and samples in the DIF3D model.

A series of MCNP cases were prepared to transition the graphite reflector and flux trap contents to current (2008) conditions. The base case had all fresh fuel, empty holder tubes in the flux trap, graphite reflector wedges without any penetrations or samples, the control blades at 23" withdrawn (which is the typical shim blade position during the bulk of the weekly operating cycle), and the regulating blade positioned at the core midplane. The model was sequentially altered to explicitly represent each wedge with its corresponding irradiation positions and typical sample loading. The final step was to model a typical sample loading in the central flux trap. Figure 2.4 identifies the locations of the reflector and flux trap irradiation positions that were altered in the model transition.

Position	Worth (%Δk/k)	
	Indiv.	**Cumm.**
L & N Wedges	-0.750	-0.750
10 Wedge ("Yellow-Green" wedge)	-0.160	-0.909
11 Wedge ("Blue-Red" and "Hanging" wedge)	-0.017	-0.926
3 Wedge	-0.065	-0.991
4 Wedge	-0.015	-1.006
6 Wedge	-0.031	-1.037
Flux Trap loaded with typical samples	+0.052	**-0.985**

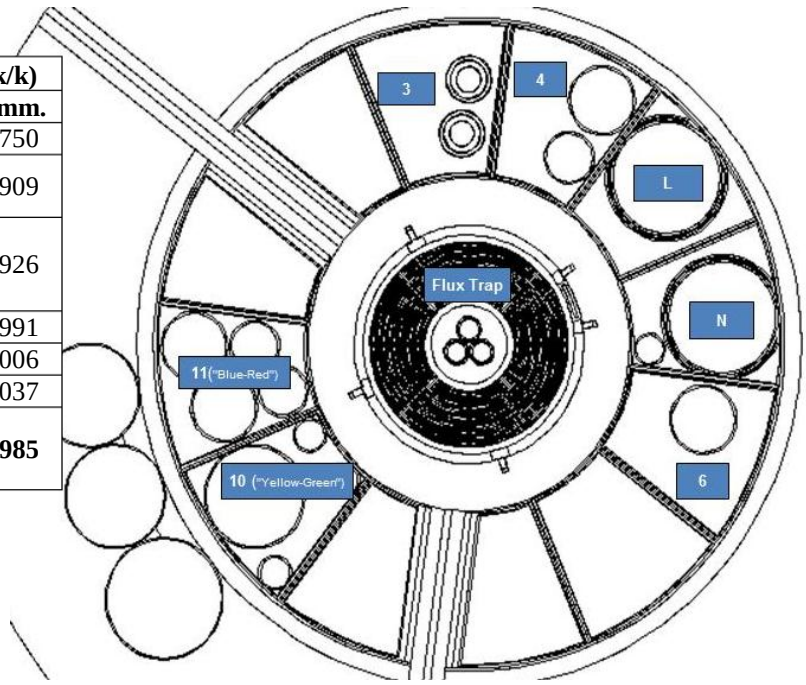

Figure 2.4. Identification of Graphite Reflector Wedges and Flux Trap With Samples in Current MURR Reactor Configuration.

The inset box in Figure 2.4 shows the individual and cumulative reactivity worth of each step of the transition as calculated by MCNP. It was known from reactivity change measurements at MURR when the Cd-lined irradiation positions in the L and N wedges were installed that the cumulative negative reactivity worth of the alteration was ~0.75% Δk/k. It can be seen that the MCNP core model predicts this reactivity worth very well, which reinforces the credibility of the model. The net cumulative effect of all reflector and flux trap alterations to reach current core conditions was -0.985% Δk/k for the HEU core.

In the same way, the DIF3D model was transitioned to the current conditions, but with an amount of natural boron smeared into the corresponding graphite wedge or flux trap sample holder that matched the reactivity worth calculated by the MCNP cases to within 0.01% Δk/k. The only deviation from this approach was for the 11-wedge, which is a helium filled aluminum can with water-filled irradiation positions. Since no graphite is present in these positions, the volume fraction of water was adjusted in the DIF3D representation of the 11-wedge to match the reactivity worth.

Table 2.3 presents the sequence of cases used to transition the MCNP and DIF3D core models loaded with HEU fuel. Both the individual and cumulative reactivity worths of each alteration in the sequence

are presented. The DIF3D model boron loading or water fraction in the graphite wedges and sample cans was adjusted empirically to match the individual worth of each alteration in the MCNP model within 0.010% Δk/k. The agreement between the DIF3D and MCNP models for the all fresh HEU core with the current configuration of the flux trap and reflector samples is 0.23% Δk/k.

Table 2.3. Reactivity Worths of Typical Samples in Graphite Reflector and Flux Trap for 2008 HEU Core.

	MCNP[3]			DIF3D			
		Worth (% Δk/k)			Worth (% Δk/k)		ppm B or water fraction change
	k-eff	Ind.	Cum.	k-eff	Ind.	Cum.	
Base Case[1]	1.09529			1.09803			
L & N Wedges	1.08637	-0.750%	-0.750%	1.08908	-0.749%	-0.749%	1280
10 wedge (Yellow-Green)	1.08449	-0.160%	-0.909%	1.08711	-0.166%	-0.915%	168
11 wedge[2] (Blue, Red, and Hanging wedges)	1.08429	-0.017%	-0.926%	1.08698	-0.011%	-0.925%	-8%
3 Wedge	1.08353	-0.065%	-0.991%	1.08621	-0.065%	-0.991%	61
4 Wedge	1.08335	-0.015%	-1.006%	1.08600	-0.018%	-1.009%	30
6 Wedge	1.08299	-0.031%	-1.037%	1.08565	-0.029%	-1.038%	40
Flux Trap Loaded with Typical Samples	1.08360	+0.052%	**-0.985%**	1.08631 (+0.23% Δk/k from MCNP)	+0.056%	**-0.982%**	82

[1] All fresh HEU fuel. Blades at 23" withdrawn; reg. blade at core midplane. Empty holder in flux trap. Graphite wedges have no samples or irradiation positions.
[2] This position is a helium-filled aluminum can with water-filled irradiation positions. In order to model the effect of the water displacement and samples, the water fraction in the DIF3D model was adjusted.
[3] MCNP runs of 60M histories had σ =11 pcm.

The details of the proposed "CD35" LEU fuel element design will be discussed in Section 3, but the description of the sample modeling in the DIF3D model of the LEU fueled reactor will be provided here to complement the description of the modeling done for the HEU fueled reactor. A similar approach to modeling the graphite reflector and flux trap samples in the DIF3D model was utilized, although the flux trap is modeled with greater axial detail in the DIF3D LEU model to improve agreement with the MCNP results for the axial power profile in plates near the flux trap, as discussed below.

Figure 2.5 shows the axial heat flux in plates 1 (innermost plate, next to the flux trap) and 24 (outermost plate, next to the control blades) of core position X1 for the so-called "FSD" (Feasibility Study design) LEU fuel element design developed in Reference 1. The calculations were performed for a core loaded with 8 fresh elements, the shim blades positioned at 23" withdrawn, and the regulating blade at the core midplane. The MCNP calculation had the graphite reflector and flux trap loaded with typical samples. The DIF3D model results labeled "DIF3D1" in Figure 2.5 had the samples represented by a smear of boron in the reflector and flux trap that matched the reactivity worth calculated by MCNP, in the same fashion as described above for the HEU core model. Thus, for the flux trap in the DIF3D1 model, a uniform concentration of boron (80 ppm in this case) was used over the entire axial range in which samples are loaded in the flux trap. For the outermost plate, the DIF3D1 model heat flux profile agrees quite well with the MCNP result near the core midplane; the agreement is not as good near the element end fittings, but this is a lower importance region of the core. However, for plate 1, which is next to the

flux trap, the DIF3D1 model under-predicts the heat flux compared with MCNP by about 11% at the core midplane. It is thought that this is due to the axial variation of the typical sample loading in the flux trap, which was modeled in detail in MCNP.

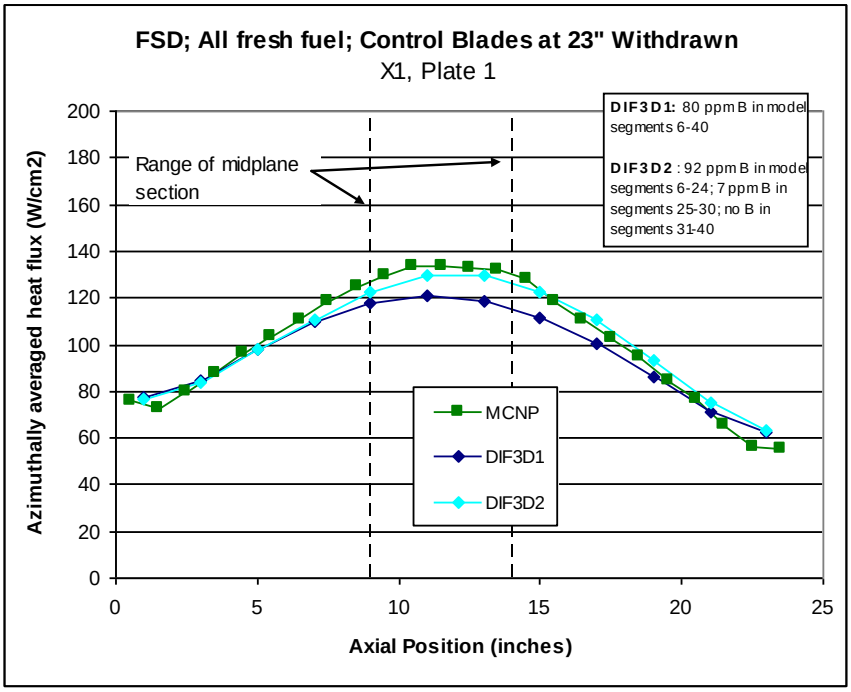

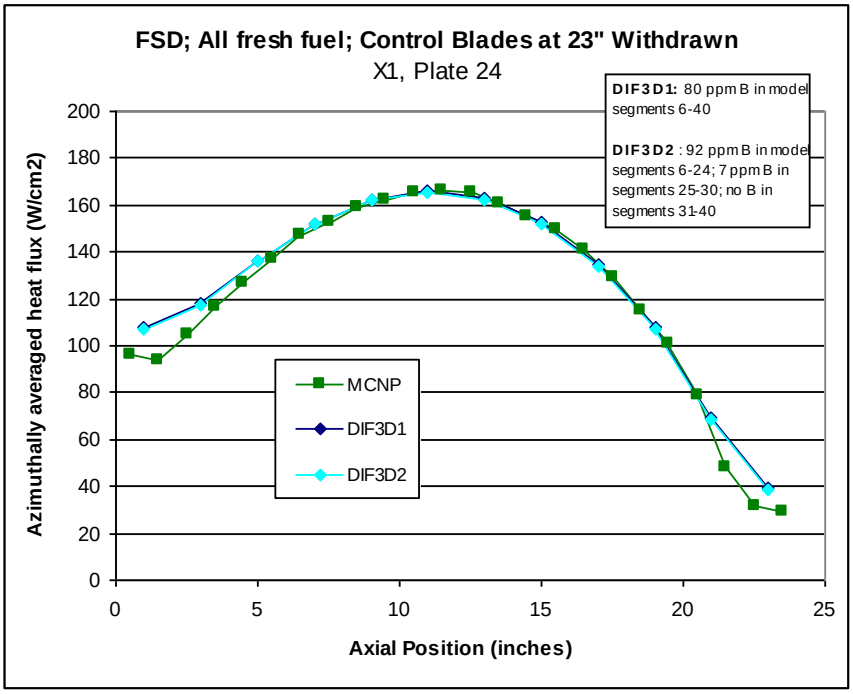

Figure 2.5. Axial Heat Flux Profile in MURR Element X1 for Feasibility Study Design. The DIF3D model uses boron loading in the flux trap as indicated in the figures.

The detailed MCNP model for the current configuration has samples or sample cans loaded in the flux trap from about 15.1 cm below the bottom of the active fuel meat to about 0.1 cm above the top of the fuel meat. In the DIF3D1 model, the three flux trap tubes were assumed to be uniformly loaded with sample cans/aluminum spacers over this axial range, which displaces the water inside the flux trap tubes. Then, a uniform loading of boron was smeared in the flux trap region to match the reactivity worth of the typical samples and spacers in the flux trap calculated by MCNP.

Figure 2.6 illustrates the MCNP model of the flux trap tubes and typical sample loading. The key parts of these figures for the present discussion are the portions contained within the blue- and red-outlined boxes. The cells inside the flux trap tubes and corresponding MCNP material numbers are indicated. The shading of the cells from lighter to darker blue indicates increasing volume fraction of water in the material. The greater the volume fraction of water in the material, the less water in the flux trap tube has been displaced by the sample cans. Materials 300-303 (for example, located in the upper portion of the flux trap tubes) contain 83% or more water by volume, and no sample material. Material 309 (located only in the center portion of Tube C) is 62% water, and material 304 is 46% water by volume. The remaining materials (305-308, 310) contain no water (all white in color in the figure), indicating that the sample cans displace all water in the flux trap tube in those locations.

Qualitatively, it can be seen that in the lower portion of the flux trap (below the red-outlined boxes that are at the core midplane) the sample cans and spacers displace the majority of the water from the flux trap tubes. In the upper portion of the flux trap (above the red-outlined boxes) it appears that very little of the water in the flux trap tubes has been displaced by the sample cans. The middle portion of the flux trap (inside the red-outlined boxes) is a high-importance region. Furthermore, it appears that roughly one-third of the cells at the core midplane have water displaced by the sample cans (cells containing materials 306 and 308), while the remaining two-thirds of the cells have a significant amount of water remaining.

Based on these observations, the DIF3D model was refined to better represent the conditions in the flux trap tubes and improve the axial heat flux profile predictions. As indicated in the legend of Figure 2.5, the flux trap in the axially-graded DIF3D2 model was modeled in 3 axial segments. The particular amounts of boron smeared in these segments are for a core loaded with the FSD LEU fuel element design. So, for example, in the lower segment, sample cans with a smear of 92 ppm boron were used to model the samples typically loaded in the flux trap. In the middle segment, a boron loading of only 7 ppm was needed to match the worth of the typical samples loaded in this axial range. In the upper segment, empty flux trap tubes (no sample cans, no boron) were modeled in the DIF3D2 model. Thus, the concentration of boron needed to match the reactivity worth of the typical sample loading is shifted towards the bottom of the flux trap in the axially-graded flux trap model. It can be seen that this adjustment to the model significantly improves the agreement between the MCNP and DIF3D models for the axial heat flux profile for plate 1, and has virtually no effect on plate 24.

This same axially-graded flux trap modeling approach was used in the DIF3D model for the CD35 fuel element design that will be described in Section 3 of this report. Table 2.4 presents the sequence of cases used to develop the MCNP and DIF3D core models of the current core configuration loaded with the proposed LEU fuel. The individual and cumulative reactivity worths of each alteration in the sequence are presented. The cumulative reactivity worth of the samples in the reflector and flux trap is -0.939% $\Delta k/k$ for the LEU fueled core. The magnitude of the reactivity worth is slightly less than the worth of the same samples in the HEU core (-0.985% $\Delta k/k$), which is expected because of the harder spectrum in the LEU core. The agreement between the DIF3D and MCNP models for the all-fresh LEU core in the current reactor configuration with typical flux trap and reflector samples is quite good, 0.09% $\Delta k/k$.

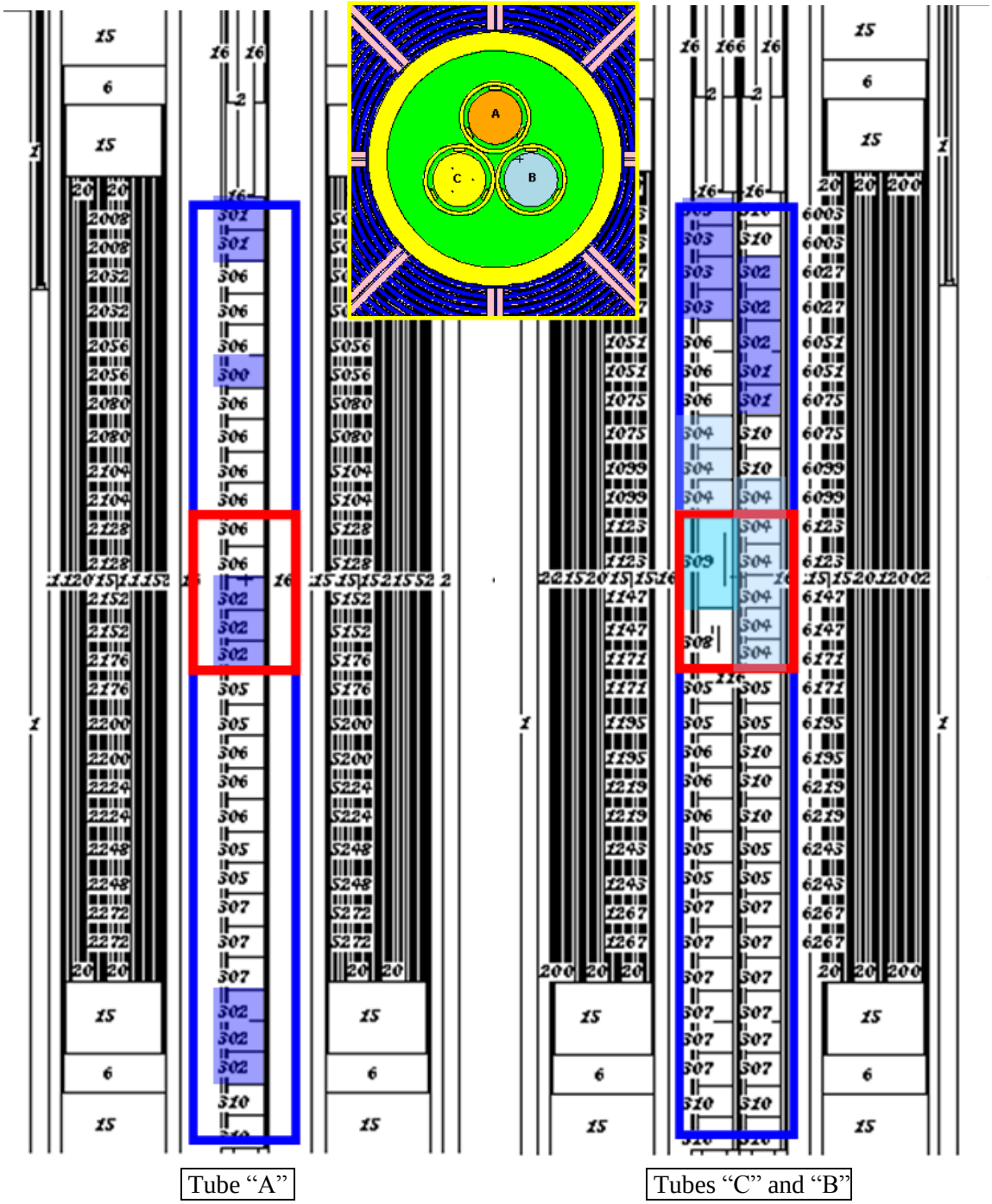

Figure 2.6. MCNP Modeling of Sample Loading in MURR Flux Trap.
The inset illustration indicates the position of the tubes in the flux trap.

Table 2.4. Reactivity Worths of Typical Samples in Graphite Reflector and Flux Trap for LEU Fueled Core.

	MCNP[3]			DIF3D			
		Worth (% Δk/k)			Worth (% Δk/k)		ppm B or water fraction change
	k-eff	Ind.	Cum.	k-eff	Ind.	Cum.	
Base Case[1]	1.07769			1.07874			
L & N Wedges	1.07001	-0.666%	-0.666%	1.07107	-0.664%	-0.664%	1020
10 wedge (Yellow-Green)	1.06808	-0.169%	-0.835%	1.06915	-0.167%	-0.831%	178
11 wedge[2] (Blue, Red, and Hanging wedges)	1.06818	+0.009%	-0.826%	1.06912	-0.003%	-0.834%	-2%
3 Wedge	1.06752	-0.058%	-0.884%	1.06852	-0.053%	-0.887%	50
4 Wedge	1.06689	-0.055%	-0.939%	1.06794	-0.051%	-0.938%	100
6 Wedge	1.06677	-0.011%	-0.950%	1.06776	-0.015%	-0.953%	20
Flux Trap Segments Near Midplane Loaded with Typical Samples	1.06781	+0.091%	-0.859%	1.06886	+0.096%	-0.857%	5
Flux Trap Segments Toward Bottom of Core Loaded with Typical Samples	1.06689	-0.081%	**-0.939%**	1.06793 (+0.09% Δk/k from MCNP)	-0.081%	**-0.938%**	94

[1] All fresh HEU fuel. Blades at 23" withdrawn; reg. blade at core midplane. Empty holder in flux trap. Graphite wedges have no samples or irradiation positions.
[2] This position is a helium-filled aluminum can with water-filled irradiation positions. In order to model the effect of the water displacement and samples, the water fraction in the DIF3D model was adjusted.
[3] MCNP runs of 60M histories had σ =11 pcm.

2.2.3 Development of Fuel Cycle Model

Depletion calculations are very important for the MURR fuel conversion analysis. The reactor has operated with a weekly fuel cycle for more than twenty years with high reliability and high utilization. The medical isotope production and many other experimental capabilities at MURR are optimized for this weekly cycle. Realistic experimental position flux levels and reaction rates must be evaluated for typical weekly cycles rather than for an all-fresh core to ensure that the conversion goal of maintaining the existing experimental performance is met. The fuel shuffling schedule of an LEU element that could efficiently and effectively match or exceed the performance of the typical HEU fuel shuffling scheme must be defined.

A depletion capability was developed with both REBUS-MCNP and REBUS-DIF3D. Modeling the complex MURR fuel shuffling sequence for a typical ("pseudo-equilibrium") core requires the evaluation of hundreds of state points. Consequently, iterative design and analysis of the fuel cycle with REBUS-MCNP is intractable. A REBUS-DIF3D model, which is much less computationally expensive, was developed and benchmarked to MCNP and measurements. Afterwards, the MCNP models were updated to include the depleted materials from REBUS-DIF3D to allow evaluations of measured critical states and

demonstrate the overall accuracy of the fuel cycle simulations. Furthermore, the MCNP models of the mixed-burnup core were used to evaluate experimental performance, calculate reactivity parameters, and calculate the detailed power distributions needed for the steady-state thermal-hydraulics analyses.

Models were developed for the 2008 reactor configuration with typical experimental loadings for current HEU operations as well as the proposed LEU fuel design. To properly model the current HEU core fuel utilization, shutdown margin, and experimental performance, it was necessary to develop a computational shuffling technique that would accurately model the actual complex cycle used at MURR. It was also necessary to develop a similar shuffling scheme for the LEU in order to calculate those parameters and demonstrate that the proposed LEU fuel element is an acceptable fuel design.

The simulation of a "pseudo-equilibrium cycle" was performed as follows. Starting with 26 fresh HEU elements, nine "pre-cycle" cores were modeled, totaling 1,794 MWd of operating time, to produce twelve pairs of fuel elements with appropriate power histories ranging from 0 to 139 MWd. Beginning with these 24 elements, an 82-week simulation of reactor operations was modeled with REBUS-DIF3D. For each modeled reactor cycle, the simulated reactor loading follows the typical loading pattern practices for the MURR. Fresh fuel elements are loaded in the 1 and 5 positions about every 4 to 5 weeks, and fuel elements are discharged from the 4 and 8 positions at the same rate, with a target burnup of 150 MWd. The fuel element positions in the MURR core are identified as shown in Figure 2.7. The simulation was conducted for the reactor with current typical reflector and flux trap sample loadings. The control blades were fixed at 23" withdrawn, which is the typical blade position during the bulk of the weekly operating cycle, while the regulating blade was positioned at the core midplane (13.375" withdrawn).

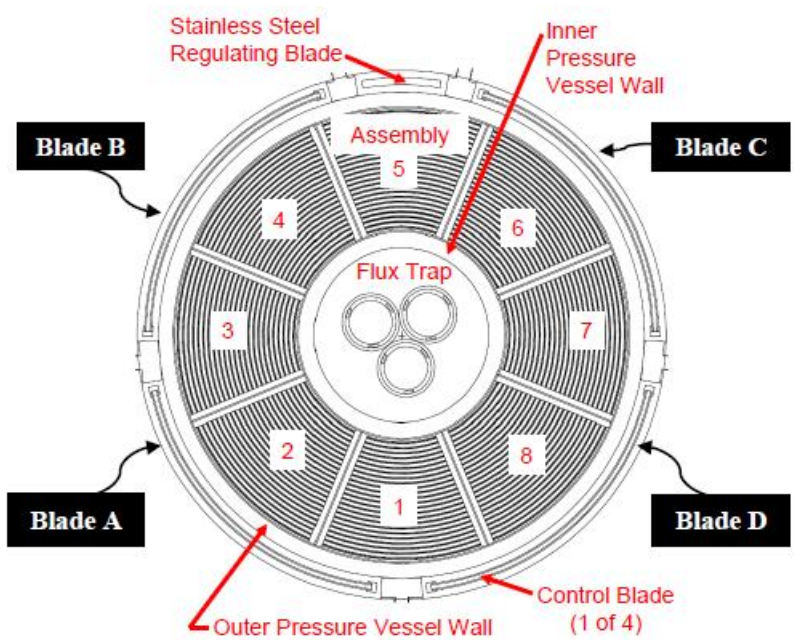

Figure 2.7. MURR Core Layout.

Figure 2.8 shows the core k-effective values at four points during each week of the simulation: day 0 (BOC; xenon free conditions), day 1, day 2 (equilibrium xenon), and 6.3 days (EOC). Results are presented for "transition" and "pseudo-equilibrium" cycles. During the transition cycles, at least two of the elements in the core model started their depletion in a pre-cycle core. Every element of the pseudo-equilibrium cycles was depleted in cores that followed typical shuffling practices. Thus, the pseudo-equilibrium cycles provide the best basis for comparison to current HEU and proposed LEU operations.

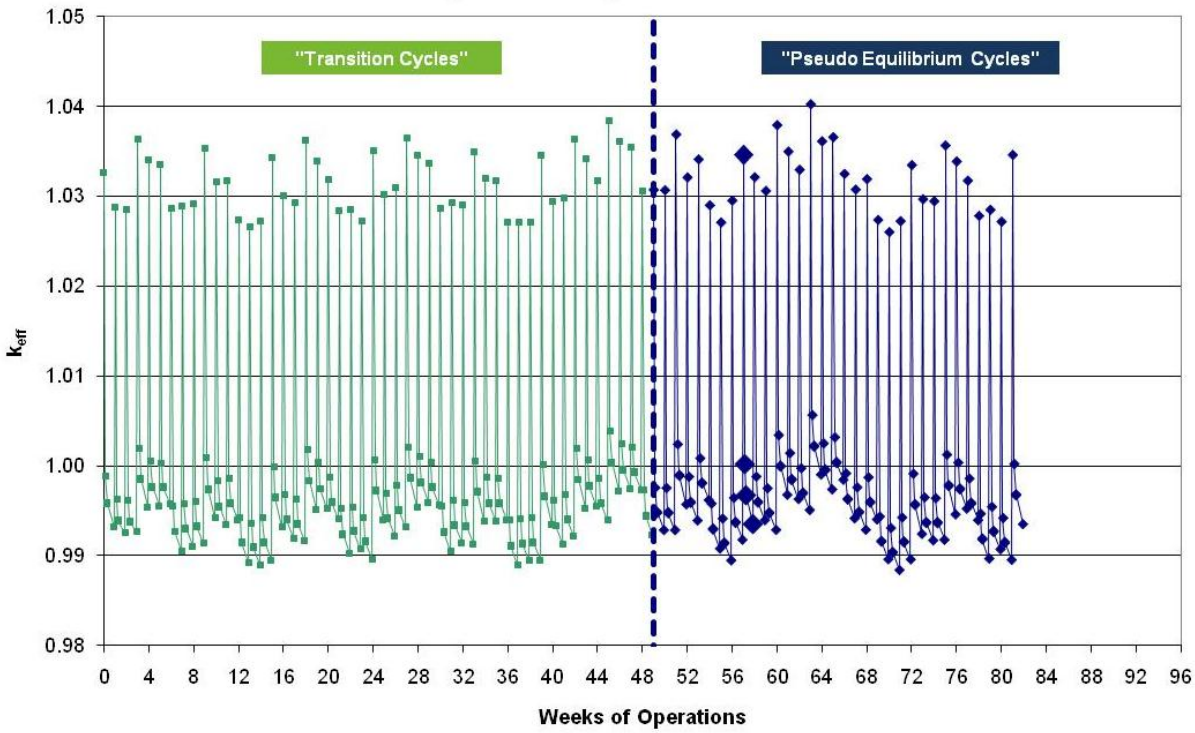

Figure 2.8. Weekly Core k-effective for MURR HEU Fuel Cycle Simulation.

With the shim blades banked at 23" withdrawn, the average core k-effective calculated by the REBUS-DIF3D simulation for the pseudo-equilibrium cycles at the end of the week is 0.99332. The critical blade height at EOC is typically closer to fully withdrawn (26"). Consequently, the REBUS-DIF3D model bias for the HEU pseudo-equilibrium cycle appears similar to the -0.49% Δk/k DIF3D model bias found for the 1971 critical experiments (see Table 2.2).

The average EOC core burnup for the HEU fuel cycle simulation is 640 MWd. Figure 2.9 shows the results of a straight REBUS-DIF3D rundown of HEU and LEU cores (no fuel shuffling), each beginning with all fresh fuel elements and the shim blades fixed at 23" withdrawn. The LEU core is loaded with elements of the design that will be described in Section 3. Assuming the same reactivity bias for the HEU core model will exist for the LEU fueled core, the estimated EOC burnup for the equilibrium LEU core is ~770 MWd. Even though the excess reactivity of the all fresh LEU core is about 1.5% Δk/k lower than for the HEU core, the shallower slope of the reactivity loss with burnup due to the higher total U-235 loading indicates that a higher fuel burnup is possible with the LEU fuel before reactivity limited end-of-life.

For the LEU fuel cycle simulation, 26 fresh elements were depleted in nine pre-cycle cores for a total of 1,982 MWd of operating time to produce twelve pairs of fuel elements with power histories ranging from 0 to 156 MWd. Using these elements as a fuel cycle inventory, a 93-week simulation of reactor operations with LEU fuel was modeled with the REBUS-DIF3D code. The simulation was performed with a core power of 12 MW, as a power uprate from 10 MW to 12 MW is anticipated in order to maintain the experimental performance of the MURR with LEU fuel.

Elements are loaded in the core about 19 times before discharge from the fuel cycle. This is the same number of times the HEU fuel is typically loaded in the MURR before discharge from the fuel cycle. While the core residence time is the same for both the LEU and HEU fuel, the discharge burnup of the LEU elements is 20% greater (about 180 MWd) due to the higher core operating power level.

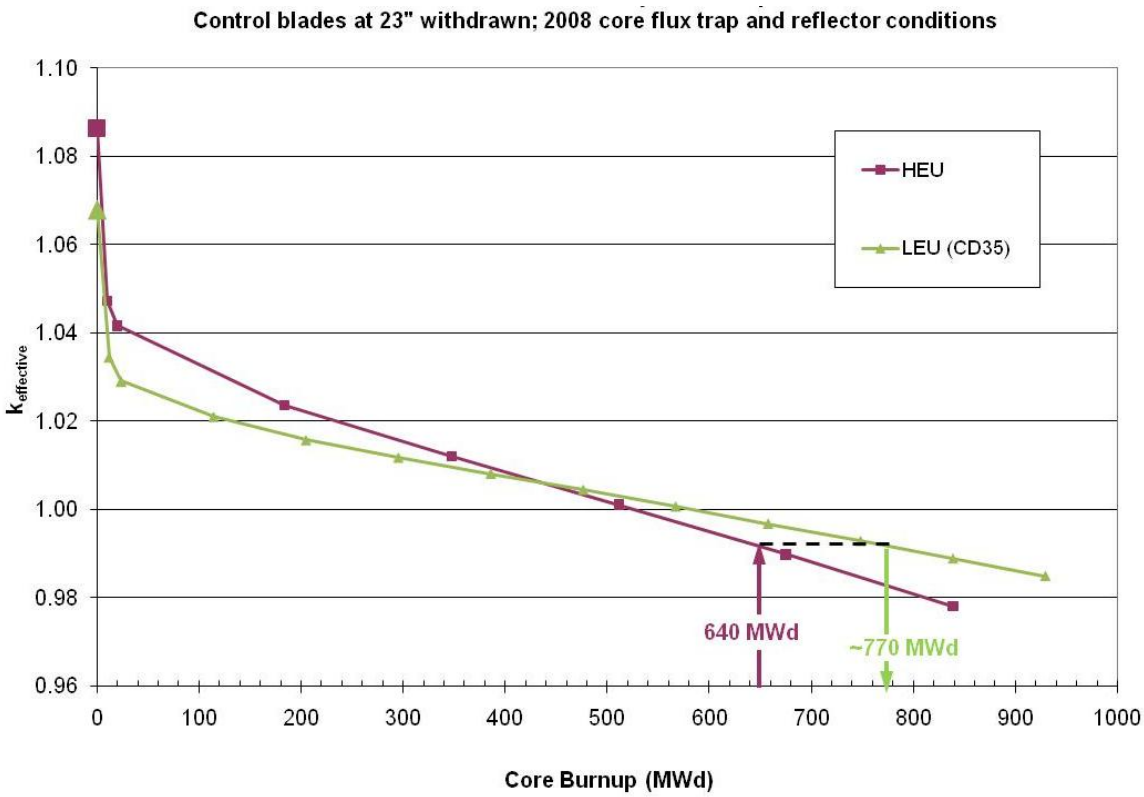

Figure 2.9. MURR Core k_{eff} vs. Burnup – Straight Rundown without Shuffling.

Figure 2.10 shows the weekly LEU core k-effective values during the simulation. As seen in the figure, the average EOC k-effective for the LEU simulation is comparable to that for the HEU fueled core simulation. Assuming the same DIF3D model bias exists for the LEU as for the HEU fueled core, "equilibrium" weekly operations with the assumed shuffling sequence utilizing the LEU fuel design will be achievable.

Lastly, Table 2.5 provides a comparison summary of the pseudo-equilibrium cycle for the HEU fueled MURR and two LEU fuel designs. The FSD results are from the Feasibility Study analysis. The CD35 results are for the proposed fuel element design. Both of the LEU fueled cores have roughly the same EOC k-effective as the HEU equilibrium core. Assuming the same reactivity bias of the DIF3D model for the LEU cores as for the HEU core, it appears that the LEU fuel design(s) will meet the weekly schedule of MURR operations. While the FSD fuel design achieves greater utilization of the fuel (fewer elements/year), the 10 mil minimum nominal clad on the fuel plates in this design would be challenging to reliably manufacture. As such, the CD35 fuel element design with a minimum nominal clad thickness of 12 mil was developed. This proposed LEU design appears suitable for the weekly fuel cycle at MURR, provided that the element can be fabricated and is demonstrated to be hydro-mechanically stable, and the fuel form is qualified. In Section 4 of this report, a more detailed analysis of the neutron physics parameters and core performance for this fuel design will be presented.

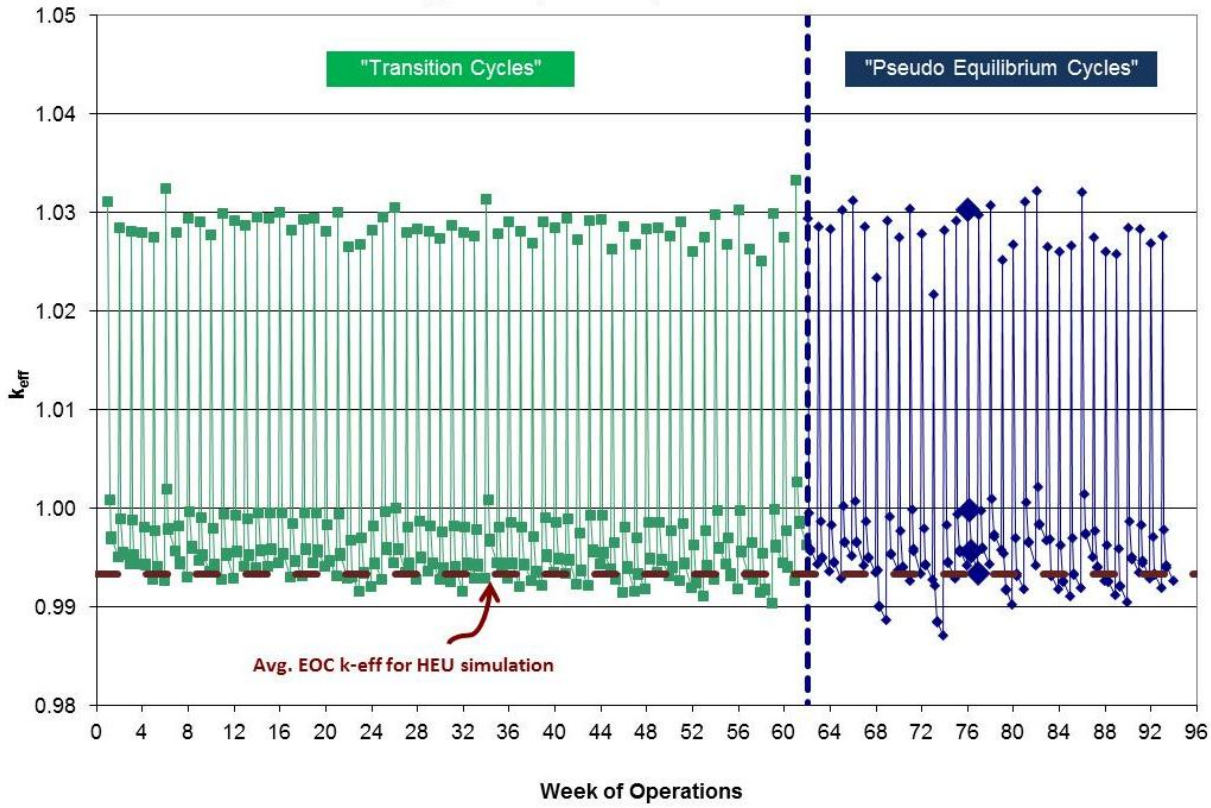

Figure 2.10. Weekly Core k-effective for MURR LEU Fuel Cycle Simulation.

Table 2.5. MURR Fuel Cycle Simulation Results for Pseudo-Equilibrium Cycle.

	HEU	LEU -- FSD	LEU -- CD35
Average BOC Core Burnup for "Pseudo-Eq." Cycles (MWd)	577	814	689
Average EOC Core Burnup for "Pseudo-Eq." Cycles (MWd)	640	890	765
Avg. BOC k-eff	1.03198	1.03087	1.02817
Average ρ swing (Δk/k)	3.77%	3.48%	3.46%
Average EOC k-eff	**0.99332**	**0.99512 (+0.18%)**	**0.99281 (-0.05%)**
Cycles Inserted before EOL	19	22	19
Average Element EOL Burnup (MWd)	149	208	180
Elements/Year	22.1	18.9	21.9

2.2.4 Credibility of the Mixed-Burnup Core Model

The MCNP and DIF3D model verification presented in Section 2.2.1 was for a core loaded with all fresh HEU fuel, and a flux trap and reflector configuration that was in place in 1971. No all-fresh core has been loaded since 1980. The MURR is always operated with a core loading of four pairs of fuel elements, with each pair being at a different burnup level. Furthermore, no measurements for an all-fresh core are available for the 2008 reactor configuration. However, the credibility of the MCNP 2008 core configuration model and the depletion methodology can be demonstrated by evaluating a series of HEU beginning-of-week core critical states and comparing the calculations with the measured data.

Depleted fuel composition data for evaluating the core critical state model in MCNP were derived from the results of the REBUS-DIF3D fuel cycle simulation discussed in the previous section. Table 2.6 provides a comparison of core k-effective calculated by MCNP and DIF3D for fresh and depleted cores. The results show very close agreement between the two codes for predicting the core k-effective, increasing confidence in the DIF3D diffusion theory model which is the basis for determining the depleted core compositions and demonstrating that the composition data can be correctly transferred from one model to the other. Furthermore, the good agreement between MCNP and DIF3D for mixed burnup cores shows that the values of boron loading used to approximate the worth of reflector wedges remain valid with burnup.

Table 2.6. Comparison of MCNP and DIF3D Core k-effective for HEU and LEU Cores.

Fuel	Condition		Blade Position (inches withdrawn)		MCNP k_{eff}	DIF3D k_{eff}	Difference ($\Delta k/k$)
			Shim blade	Regulating blade			
HEU	All Fresh	No Xe	23.0	13.4[1]	1.08360 ± 12 pcm	1.08630	0.23%
HEU	Mixed[2]	No Xe	17.8	10	1.00022 ± 10 pcm	1.00002	-0.02%
HEU	Mixed[2]	Eq Xe	24.0	15	0.99983 ± 10 pcm	1.00019	0.04%
LEU	All Fresh	No Xe	23.0	13.4[1]	1.06689 ± 11 pcm	1.06793	0.09%
LEU	Mixed[3]	No Xe	17.6	10	1.00008 ± 8 pcm	1.00010	0.002%
LEU	Mixed[3]	Eq Xe	24.3	15	1.00001 ± 10 pcm	0.99918	-0.08%

[1] Regulating blade position for all fresh core calculations is at core midplane.
[2] Week 58 of HEU fuel cycle simulation.
[3] Week 76 of LEU (CD35) fuel cycle simulation.

A series of 15 Estimated Critical Position (ECP) calculations were performed to determine whether the overall depletion scheme provides a good estimate of reactor performance. Each case was a measured critical state at hot conditions. Small differences between the nominal water temperatures and measured temperatures were corrected by applying the reactivity coefficients of HEU operations at MURR. The cores analyzed covered a broad range of fuel loadings (e.g., two fresh elements in the core, or none), a variety of flux trap loading states (including an empty flux trap), and notably, a broad range of control blade history states.

Burned fuel material compositions for each element in the critical states were derived from the results of the REBUS-DIF3D fuel cycle simulations. The full set of results for the pseudo-equilibrium cycles were searched to find the closest element average burnup match at a beginning-of-week step. The REBUS-DIF3D materials were tracked as 12 axial regions in each individual plate. That data were mapped to the

24 axial region MCNP model by plate and then converted to MCNP input cards for each plate by an automated procedure.

Table 2.7 summarizes the cases evaluated, including the deviation of MCNP k-effective from 1.0. It is clear that many cases had excellent agreement, but also clear that some cases had a large deviation from critical. The deviations were compared to element burnup, flux trap state, blade insertion, and prior history of the control blades. The only trend discovered was the control blade history.

MURR control blades are shuffled in a multi-year scheme analogous to fuel shuffling. Only the region of the blade tip is expected to deplete. Within the first two days of the one week cycle, the blades move from a typical position of 17 inches withdrawn at the beginning-of-cycle to 23 inches withdrawn after xenon builds in. Thus, the Boral material depletes in the region near the tip, which is in a position of higher neutron fluence.

Figure 2.11 illustrates the clear trend of MCNP deviation from critical vs. the prior history of the control blades. Figure 2.12 shows the trend of control blade withdrawal vs. blade history, which is consistent with Boral depletion in the blade.

Table 2.7. Summary of Critical States Evaluated for Partially Burned Cores.

Date of Core BOC	Fuel Element Burnup (MWd)					Flux Trap Reactivity[1] (%Δk/k)	Average Prior Days for Control Blades	Critical Bank Height[2] (inches withdrawn)	MCNP Deviation from Critical[3] (%Δk/k)
	X1/ X5	X2/ X6	X3/ X7	X4/ X8	Sum				
04/23/05	32	92	73	95	584	0.478	271	17.97	-0.263%
05/02/05	38	140	44	73	590	0.474	280	18.02	-0.228%
05/09/05	0	117	63	115	590	0.427	287	17.63	-0.260%
05/16/05	17	137	52	82	576	0.432	294	17.93	-0.270%
05/30/05	9	139	21	124	586	0.474	308	18.06	-0.144%
07/11/05	29	136	40	84	578	0.464	350	17.98	-0.257%
06/16/00	54	72	41	143	620	0.346	1040	17.22	-1.301%
08/07/00	16	98	68	117	598	0.384	1092	17.02	-1.198%
11/15/00	0	139	56	108	606	0.359	1192	16.72	-1.307%
12/17/01	22	124	69	91	612	0.348	1709	16.64	-1.743%
12/31/01	14	131	72	87	608	0.340	1723	16.66	-1.705%
04/22/02	0	118	64	114	592	0.418	1835	16.00	-1.735%
08/08/05	0	143	38	115	592	0	378	18.52	-0.087%
09/04/00	24	90	50	141	610	0	1120	17.81	-1.074%
02/04/02	11	136	61	96	608	0	1758	17.03	-1.630%

[1] The flux trap reactivity indicates the worth of the flux trap contents relative to an empty flux trap.
[2] Critical bank heights reported here are corrected for small differences between the nominal water temperatures modeled and those measured at the critical state.
[3] MCNP deviation from critical is (k-1)/k, corrected for the difference between flux trap worth of the critical state and flux trap worth modeled with the nominal sample loading (for cases with nonzero flux trap worth).

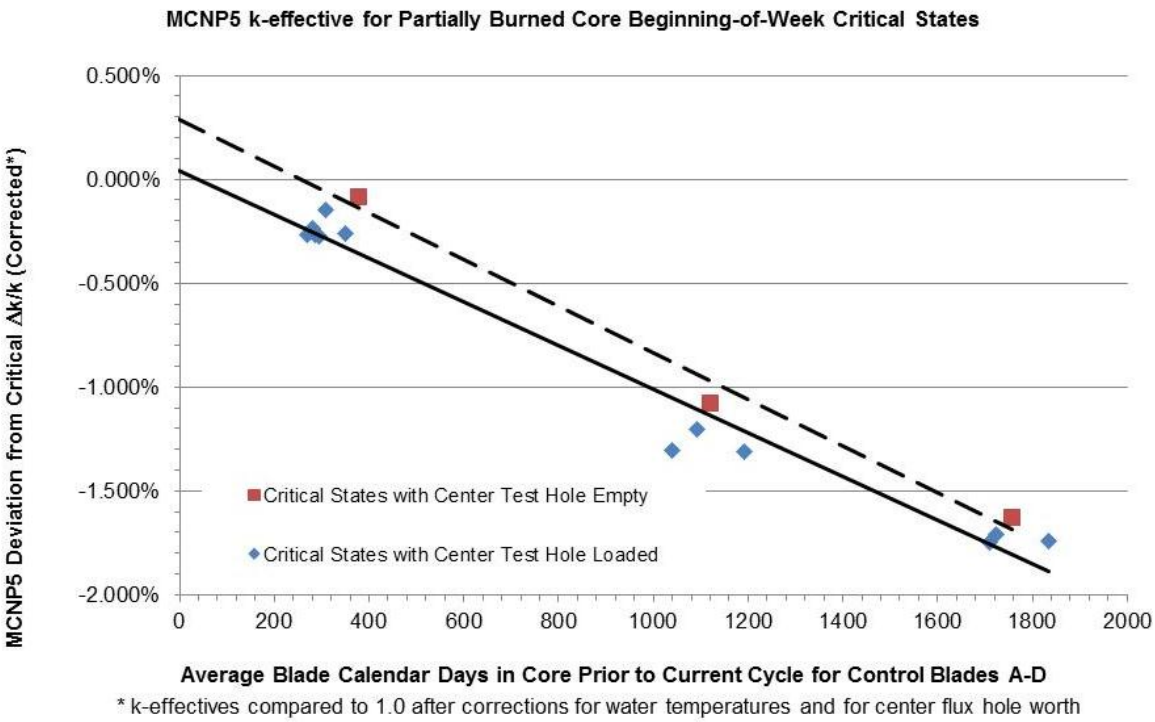

Figure 2.11. ECP Deviation from Critical vs. Blade History.

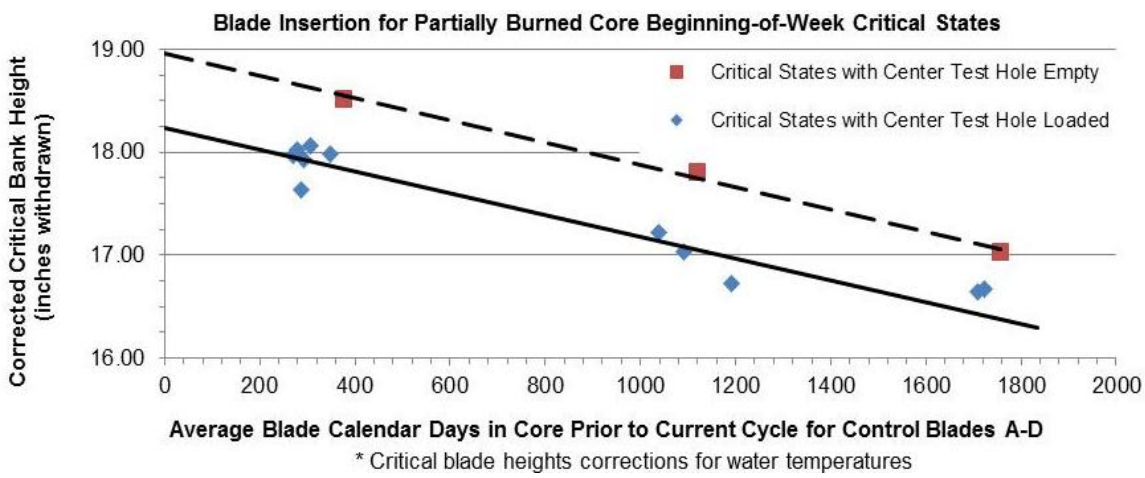

Figure 2.12. Critical Withdrawl of Shim Blades vs. Blade History.

The MURR calculations in Table 2.7 were based on fresh control blade compositions in the MCNP model. Seven of the 15 ECP cases had little prior use of the control blades: 271-378 average calendar days of prior use. The RMS bias for those seven cases was 0.226% Δk/k. Furthermore, the trend lines drawn in Figure 2.11 indicate that if fresh shim blades were in the MURR, the agreement of the MCNP model with measured criticals for mixed-burnup cores would be quite good.

For the cases in Table 2.7, the average residence time of the shim blades in the reactor ranges from ~1 to 5 years. Recently, a study was completed to assess the depletion of the poison material in the shim blades as a function of days of prior blade use and axial position in the blade [13]. Blades are typically resident for about 2 to 8 years, and average about 4 years, before being retired. During this time, the B-10 in the bottom few inches of the control blades is observed to deplete significantly, as this portion of the blade

always resides in the range of the active core height. The results of control blade modeling are summarized in Figure 2.13, which shows the axial distribution of the B-10 in the control blade meat for blades with different residence times. As can be seen from the figure, at the end of blade life, the bottom four inches of the blade has been almost depleted of any poison material.

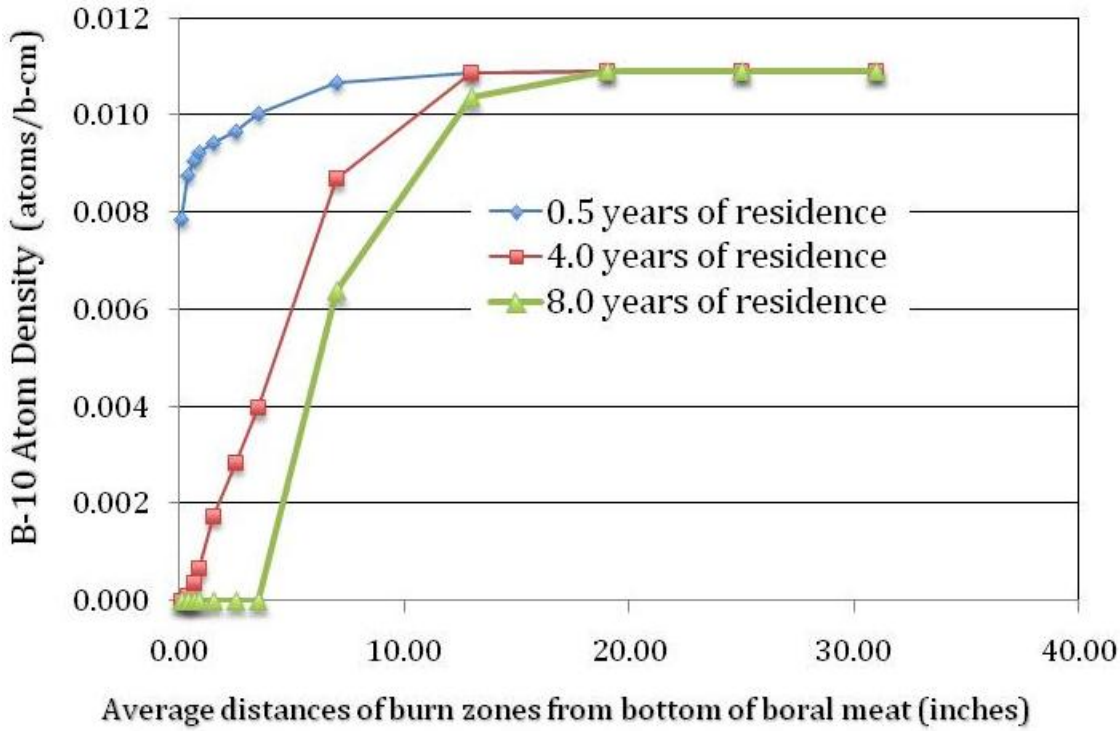

Figure 2.13. Effect of Residence Time on B-10 Atom Density in MURR Control Blades.

Data presented in Table 2.7 above show the deviation (%Δk/k) of the core k_{eff} from critical for ECPs for various blade histories when the blades are modeled at their fresh composition. Table 2.8 below compares results for selected cases from Table 2.7 with fresh blades and with the blade burnup modeled. When all-fresh control blades are used in the MCNP simulation (the column labeled "No Control Blade Burnup"), cores with the combination of blades that have the greatest total burnup, and correspondingly the lowest measured critical blade heights, have the greatest deviation from critical at the ECP. However, when the blades are modeled with the depleted blade compositions (the column labeled "Control Blade Burnup"), the deviation from critical at the ECP is smaller. For the case with the maximum control blade history, the deviation from critical is reduced from 1.735% to 0.422%.

Figure 2.14 shows plots of the deviation of the core k_{eff} from critical at the ECPs when the blades are modeled as fresh and with their burnup history. The result of adding the modeled depleted blades to the existing HEU MURR core model shows a significant improvement; the average deviation from critical is -0.41% Δk/k when the blade depletion is modeled, compared with -1.08% Δk/k if the blades are modeled as fresh. There is still a small negative bias in the ECPs versus blade burnup when using the modeled depleted blade in the MCNP model. The bias is seen as the slight negative slope in the trend line fitting the solid red squares in Figure 2.14, and could be due to under-depleting the boron-10 in some of the larger axial zones above the blade tip where smaller divisions could have been more appropriate. Another

Table 2.8. %Δk/k Deviation for Estimated Critical Positions for Fresh Blades and Depleted Blades for Partially Burned Cores.

Date of Core BOC	Average Prior Days for Control Blades	Critical Banked Height (inches)	No Control Blade Burnup (%Δk/k)	Control Blade Burnup (%Δk/k)
05/09/2005	287	17.63	-0.260	-0.232
05/30/2005	308	18.06	-0.144	-0.139
06/16/2000	1040	17.22	-1.301	-0.730
11/15/2000	1192	16.72	-1.307	-0.532
12/17/2001	1709	16.64	-1.743	-0.390
04/22/2002	1835	16.00	-1.735	-0.422

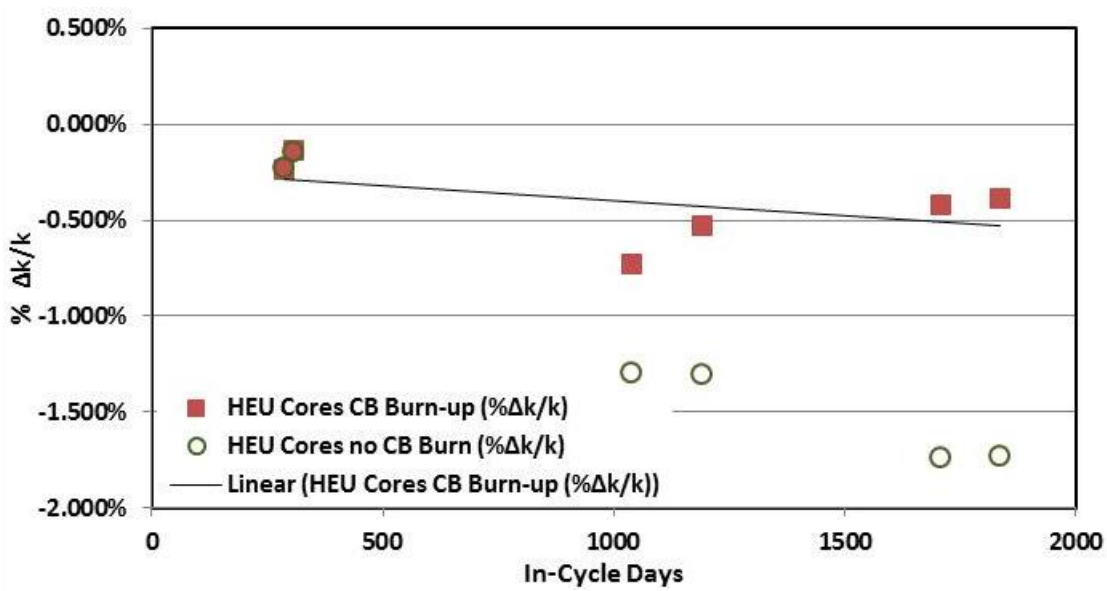

Figure 2.14. ECP Deviation From Critical With ("CB Burnup") and Without ("no CB Burn") Modeled Control Blade History.

contributor to this negative bias could be the MCNP models for the partially burned fuel assemblies in the weekly start-up cores.

Lastly, while the fuel cycle simulations for the HEU and LEU fueled cores were performed with a set of four fresh shim blade compositions, the blades are parked near the top of the active core height (23" withdrawn) where they reside during the bulk of the weekly operating cycle. In this position, the blades have a reduced impact on the axial power profile and the fuel depletion. When calculating the detailed power distributions (Section 4 of this report) that will be used for steady-state thermal-hydraulic safety analyses, the effect of shim blade depletion and mismatch of the shim blade heights relative to one another will be evaluated.

2.2.5 Azimuthal Discretization of Fuel Plates for Detailed Power Distribution Analysis

Thermal-hydraulic safety calculations will be performed utilizing detailed power distribution data calculated by MCNP. The power distribution in the MURR varies most significantly in the axial and radial (plate-by-plate) directions. The power distribution also varies in the azimuthal direction along the width of the fuel plates in the MURR elements, and can peak sharply at the edge of the fuelled section of the plate due to an increase in the local water-to-fuel ratio near the edge of the fuel meat. The azimuthal power peaking is evaluated from MCNP calculations by azimuthally subdividing the tally zones of the fission reaction tallies in the fuel meat. In the Feasibility Study, tally zones were created by subdividing the fuel meat in each plate into 9 "stripes," with each stripe covering the same angular span of 5 degrees, as shown in Figure 2.15.

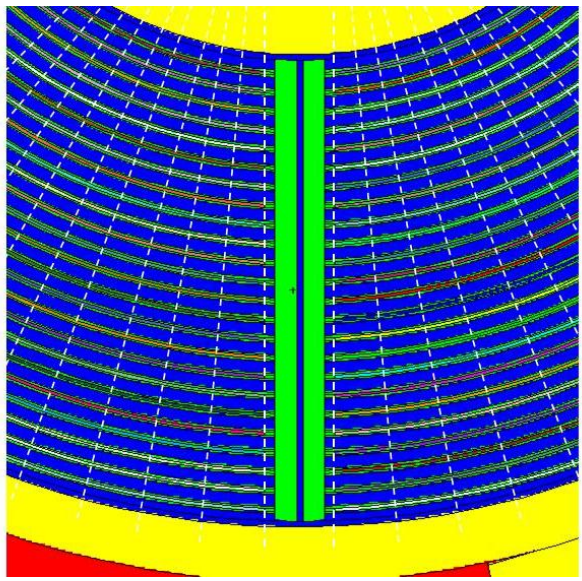

Figure 2.15. Azimuthal Striping Detail with Equal-Angle Stripes at Edge of Fuel Meat.
Note that for the wider plates, the width of the tally stripe increases.

The total width (arc length) of the fuel foils increases by a factor of 2.4 from the innermost to the outermost plates. Consequently, when the tally stripes in the MCNP model cover an "equal angle" of the fuel meat width, the width of the stripe along the edge of the fuel meat over which the power distribution is tallied increases by a similar factor of 2.4. As the size of the tally zone increases, the azimuthal peaking factor on the power distribution will be underpredicted for the outermost plates relative to the innermost plates of the element.

This can be seen in Figure 2.16, which provides the azimuthal peaking factor in each plate of an LEU-FSD element in a representative core. For each plate, the azimuthal peaking factor is the axially-averaged power density of the stripe with the highest power density divided by the average power density in the plate. The "hot stripe" is always along the edge of the fuel meat near the element side plate. The azimuthal peaking factor is generally lower for the innermost and outermost plates because the neutron spectrum is naturally more thermalized near the flux trap and beryllium reflector, so that the effect of higher water-to-fuel ratio near the edge of the plate is less pronounced. For the plates in the interior of the element, the spectrum is harder, so the effect of larger relative amounts of water near the edge of the fuel meat is more pronounced.

When the tally stripes along the edge of the fuel meat cover the same angle for all plates, as in the curve labeled "9 Stripes, 5 degrees," the azimuthal peaking factor is highest for plate 6. This plate has a total meat width of 5.60 cm, and an edge-stripe width of 6.23 mm, which is one-ninth of the total meat width. For the wider plates toward the outer portion of the element, the tally stripe becomes longer in dimension when the meat width is subdivided by equal-sized angle. For example, plate 20 has an edge stripe dimension of 10.26 mm. The wider the tally zone, the less pronounced the calculated azimuthal peaking.

In the present work, the azimuthal striping detail for the power distribution tallies was altered so that the first three tally stripes along the edge of the fuel meat all had the same arc length for all fuel plates. The remainder of the fuel meat was divided into three "equal-angle" stripes. The use of equal-angle striping for tallies in the center of the fuel foil in the azimuthal direction is satisfactory because the power profile is relatively flat in this region of the fuel meat.

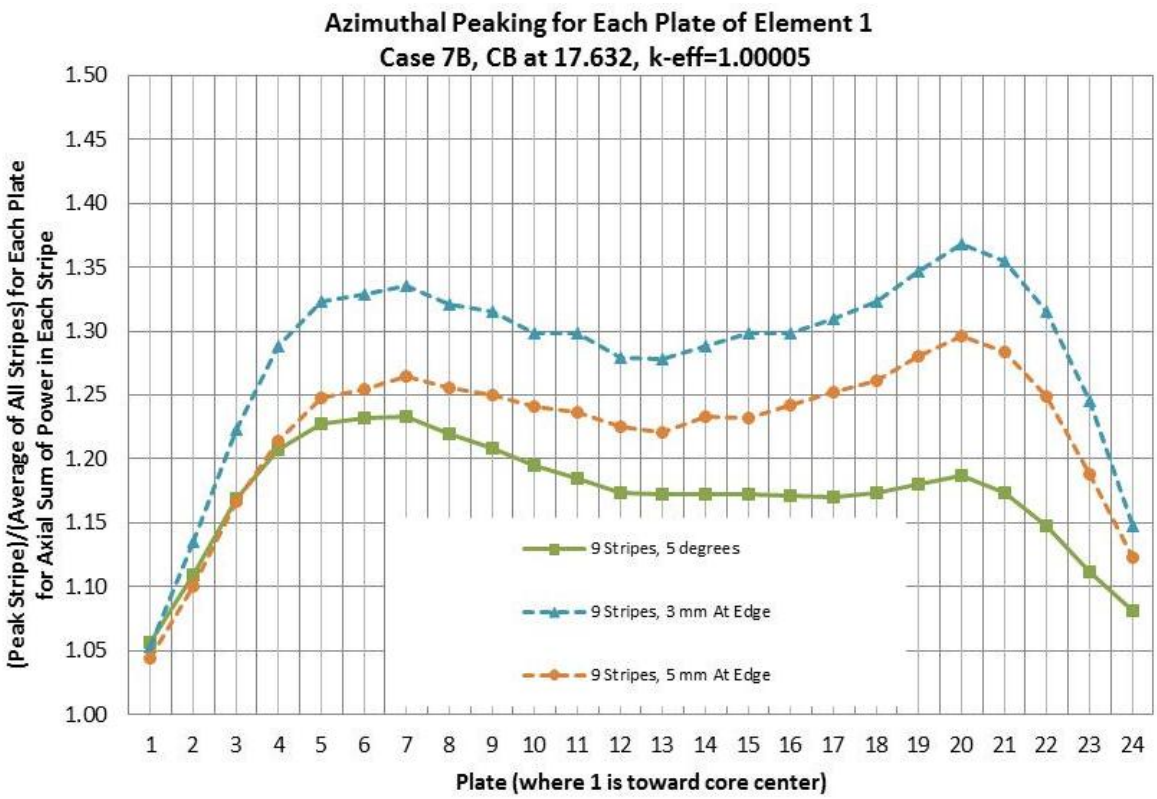

Figure 2.16. Azimuthal Peaking Factor For Representative Core Loaded with LEU-FSD.

When the tally zone along the edge of the fuel meat is set by "equal width," the calculated azimuthal peaking for the wider interior plates is greater, as can be seen in Figure 2.15. So, for example, the case with a 5 mm tally stripe along the edge of the fuel meat for all plates shows that the highest azimuthal peaking occurs in plate 20. If the tally stripe at the edge of the fuel meat is reduced to 3 mm, the calculated azimuthal peaking factor increases further.

The results in Figure 2.16 show that the azimuthal peaking factor is sensitive to the dimension of the tally stripe. Therefore, the proper size of the stripe must be determined to ensure that azimuthal peaking factors used by the PLTEMP code [14] are appropriately calculated for the MURR. The critical parameter for the PLTEMP calculation is the predicted convective heat flux from the plate into the coolant channel. Therefore, the azimuthal mesh intervals at the outer edges of the fuel meat in the MCNP calculation need to be sized to account for the azimuthal conduction of heat at the edge of the fuel.

The fuel plates proposed for the conversion to LEU fuel consists of a fuel foil, a thin layer of zirconium on each face of the foil, and a layer of aluminum clad covering the two exterior faces of the zirconium. Furthermore, the fuel plates are supported by a side plate made of aluminum. Although the MURR plates are very thin, the zirconium and aluminum cladding and the fuel have very good thermal conductivities. Significant temperature gradients in the azimuthal direction could lead to a convective heat flux distribution that is significantly different from the power distribution. To determine the impact of lateral conduction in the azimuthal and axial directions on the azimuthal distribution of the convective heat flux, 3-D CFD [15] simulations, which account for conduction (solids and fluid) and convection, were performed at steady state conditions of the MURR [16]. The analysis was performed for a hot channel in the FSD fuel element design. Since the CD35 plates have a thicker aluminum clad, the heat conduction, which reduces the convective heat flux into the water channel, will be greater than for the FSD. Thus, the results obtained in Reference 16 will be conservative for the CD35 design.

Figure 2.17 illustrates the hot channel analyzed in the CFD simulation. The component labeled "stiffener" in the figure is the side plate. CFD simulations were performed where: (1) the one mil (0.001 inch) zirconium layer between the fuel foil and the aluminum cladding was treated as aluminum (total cladding (Zr + Al) thickness of ten mil); (2) the cladding was split into two layers, 1.25 mil of zirconium, and 8.75 mil of aluminum; and (3) same as case (2) with a water gap of 0.5 mil between the plate and the stiffener. The last case is a conservative simulation of an imperfect contact between the fuel plate and the side plate.

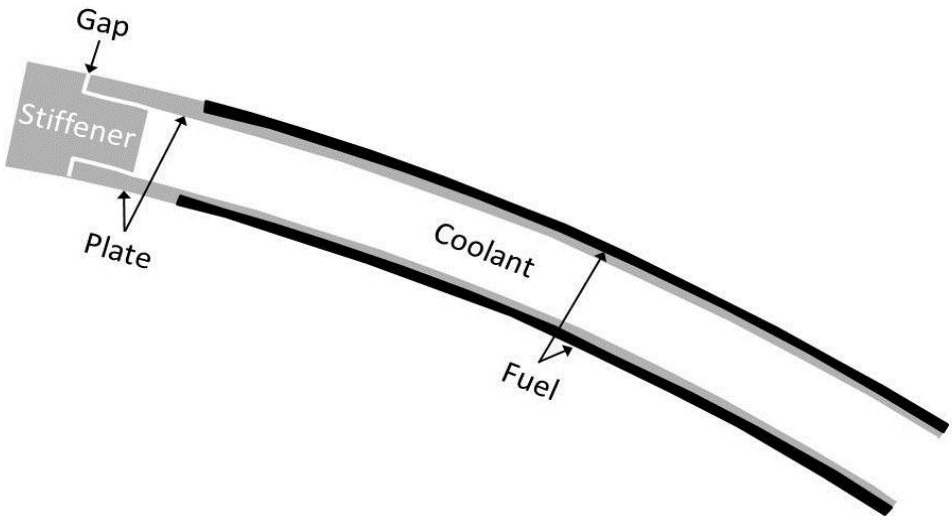

Figure 2.17. Simulated Geometry in CFD Analysis of MURR Hot Channel.

Axial and azimuthal power distributions by plate in the FSD element were calculated using MCNP. The total heat flux, i.e. power distribution, data from the MCNP calculation were fit to the axial and azimuthal dimensions and provided as a correlation to the CFD analysis.

Figure 2.18 shows the azimuthal heat flux distribution computed by the CFD analysis for the three cases analyzed at the axial position in the channel where the power density peaks (23.6 cm from the bottom of the fuel meat). The effect of azimuthal conduction on the convective heat flux is insignificant at distances greater than 5.0 mm from the edge of the fuel meat. However, the convective heat flux peaks at about 3.0 mm from the edge of the fuel meat and drops sharply towards the edge of the meat (moving towards the side plate). The effect of the zirconium layer (between the fuel foil and the aluminum cladding) and that of the water gap (between the plates and the side plate) on the azimuthal distribution of the convective

heat flux are also insignificant. From this analysis, it is concluded that the representation of the fuel meat at the edge of the fuel plate by a 5 mm stripe at the average power density in the stripe would give a conservative estimate of the convective heat flux into the water channel. Thus, azimuthal tally stripes of 5 mm along the edge of the fuel meat for all fuel plates will be used for obtaining the power distribution results from MCNP.

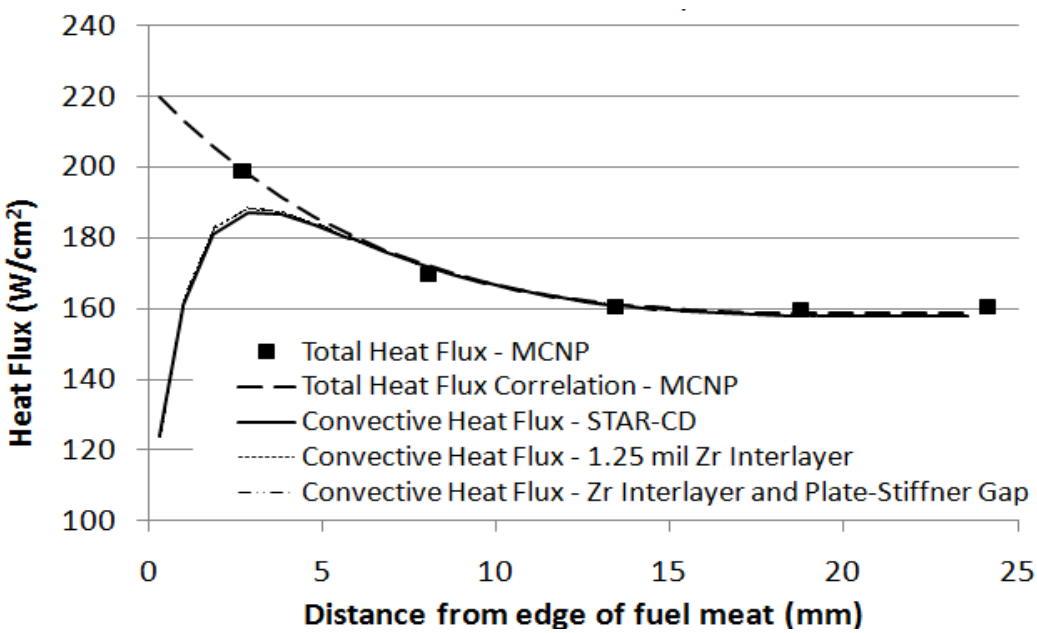

Figure 2.18. Azimuthal Heat Flux Distribution for MURR Hot Channel.

3.0 DEVELOPMENT OF LEU FUEL ELEMENT DESIGN

An extensive study was completed in 2009 to assess the feasibility of safely replacing the HEU fuel in MURR with an LEU fuel element design under a set of manufacturing assumptions. [1] A fuel element design was developed and the study concluded that conversion of the fuel with that element design would meet the goals of reactor safety, provide adequate shutdown margin, and maintain the operations and experimental performance of the MURR.

One of the manufacturing assumptions applied in the development of the "FSD" (Feasibility Study Design) fuel element design was that the fuel plates could be reliably manufactured with a nominal clad thickness as thin as 10 mil. Subsequent experiments and feedback from the Fuel Development (FD) and Fuel Fabrication Capability (FFC) pillars of the GTRI RERTR program was that the minimum nominal clad in the fuel plates would need to be increased to 12 mil in order to have a reliable manufacturing process.

The Reactor Conversion (RC) program has responded by developing a new LEU fuel element design that meets this constraint. Several contingency designs were explored, followed by optimization of a design that meets the conversion goals. The newly designed fuel element that is now proposed has been labeled "CD35," and is constructed with 23 fuel plates (instead of 24 plates as in the FSD and HEU elements). The element still uses graded foil thicknesses to flatten the radial heat flux profile, but the thinnest nominal clad is 12 mil (versus 10 mil in the FSD) and the thinnest total plate thickness is 44 mil (versus 38 mil in the FSD).

In the following sections, the basic neutron physics effects that drove the LEU design process are first discussed. Following that, the specific details of the evolution of the LEU element design that led to the CD35 design will be elaborated.

3.1 Preliminary Studies in LEU Fuel Element Design

Scoping studies were completed in 2006 and 2007 to understand the impact of LEU element design features that affected parameters such as excess reactivity (which affects the length of the weekly operations cycle) and fuel lifetime (which impacts fuel costs and on-site fuel storage requirements). Further studies were conducted to evaluate the power density and heat flux profiles in the element, and design features that would optimize the detailed power distributions to maintain safety margins. The conclusion was to fabricate an element with graded fuel foils in the plates, where thinner meat thicknesses were employed near the center flux trap and beryllium reflector to flatten the heat flux profile.

The non-uniform meat, clad, and plate thicknesses of the LEU fuel element are an essential feature of the element design. Initial scoping studies with MCNP concluded that a design with 24 uniform LEU fuel plates with the same dimensions as the HEU fuel could provide sufficient, albeit lower, excess reactivity for a core operating at 10 MW. However, such a design would not satisfy power peaking limits since the harder neutron spectrum within the LEU core increases the propensity for peaking at the edges of the core in the vicinity of the flux trap and the reflector. The high power peaking would reduce the allowable power level at LSSS conditions. Further studies confirmed the need to increase the water-to-metal ratio in order to gain excess reactivity and the need to make the fuel foils with the highest power peaking factors thin to reduce the heat flux peaking factors and limit the number of fuel elements in the fuel cycle.

The preferred approach to increase the water-to-metal ratio in the LEU element selected in the Feasibility Study was to make the fuel plates thinner than the uniform 50 mil plates in the HEU element. Furthermore, the fuel foil thicknesses were varied by plate to reduce the heat flux peaking factors. The anticipated high peak fuel burnup limit for the U-10Mo fuel means that higher power peaking factors

could be managed without needing to decrease the ^{235}U loading density to avoid limiting fuel element lifetime. However, to avoid limiting the safe operating power level due to heat flux peaking, the thickness of the meat in plates 1, 2, and 24 was reduced to lower their hot stripe heat flux. Using this approach, the proposed element design consisted of fuel meat thicknesses that vary by a factor of two. Additionally, the reduction of the heat flux peaking factors allows for the power uprate from 10 to 12 MW that is necessary to maintain current experimental performance and materials irradiation capabilities.

3.2 LEU Fuel Element Design Optimization

The element design developed during the Feasibilty Study was able to satisfy the converion goals of 1) reactor safety, 2) adequate shutdown margin, and 3) maintaining the operations and experimental performance of MURR. One of the key features contributing to the success of the element design was increasing the water-to-metal ratio, which was accomplished by reducing the thickness of all the fuel plates so that less water was displaced. This enabled the coolant channels between adjacent fuel plates to increase in thickness from 80 mil for the HEU element to 92 mil for the FSD.

To increase the minimum nominal clad thickness from 10 to 12 mil, one could envision simply keeping the foils the same thickness as in the FSD and putting thicker clad on the fuel plates. This, however, would reduce the water-to-fuel ratio by displacing moderator, and reduce the fuel reactivity. This can be seen in Figure 3.1, which shows the results of a straight rundown of a core initially loaded with 8 fresh elements for the FSD and for a non-optimized variation in which the clad was simply made thicker to satisfy the constraint of a minimum nominal clad of 12 mil. The core reactivity decreases by about 1% $\Delta k/k$ from this design change. Consequently, the total core burnup at reactivity limited EOC would be roughly 200 MWd lower than for the FSD, decreasing the fuel discharge burnup and increasing the number of elements needed per year.

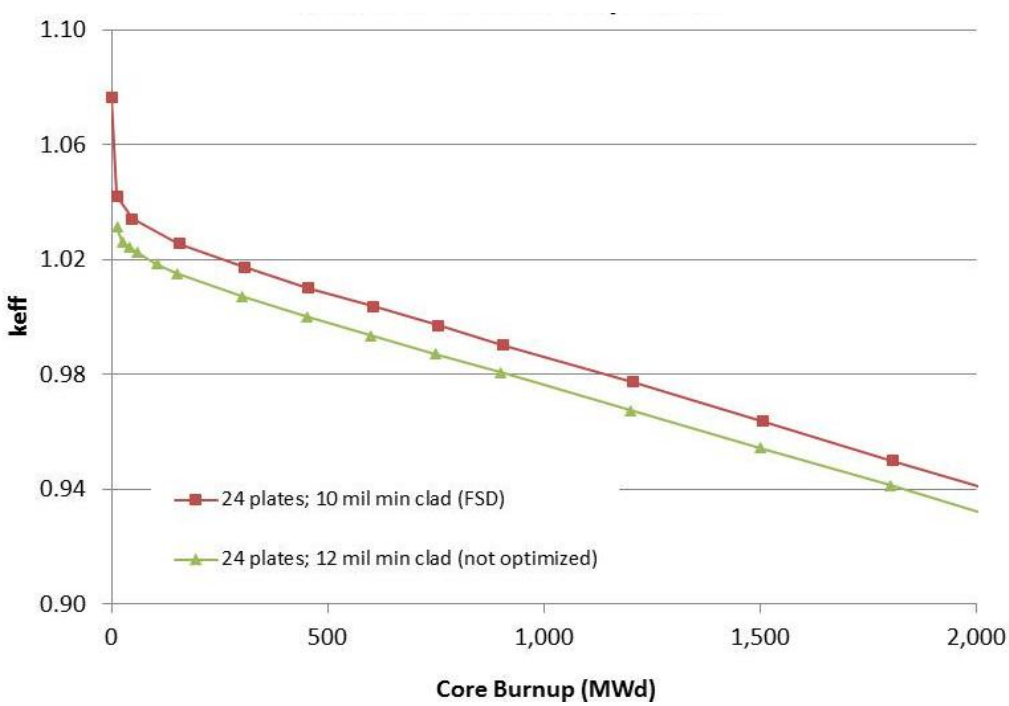

Figure 3.1. Comparison of Core k_{eff} vs. Burnup for FSD and Non-Optimized Element.

A series of scoping cases were evaluated to optimize the LEU fuel element design with the constraint of a minimum nominal clad of 12 mil. In addition to reactivity effects, which affects the weekly cycle length

and/or the consumption rate of fuel elements in the MURR fuel cycle, any design modification also potentially affects the core power distribution. This is highly important, as the steady-state thermal-hydraulic safety analyses are required to show sufficient margins to the onset of flow instability (OFI) and critical heat flux (CHF) at the reactor's Limiting Safety System Sessing (LSSS) conditions. These margins are generally influenced by the axially-averaged hot-stripe heat flux in the core (which affects flow instability) and the local peak heat flux (which affects CHF). Changing the thickness of the coolant channels can also have an impact on the safety margins, but the effect on the safety margins due solely to a change in the channel thickness is less than any resulting change in the heat flux.

Only a few LEU element designs with 24 fuel plates and thinnest nominal clad of 12 mil were evaluated. In order to regain the core excess reactivity that is lost when the water is displaced by the thicker clad, fuel must be added to the plates in the high-importance regions next to the flux trap and reflector. This penalizes the design by increasing the power peaking. Consequently, most of the effort was placed on reducing the number of plates to maintain the water-to-fuel ratio and on flattening the power distribution.

Results for a number of 23-plate designs that were evaluated in the design optimization study are presented in Table 3.1. The HEU and FSD results are shown for comparison purposes. The cases beneath the FSD results are generally sorted by decreasing hot-stripe heat flux, because preliminary calculations had shown that the margin to OFI would likely be the most limiting for the MURR steady-state safety basis. The data parameters summarized in the table are as follows:

- Fuel design identifier.
- Number of plates.
- Thinnest nominal clad. The constraint for the LEU fuel element design with U-10Mo foils is 12 mil.
- Thickness of the thinnest fuel plate in the element. Fuel plate thickness affects the hydro-mechanical stability of the plate.
- Coolant channel thicknesses for the outer channels of the element (i.e., channel between plate 1 and inner pressure vessel, and between outermost plate and outer pressure vessel) and for the interior channels (i.e., between fuel plates). For a few designs that were evaluated, the water channels were non-uniform to place more coolant near plates that have greater power peaking.
- Meat thickness for plates 1, 2, 3, and the last plate (i.e., plate 23 or 24). The heat flux peaking generally occurs in one of these plates in the LEU fuel elements.
- Total loading of U-235 in the fresh element.
- Reactivity data. First is the k-effective of a core loaded with 8 fresh elements of the fuel design and the shim blades at 23"; the reflector and flux trap were loaded with typical samples for MURR. Second is the difference in fresh core k-eff relative to the FSD.
- Peak hot-stripe and local heat flux data are provided for two core states. The hot-stripe heat flux is the largest axially-averaged heat flux, taking into account the azimuthal (edge effects) and radial (plate-by-plate) power distribution. Also indicated is the plate for which the heat flux is greatest. It is assumed that half of the power of each fuel plate exits each of its two faces. Figure 3.2 plots the hot-stripe heat flux by plate in a fresh core loaded with each of the 23-plate designs.

  The two core states are a) an all-fresh core loaded with typical samples and the blades at critical, and b) a mixed burnup core with no samples or holder in the flux trap; this core state was the limiting case for OFI in the FSD. The all fresh core state was evaluated for all designs, and serves as the starting point for evaluation. If a design was considered a good candidate for further analysis, the fuel cycle simulation was performed in REBUS-DIF3D to develop the mixed burnup core compositions.

In order to give the reader an appreciation for the tradeoffs associated with the LEU element optimization, summary notes describing the alterations and impacts on performance are provided below.

Table 3.1. Design Parameters for LEU Fuel Element Optimization Study.

Fuel Design	# Plates	Thinnest Nominal Clad (mil)	Thinnest Plate (mil)	Coolant Channel Thickness (mil)		Meat Thickness (mil) Plates 1-2-3-Last	^{235}U mass (g)	Reactivity		Heat Flux (W/cm^2)			
										All Fresh Core, Typical Samples in FT		Mixed Core, No Samples in FT	
				Outer	Interior			k_{eff} with blades at 23"	Diff. from FSD (Δk/k)	Peak HSHF[1] (Plate)	Peak HF[2] (Plate)	Peak HSHF[1] (Plate)	Peak HF[2] (Plate)
HEU	24	15	50	110[3] 90[4]	80	20-20-20-20	775	1.08326		126.8 (1)	181.4 (1)	137.0 (1)	188.8 (1)
FSD	24	10	38	95	92	9-12-18-17	1439	1.07636		137.4 (3)	219.2 (24)	141.5 (3)	213.5 (24)
CD1	23	12	44	98	92	7-9-12-14	1447	1.05903	-1.52%	110.5 (5)	197.4 (23)		
CD19	23	12	44	86	93	11-15-20-17	1527	1.07215	-0.36%	138.5 (3)	217.5 (23)	142.3 (3)	209.0 (23)
CD21	23	12	44	86	93	10-14-19-17	1521	1.07119	-0.45%	134.3 (3)	218.2 (23)		
CD32	23	12	44	99.5	92	9-13-17-17	1511	1.06629	-0.88%	127.0 (3)	219.6 (23)		
CD33	23	12	44	95.5	93-92-93[5]	9-13-17-17	1511	1.06733	-0.79%	127.0 (3)	220.0 (23)		
CD35	**23**	**12**	**44**	**95.5**	**93-92-93[5]**	**9-12-16-17**	**1507**	**1.06703**	**-0.81%**	**125.3 (4)**	**222.2 (23)**	**133.1 (23)**	**208.9 (23)**

[1] Axially-averaged hot-stripe heat flux.
[2] Peak of 3-D heat flux calculated by MCNP tallies.
[3] Channel 1 between inner pressure vessel and plate 1 for HEU element is 110 mil.
[4] Channel 25 between plate 24 and outer pressure vessel for HEU element is 90 mil.
[5] See Figure 3.2 for location of 93 and 92 mil coolant channels.

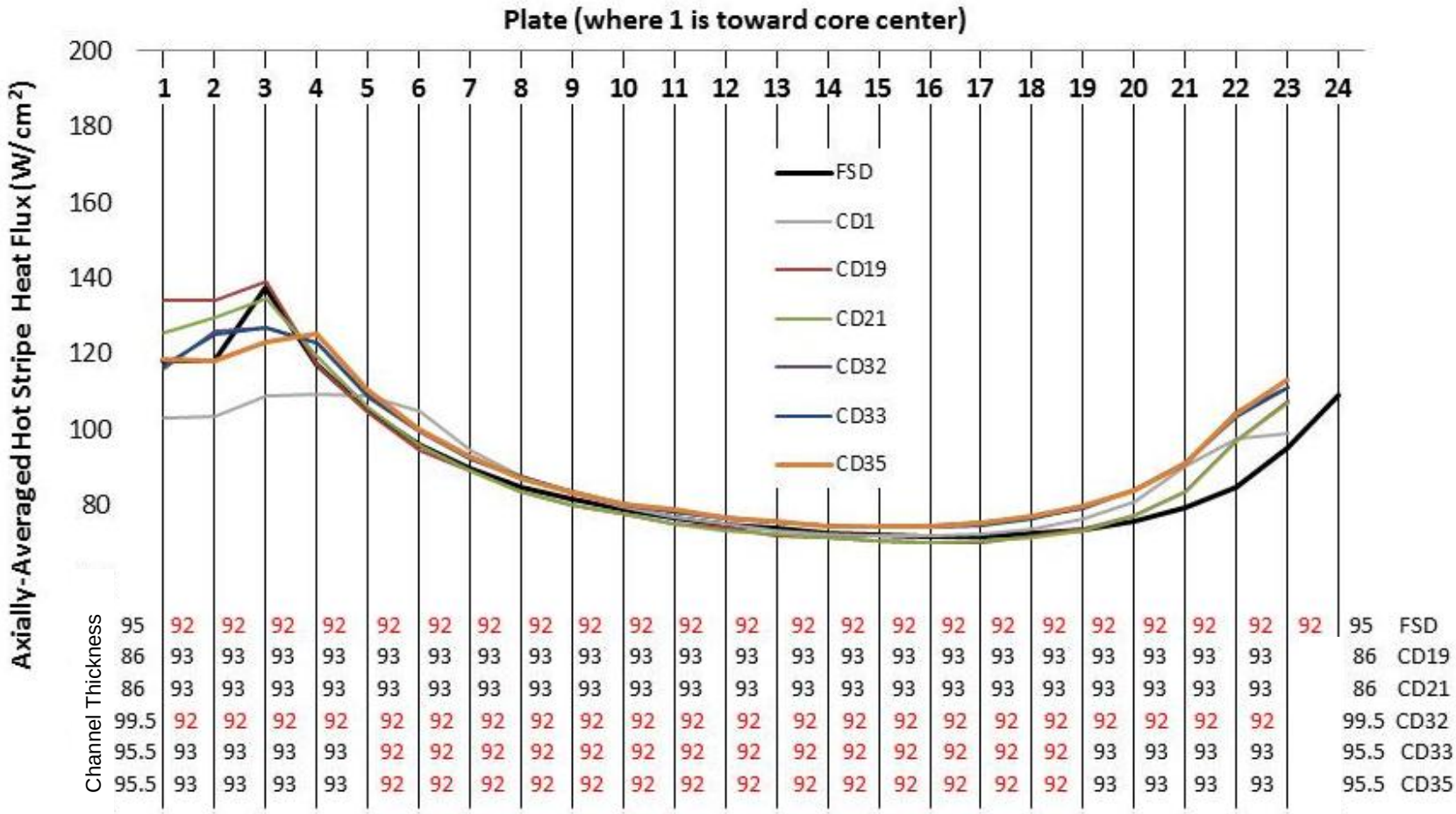

Figure 3.2. Hot-Stripe Heat Flux by Plate for Candidate LEU Element Designs in All Fresh Core.

CD1. The first 23-plate contingency design considered has the lowest hot-stripe and peak heat flux (110.5 and 197.4 W/cm^2, respectively). This design would likely have a greater margin to OFI and CHF than the other element designs, but there is a significant excess reactivity penalty relative to the FSD (-1.52% Δk/k). This would increase the number of elements needed per year. By a very rough estimate, employing the CD1 element design will require ~23 elements/year, which is more than the 22 elements/year needed currently for HEU fuel.

CD19. Of the 23-plate designs evaluated, CD19 is among the best in regard to excess reactivity. However, the hot-stripe heat flux is slightly greater than for the FSD, which would likely reduce the margin to OFI. Another challenge of this design is the smaller channel 1 thickness (86 mil vs. 95 mil for the FSD). The tolerance on the channel 1 thickness due to manufacturing is ±22 mil, so the minimum channel 1 thickness is reduced to 64 mil, which could lead to OFI in this channel.

CD21. Relative to CD19, this design thinned the meat in plates 1, 2, and 3 by 1 mil to reduce the power peaking in the inboard plates. There is a slight reactivity penalty for doing this (0.09% Δk/k). The hot-stripe heat flux decreases by 3.0% (relative to CD19) due to this change. However, the peak heat flux is approximately the same as for the FSD, and the outermost channel is nominally thinner than for the FSD (86 vs. 95 mil), which could cause CHF limitations.

CD32. Relative to CD21, two changes are made in this design. First, the meat of the inboard plates is thinned (by 1 mil for plates 1 and 2; by 2 mil for plate 3). Furthermore, the interior channel thickness is decreased from 93 to 92 mil, which gives more water in channels 1 and 24 – 99.5 mil vs. 86 mil. The peak heat flux is about the same as for the FSD, and the hot-stripe heat flux is about 7.6% lower (127.0 vs. 137.4 W/cm^2). However, there is a reactivity penalty of 0.88% Δk/k relative to FSD.

CD33. This design has mixed interior channel thicknesses in an attempt to put more coolant around the inboard (and outboard) plates, which are more limiting. Channels 2-5 and 20-23 are widened by 1 mil by taking coolant from channels 1 and 24. No changes were made to the meat thicknesses relative to the CD32 design. Because of the changes to the channel thickness, the excess reactivity increased 0.09% Δk/k relative to CD32. The hot-stripe heat flux and peak heat flux remain about same as CD32, however.

CD35. It was observed in the CD33 results that plates 2 and 3 have the highest hot-stripe heat flux, and that they differ by only about 1.5%. The design was altered by thinning the meat of these two plates. No other adjustments to the CD33 element design (e.g., channel thicknesses) were made. The excess reactivity decreased only slightly, to -0.81% Δk/k relative to the FSD, as a result of this change. The peak heat flux for the all fresh core is only about 1.2% higher than for the FSD, while for the burned core the peak heat flux is about 2.2% lower,. More notably, the hot-stripe heat flux is decreased by 8.8% relative to the FSD for the all fresh core, and by 6% for the mixed burnup core. Furthermore, the thicknesses of the coolant channels surrounding the peak plate are increased by 1.1% (93 vs. 92 mil) relative to the FSD element design.

The effects observed while altering the LEU fuel element design parameters demonstrate the tradeoffs that are inherent to design optimization processes. The CD35 design appeared to be the best candidate design that meets the constraint of a thinnest nominal clad of 12 mil in a flow instability limited core. While the excess reactivity is reduced by 0.81% Δk/k relative to the optimized design when the clad thickness is constrained to 10 mil (FSD), the hot-stripe heat flux is decreased by ~9%, which will improve the margin to OFI.

Table 3.2 provides a comparison of the nominal design parameters for the HEU and CD35 (LEU) fuel element designs.

Table 3.2. Nominal HEU and LEU Fuel Plate Dimensions.

Plate	HEU					LEU – CD35 Design				
	Clad I.R. (inches)	Meat width (inches)	Meat thickness (mil)	Clad thickness (mil)	^{235}U Content (grams)*	Clad I.R. (inches)	Meat width (inches)	Meat thickness (mil)	Clad thickness (mil)	^{235}U Content (grams)**
1	2.770	1.703	20	15	19.26	2.756	1.690	9	17.5	18.09
2	2.900	1.805	20	15	20.39	2.893	1.797	12	16	25.66
3	3.030	1.907	20	15	21.53	3.030	1.905	16	14	36.26
4	3.160	2.010	20	15	22.66	3.167	2.012	20	12	47.89
5	3.290	2.112	20	15	23.79	3.304	2.120	20	12	50.45
6	3.420	2.214	20	15	24.93	3.440	2.227	20	12	52.99
7	3.550	2.316	20	15	26.06	3.576	2.334	20	12	55.53
8	3.680	2.418	20	15	27.19	3.712	2.440	20	12	58.07
9	3.810	2.520	20	15	28.33	3.848	2.547	20	12	60.61
10	3.940	2.622	20	15	29.46	3.984	2.654	20	12	63.16
11	4.070	2.724	20	15	30.59	4.120	2.761	20	12	65.70
12	4.200	2.826	20	15	31.73	4.256	2.868	20	12	68.24
13	4.330	2.928	20	15	32.86	4.392	2.974	20	12	70.78
14	4.460	3.031	20	15	33.99	4.528	3.081	20	12	73.32
15	4.590	3.133	20	15	35.12	4.664	3.188	20	12	75.86
16	4.720	3.235	20	15	36.26	4.800	3.295	20	12	78.41
17	4.850	3.337	20	15	37.39	4.936	3.402	20	12	80.95
18	4.980	3.439	20	15	38.52	5.072	3.508	20	12	83.49
19	5.110	3.541	20	15	39.66	5.208	3.615	20	12	86.03
20	5.240	3.643	20	15	40.79	5.345	3.723	20	12	88.59
21	5.370	3.745	20	15	41.92	5.482	3.830	20	12	91.15
22	5.500	3.847	20	15	43.06	5.619	3.938	20	12	93.71
23	5.630	3.949	20	15	44.19	5.756	4.048	17	16	81.87
24	5.760	4.052	20	15	45.32					
Total					**775.0**					**1506.8**

*± 1.0% per plate
**± 11% in plate 1; ± 8.3% in plate 2; ± 6.3% in plates 3, ± 5.0% in plates 4-22; ± 5.9% in plate 23

4.0 NEUTRON PHYSICS FOR HEU AND LEU FUELED CORES

The MURR is an active research facility providing testing and irradiation services to a variety of users. Steady-state neutron physics analyses are performed to ensure that the reactor will be able to continue to provide these services with the LEU fuel after conversion. More importantly, the neutron physics analyses evaluate the parameters necessary to ensure that the facility will continue to operate safely, and with sufficient safety margins, with the new fuel. Table 4.1 provides a summary comparison of reactor physics parameters for the HEU and LEU (CD35) fuel elements in the MURR that pertain to safety. These safety parameters, and performance parameters, with the LEU fuel are described below.

Table 4.1. Summary of Reactor Physics Parameters Calculated by MCNP for MURR.

Simulated Core:	HEU		LEU	
	Fresh	**Mixed Core**	**Fresh**	**Mixed Core**
Hot[1] Excess Reactivity (% Δk/k)	8.5	4.0	7.0	3.6
Cold[2] Excess Reactivity (% Δk/k)	8.6	4.1	7.0	3.6
Cold Reactivity with All Blades In[3] (% Δk/k)	-11.6	-17.2	-10.0	-14.0
Total Bank Worth at Cold Conditions[4] (% Δk/k)	-20.2	-21.3	-17.0	-17.7
Cold Minimum Shutdown Margin[5] (% Δk/k)	- 4.3	- 9.7	- 3.9	- 7.6
Critical Shim Blade Position (inches withdrawn)[6]	12.91	17.81	13.26	17.57
Axially-Averaged Hot-Stripe Heat Flux (W/cm^2)				
Samples in FT & Reflector (typical operating mode)	126.8	131.3	125.8	149.0
Maximum of all perturbed core cases (see Section 4.2)	139.2	141.3	144.0	156.8
Peak Heat Flux (W/cm^2)				
Samples in FT & Reflector (typical operating mode)	181.4	185.3	222.2	210.8
Maximum of all perturbed core cases (see Section 4.2)	197.6	189.9	234.0	228.1
Effective Delayed Neutron Fraction [6]	0.80%	0.79%	0.79%	0.77%
Prompt Neutron Lifetime (μs) [6]	49.5	57.8	38.7	43.8
Primary Coolant Void Coefficient (% Δk/k/% void) [6]				
0 to 0.5% void	-3.38E-03	-2.76E-03	-3.04E-03	-2.76E-03
0.5 to 1.0% void	-3.23E-03	-2.88E-03	-2.93E-03	-2.65E-03
1.0 to 5.0% void	-3.33E-03	-2.91E-03	-3.04E-03	-2.77E-03
Coolant Temperature Coefficient (% Δk/k/deg-K) [6]				
293.6 to 400K	-4.83E-05	-6.52E-05	-1.85E-05	-2.64E-05
Fuel Temperature Coefficient (% Δk/k/deg-K) [6]				
400 to 500K	-	-	-2.07E-05	-2.04E-05
500 to 600K	-	-	-1.99E-05	-1.93E-05

Notes:
1: Hot conditions are for 10 MW operations with HEU, 12 MW operations with LEU.
2: Cold conditions are isothermal after forced convection pumps are running (increased pressure in coolant channels increases moderator density relative to stagnant state).
3: "All Blades In" is defined as Boral control blades A-D fully inserted, but steel regulating blade parked at 10" withdrawn.
4: Total worth of blades A-D with the regulating blade fixed at 10" withdrawn.
5: "Minimum Shutdown Margin" case is most reactive blade and regulating blade fully withdrawn, others fully inserted
1-5: k_{eff} for MCNP calculations had $\sigma < 12$ pcm; reactivities reported have $\sigma < 0.015\%$ Δk/k
6: BOC, so no Xe or I. No Sm for fresh cores; Sm per prior depletion history for mixed cores. Typical samples loaded in flux trap; k_{eff} for MCNP calculations had $\sigma \leq 4$ pcm; consequently, reactivity coefficients reported have $\sigma < 6\%$.

4.1 Selection of HEU and LEU Reference Cores

In order to perform a comparison between HEU and LEU fuel, it is necessary to define reference cores that could be compared in order to demonstrate acceptability of all major parameters: fuel cycle performance, shutdown margin, reactivity coefficients, thermal-hydraulic steady-state safety margins, and experimental performance. It was decided that these reference cores should be close to limiting in order to provide additional confidence that the safety margin calculations treat the potentially limiting power shapes from the HEU and LEU fuel element.

The typical condition for the MURR core fuel loading is eight elements with a mixture of burnups. The eight elements are loaded as four pairs, with the elements in each pair having similar burnup because they generally have had the same operating history. The elements in each pair are loaded opposite each other in the core, as illustrated in Figure 4.1. The burnup values are calculated from the fuel cycle simulation described in Section 2.2.3. The fuel shuffling sequence modeled in the simulation was based on typical MURR practices.

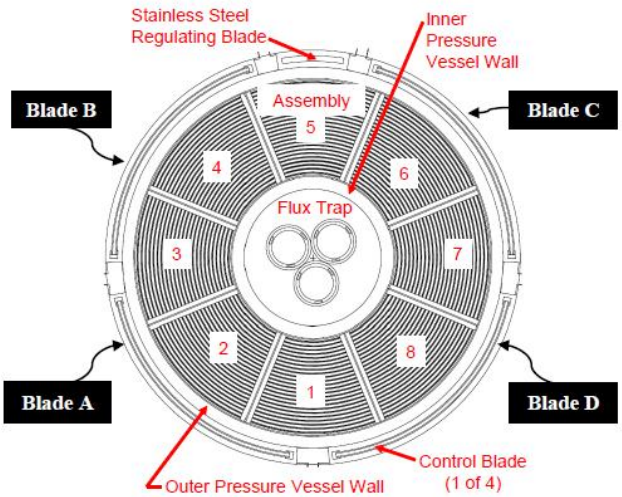

Core Positions	Typical BOC Burnup Range (MWd)[1]	Reference Core BOC Burnup (MWd)[1]
1 and 5	HEU: 0 to 40 (17 avg.) LEU: 0 to 50 (20 avg.)	HEU: 0 LEU: 0
3 and 7	HEU: 35 to 75 (54 avg.) LEU: 40 to 90 (64 avg.)	HEU: 65 LEU: 77
2 and 6	HEU: 65 to 110 (91 avg.) LEU: 85 to 135 (108 avg.)	HEU: 81 LEU: 96
4 and 8	HEU: 105 to 140 (127 avg.) LEU: 125 to 170 (153 avg.)	HEU:142 LEU: 170

[1] Burnup values from fuel cycle simulation in REBUS-DIF3D

Figure 4.1. MURR Core Layout with Typical BOC Burnups.

Core configurations with potentially high power peaking were identified from the fuel cycle simulation to be analyzed for thermal-hydraulic behavior and confirm compliance of the proposed LEU fuel element design with operating limits (e.g., flow instability). The fuel cycle simulations provided a collection of more than 325 HEU core states (4 state points per week x 82 weeks), and nearly 375 LEU core states (4 state points per week x 93 weeks).

Each of these state points from the REBUS-DIF3D model was examined and sorted to rank the cases with the highest peak heat flux in the core. As expected, it was found that the highest heat flux always occurs in cases where a fresh element is loaded next to an element that is near its discharge burnup. Other criteria were also used to filter the cases down to a small collection of "worst case" scenarios. For example, as described in section 2.2.3, the fuel cycle simulations were initiated with 26 all fresh HEU or LEU fuel elements, so a number of "transition cycles" existed in the simulations before a regular sequence of loading patterns that fit the typical weekly operations of MURR was established. Therefore, only cores after the transition cycles were considered for detailed thermal-hydraulics analysis.

Based on the selection criteria, the core conditions in week 58 (out of 82) of the HEU fuel cycle simulation and in week 76 (out of 93) of the LEU fuel cycle simulation were chosen for more detailed

evaluation. The burnups of the elements in the core positions of the HEU and LEU reference cores are provided in Figure 4.1. Depleted fuel material compositions were extracted from the REBUS-DIF3D results for each plate and axial depletion zone in the model; this consisted of 2,304 fuel compositions (8 elements x 24 plates x 12 axial zones) for the HEU core and 2,208 fuel compositions (8 x 23 x 12) for the LEU core. This data was utilized as material composition data for a detailed MCNP model for the calculation of estimated critical positions, detailed power distributions that could be used for the thermal-hydraulics analyses, and the evaluation of performance parameters such as the neutron flux in irradiation positions.

4.2 Power Distributions for Steady-State Safety Margin Evaluations

Power distributions were calculated with MCNP by tallying the fission power (f7 tally) within 24 axial, 9 azimuthal, and either 24 (HEU) or 23 (LEU) radial segments (plate-by plate) of the fuel meat in the entire core of eight elements (i.e., either 5,184 (HEU) or 4,968 (LEU) segments per element). Power distributions were calculated for a variety of critical configurations of various cores in order to identify the highest peaking factors that might limit the margin to onset of flow instability (OFI) and/or critical heat flux (CHF). The MCNP tallies were normalized by a post-processor to facilitate studies of different core power levels and different levels of tally detail. It should be noted that credit for power deposition outside the fuel is not modeled here, but is taken into account in the thermal-hydraulic safety margin calculation.

Power peaking is dependent upon the mix of burnup states among the elements in the core, upon the core xenon buildup state, upon critical control blade compositions and positions, and upon the experiment/sample loadings, particularly in the flux trap. A number of cases that covered the range of expected variations in these conditions were examined. In the results presented on the following pages, cases are labeled with a nomenclature CFb, where C indicates the fuel type and its burnup condition, F indicates the flux trap loading, and b indicates the control blade conditions.

The core fuel type and burnup conditions (“C” in the case name label) examined are as follows:

HEU		LEU	
C=1	All elements fresh, BOC (no Xe)	C=5	All elements fresh, BOC (no Xe)
C=2	All elements fresh, day 2 (eq. Xe)	C=6	All elements fresh, day 2 (eq. Xe)
C=3	Reference mixed core, BOC (no Xe)	C=7	Reference mixed core, BOC (no Xe)
C=4	Reference mixed core, day 2 (eq. Xe)	C=8	Reference mixed core, day 2 (eq. Xe)

Low-power physics testing will be conducted for initial LEU cores loaded with all fresh elements. So, in addition to evaluating the power distribution for the reference mixed cores, cores loaded with eight fresh elements of either HEU or LEU were also evaluated. For actual operations with all fresh LEU fuel, some of the elements will be constructed with borated Al-6061 side plates to provide reactivity hold-down. The borated side plates should reduce the azimuthal power peaking factors, while the radial and axial peaking factors should be reduced due to less difference in burnup among the fuel elements, so that the overall peaking will be within the range of the cases analyzed here. Thus, it is expected that the first all fresh operating cores of MURR with LEU fuel will be bounded by the present analysis.

Two flux trap loading conditions were considered. The nominal case, indicated by F=A in the case name label, has the flux trap loaded with typical samples for MURR operations. An off-nominal “empty trap” case, in which the flux trap is emptied of samples and the holder apparatus, is indicated by F=B.

The control blade condition assumed in the fuel cycle simulation was that all blades were at their fresh composition and banked in position. The effect of perturbations of the effective control blade B-10

concentration due to depletion and mismatched positioning of the blades on the core power distribution was examined since variations of this sort can exist in MURR. Shim blades in the MURR will be at different points in their lifetime, and as discussed in Section 2.2.4, the B-10 concentration depletes significantly in the bottom four inches of a given blade towards the end of its life of 8 years. The differences in the B-10 concentration at the tip of the shim blades can create a tilt in the core power distribution. Furthermore, the MURR Technical Specifications allow for the height of the blade tips to be mismatched by up to one inch. As an extreme scenario, perturbed heat flux profiles were calculated with two of the blades at their end of life (8 years) and positioned one inch above the other two blades, which were assumed to be fresh.

Calculations for the reference LEU core found that the power peaks in the fresh element in position 1 near its interface with element in position 8 that is near its discharge burnup. The largest perturbation of the peak heat flux will occur under conditions where two blades (e.g., A and D) in that region of the core are highly depleted and the remaining blades (e.g., B and C) are fresh, pushing the power even more to that region of the core. Allowing the depleted blades to be further withdrawn up to the Technical Specification limit creates an even greater power tilt. The cores for each fuel type (HEU and LEU) were evaluated under three conditions with regard to blade depletion and positioning, which is indicated by the character "b" in the case name.

b=Blank	All blades fresh and banked.
b=1	Blades C and D at 8 years depletion, blades A and B fresh. Blades C and D positioned 1 inch higher than A and B, per Technical Specification.
b=2	Blades A and D at 8 years depletion, blades B and C fresh. Blades A and D positioned 1 inch higher than B and C, per Technical Specification.

In the results presented below, the heat flux will be treated as the figure-of-merit for comparing the core states and predicting the potential impact on safety margins. The reason for this can be understood from Figure 4.2, which illustrates the radial (plate by plate) shapes of power (W), power density (W/cm^3), and heat flux (W/cm^2) for one of the reference cores of the LEU design (mixed burnup + BOC + loaded flux trap + control blades all fresh and banked = Case 7A). *Power* within a segment of an outboard plate is higher than power within the equivalent segment of an inboard plate because of the greater fuel volume. Since the volume of coolant being heated increases at the same rate as the volume of fuel in which power is tallied (i.e., the longer the arc length of the plate, the longer the arc length of the coolant channel), the higher power in outboard plates does not imply a more challenging case for thermal margin. *Power density* is higher for thin foils than for thick foils (for two plates producing the same total power), but the volume of coolant being heated is directly proportional to the fuel surface area, not the fuel thickness. Consequently, *heat flux* is the appropriate quantity to compare among segments tallied in order to predict heat transfer to the coolant.

Figure 4.3 shows the hot stripe heat flux radial peaking factor in LEU cores for several conditions of fuel burnup, day in the cycle, flux trap loading, and control blade configuration. These figures illustrate some of the factors that influence the heat flux profile in the core. First, the mix of burnup states of the elements within the core largely determines the power sharing between elements. A core with fresh elements alongside elements that will be discharged at the end of the cycle is expected to have the highest element peaking factor since the fresh elements will produce a greater fraction of the total power. For the reference mixed burnup LEU core at BOC, the fresh elements produce about 7% more power than all previously burned elements, and about 10% more than the previously burned elements at the end-of-cycle.

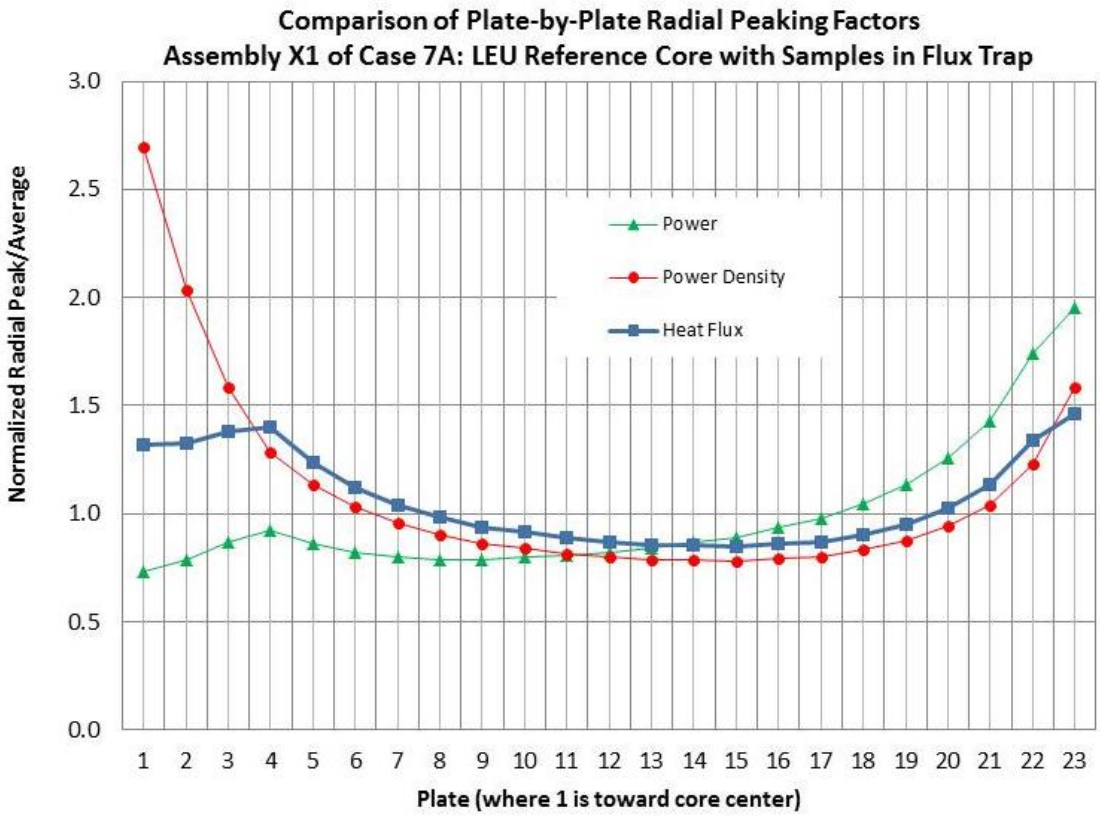

Figure 4.2. Normalized Radial Power Factors in Fresh Element in LEU Reference Core.

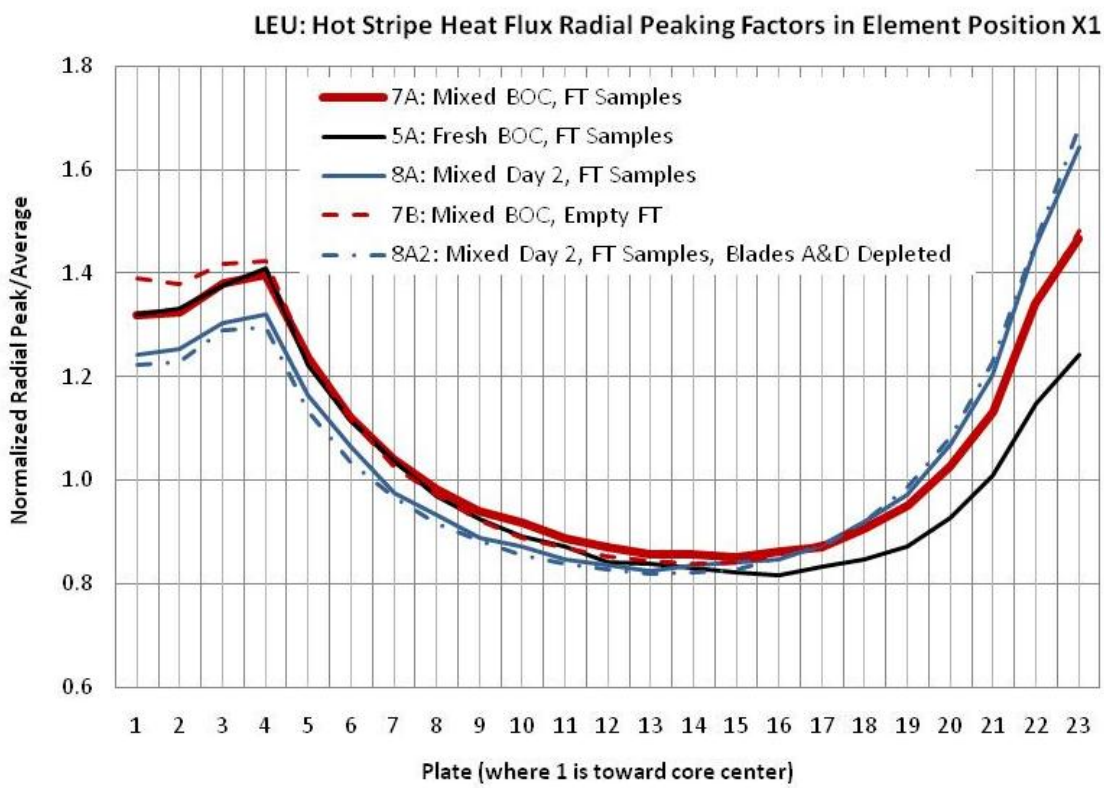

Figure 4.3. Hot-Stripe Heat Flux Radial Peaking Factor in Fresh Element in LEU Cores.

Case 5A is loaded with all fresh elements. The critical blade position is more deeply inserted for this core (13.3" withdrawn) than for the reference mixed core (Case 7A, 17.6" withdrawn) to compensate for the higher excess reactivity at BOC. Figure 4.3 illustrates the effect that the critical control blade position has on heat flux profile. The hot stripe peaking factor for plate 23 is 15% lower in the all fresh core because the radial power profile is suppressed in the outer plate(s) when the blades are more deeply inserted. This effect is important for margin to flow instability, which is largely driven by the axially averaged heat flux which contributes to the total coolant temperature rise in the channel adjacent to the plate. The deeper blade insertion would naturally cause a shift in the power profile towards the innermost plates, but because the overall power share of the fresh element is reduced due to the more even power sharing in the all-fresh core, no increase in the hot-stripe peaking factor in the innermost plates is observed.

The lower blade also increases axial peaking, particularly in the outer plates. The change in axial peaking is not important for margin to flow instability, but this effect is important to CHFR. From preliminary calculations it appears that the steady-state safety limits in MURR will be limited by flow instability, but critical heat flux analysis will be included in the detailed safety analysis to verify this.

A third factor affecting the heat flux profile is the time in the cycle, and is illustrated by the Case 8A results in Figure 4.3. As xenon builds up to equilibrium during operation, the control blades are withdrawn to compensate for the negative reactivity effect of the xenon. The change in control blade position shifts the power radially outward and axially upward, as discussed above. The xenon may also alter the power shape directly since it builds up in the regions of highest power.

Fourth, the flux trap contents can affect the heat flux profile. Having no samples or sample holder in the flux trap region is an off-normal condition for the MURR, but is one that will be evaluated for its effect on the power distribution and safety limits, nonetheless. When the sample holder is not inserted in the flux trap region, the core reactivity decreases due to the positive void coefficient of this region, and removing the sample holder and samples increases the amount of water in the flux trap. Decreasing core reactivity means the critical blade position is higher when only water is in the flux trap region. Further, increasing the amount of moderation from the flux trap region has a direct effect on the power in the interior plates, as can be seen in the curve for Case 7B in Figure 4.3.

The final factor affecting the heat flux profile is the control blade history and positioning. As discussed above, accounting for the depletion of the control blades being different for each blade, as well as the mismatch of the blade heights up to the Technical Specification limit, will introduce a power tilt in the core. This can be seen in the Case 8A2 curve in Figure 4.3, which shows that the hot stripe heat flux peaking factor increases in the outer plates (and decreases in the inner plates) relative to Case 8A.

After considering all of the various contributors to power peaking discussed above, power distributions were calculated for 24 cases that enveloped the distinct combinations of effects for each fuel type. The atom densities of the fuel compositions for each core state were read from REBUS-DIF3D depletion results to automatically update an MCNP input file. A search was then performed with MCNP to find the critical blade position for the core (i.e., blades moved until MCNP predicted a k-effective of 1.0). The 24 cases for the HEU fuel are summarized in Table 4.2, showing the core conditions and the calculated critical blade height for each case. The 24 cases for the LEU core are summarized in Table 4.3.

Finally, a post-processor was applied to read the mctal file and produce power distribution edits suitable for the thermal-hydraulics analyses of flow instability and critical heat flux. The peak hot-stripe and local heat fluxes for each case are summarized in Tables 4.4 and 4.5 for the HEU and LEU cores, respectively. The location of the peak in terms of element position, azimuthal stripe, plate, and axial position (for local heat flux) is also indicated.

Table 4.2. Summary of Power Distribution Evaluations – HEU Cores.

Core state that may bound power peaking				Element Burnup (MWd) at Beginning of Week						Critical Blade Position (Inches withdrawn)			
Case	Burnup State	Time (Days)	Flux Trap	X1 X5	X2 X6	X3 X7	X4 X8	Fresh Blades	Depleted Blades	Fresh Blades	Depleted Blades	Reg Blade	MCNP k-eff
1A	Fresh	0	Samples	0	0	0	0	A, B, C, D		12.911		10	0.99983
1A1	Fresh	0	Samples	0	0	0	0	A, B	C, D	10.307	11.307	10	1.00020
1A2	Fresh	0	Samples	0	0	0	0	B, C	A, D	10.466	11.466	10	1.00009
2A	Fresh	2	Samples	0	0	0	0	A, B, C, D		16.782		15	1.00017
2A1	Fresh	2	Samples	0	0	0	0	A, B	C, D	14.423	15.423	15	1.00002
2A2	Fresh	2	Samples	0	0	0	0	B, C	A, D	14.556	15.556	15	1.00014
3A	“Week 58”	0	Samples	0	81	65	142	A, B, C, D		17.809		10	1.00044
3A1	“Week 58”	0	Samples	0	81	65	142	A, B	C, D	15.473	16.473	10	0.99999
3A2	“Week 58”	0	Samples	0	81	65	142	B, C	A, D	15.536	16.536	10	0.99985
4A	“Week 58”	2	Samples	0	81	65	142	A, B, C, D		24.031		15	1.00020
4A1	“Week 58”	2	Samples	0	81	65	142	A, B	C, D	22.394	23.394	15	1.00014
4A2	“Week 58”	2	Samples	0	81	65	142	B, C	A, D	22.373	23.373	15	0.99993
1B	Fresh	0	Empty	0	0	0	0	A, B, C, D		13.295		10	0.99974
1B1	Fresh	0	Empty	0	0	0	0	A, B	C, D	10.694	11.694	10	1.00000
1B2	Fresh	0	Empty	0	0	0	0	B, C	A, D	10.873	11.873	10	1.00006
2B	Fresh	2	Empty	0	0	0	0	A, B, C, D		17.367		15	0.99985
2B1	Fresh	2	Empty	0	0	0	0	A, B	C, D	15.041	16.041	15	0.99993
2B2	Fresh	2	Empty	0	0	0	0	B, C	A, D	15.187	16.187	15	1.00006
3B	“Week 58”	0	Empty	0	81	65	142	A, B, C, D		18.380		10	0.99969
3B1	“Week 58”	0	Empty	0	81	65	142	A, B	C, D	16.125	17.125	10	1.00010
3B2	“Week 58”	0	Empty	0	81	65	142	B, C	A, D	16.216	17.216	10	0.99998
4B	“Week 58”	2	Empty	0	81	65	142	A, B, C, D		26.000		15	1.00029
4B1	“Week 58”	2	Empty	0	81	65	142	A, B	C, D	24.569	25.569	15	0.99988
4B2	“Week 58”	2	Empty	0	81	65	142	B, C	A, D	24.664	25.664	15	1.00016

“Samples” indicates a typical loading of samples in all three flux trap tubes.
“Empty” indicates neither samples nor tubes in the flux trap (i.e., "empty island" configuration).
Full blade withdrawal is 26 inches.

Table 4.3. Summary of Power Distribution Evaluations –LEU Cores.

Core state that may bound power peaking				Element Burnup (MWd) at Beginning of Week						Critical Blade Position (Inches withdrawn)			
Case	Burnup State	Time (Days)	Flux Trap	X1 X5	X2 X6	X3 X7	X4 X8	Fresh Blades	Depleted Blades	Fresh Blades	Depleted Blades	Reg Blade	MCNP k-eff
5A	Fresh	0	Samples	0	0	0	0	A, B, C, D		13.259		10	1.00016
5A1	Fresh	0	Samples	0	0	0	0	A, B	C, D	10.656	11.656	10	0.99993
5A2	Fresh	0	Samples	0	0	0	0	B, C	A, D	10.814	11.814	10	0.99999
6A	Fresh	2	Samples	0	0	0	0	A, B, C, D		17.193		15	0.99985
6A1	Fresh	2	Samples	0	0	0	0	A, B	C, D	14.912	15.912	15	1.00001
6A2	Fresh	2	Samples	0	0	0	0	B, C	A, D	15.027	16.027	15	0.99990
7A	“Week 76”	0	Samples	0	96	77	170	A, B, C, D		17.567		10	1.00008
7A1	“Week 76”	0	Samples	0	96	77	170	A, B	C, D	15.209	16.209	10	0.99975
7A2	“Week 76”	0	Samples	0	96	77	170	B, C	A, D	15.351	16.351	10	1.00014
8A	“Week 76”	2	Samples	0	96	77	170	A, B, C, D		24.314		15	1.00001
8A1	“Week 76”	2	Samples	0	96	77	170	A, B	C, D	22.765	23.765	15	1.00004
8A2	“Week 76”	2	Samples	0	96	77	170	B, C	A, D	22.698	23.698	15	0.99986
5B	Fresh	0	Empty	0	0	0	0	A, B, C, D		13.650		10	0.99998
5B1	Fresh	0	Empty	0	0	0	0	A, B	C, D	11.080	12.080	10	1.00003
5B2	Fresh	0	Empty	0	0	0	0	B, C	A, D	11.258	12.258	10	1.00009
6B	Fresh	2	Empty	0	0	0	0	A, B, C, D		17.891		15	0.99997
6B1	Fresh	2	Empty	0	0	0	0	A, B	C, D	15.580	16.580	15	0.99988
6B2	Fresh	2	Empty	0	0	0	0	B, C	A, D	15.741	16.741	15	1.00017
7B	“Week 76”	0	Empty	0	96	77	170	A, B, C, D		18.193		10	1.00013
7B1	“Week 76”	0	Empty	0	96	77	170	A, B	C, D	15.933	16.933	10	1.00012
7B2	“Week 76”	0	Empty	0	96	77	170	B, C	A, D	16.030	17.030	10	1.00003
8B	“Week 76”	2	Empty	0	96	77	170	A, B, C, D		26.000		15	0.99917
8B1	“Week 76”	2	Empty	0	96	77	170	A, B	C, D	25.621	26.000	15	0.99998
8B2	“Week 76”	2	Empty	0	96	77	170	B, C	A, D	25.312	26.000	15	0.99986

“Samples” indicates a typical loading of samples in all three flux trap tubes.
“Empty” indicates neither samples nor tubes in the flux trap (i.e., "empty island" configuration).
Full blade withdrawal is 26 inches.

Table 4.4. Summary of Key Hot-Stripe and Local Heat Fluxes Evaluated for HEU Cores.

	Hot Stripe Heat Flux (W/cm^2)		Local Heat Flux (W/cm^2)	
Case	Peak	Location[1]	Peak	Location[2]
1A	126.8	X2 S9 P1	181.4	X4 A15 S9 P1
1A1	132.1	X7 S9 P1	187.8	X7 A15 S9 P1
1A2	130.7	X1 S9 P1	184.0	X2 A16 S1 P1
2A	122.4	X5 S1 P1	173.4	X7 A14 S9 P1
2A1	126.5	X7 S9 P1	176.2	X7 A14 S9 P1
2A2	124.9	X1 S9 P1	173.0	X7 A15 S9 P1
3A	131.3	X5 S1 P1	185.3	X5 A14 S1 P1
3A1	131.5	X1 S1 P1	180.9	X5 A15 S9 P1
3A2	134.0	X1 S1 P1	181.3	X1 A14 S1 P1
4A	125.5	X5 S1 P1	168.0	X5 A13 S1 P1
4A1	125.4	X1 S1 P1	165.6	X5 A13 S1 P1
4A2	126.2	X1 S1 P1	165.6	X5 A13 S1 P1
1B	133.3	X5 S1 P1	194.4	X2 A17 S1 P1
1B1	139.2	X7 S1 P1	**197.6**	X7 A16 S1 P1
1B2	137.0	X1 S9 P1	195.0	X1 A17 S9 P1
2B	128.4	X5 S1 P1	178.6	X6 A15 S9 P1
2B1	131.9	X7 S9 P1	180.2	X6 A15 S9 P1
2B2	131.4	X1 S1 P1	180.3	X7 A15 S9 P1
3B	137.0	X5 S1 P1	188.8	X1 A15 S1 P1
3B1	138.6	X1 S1 P1	187.5	X1 A14 S1 P1
3B2	**141.3**	X1 S1 P1	189.9	X1 A14 S1 P1
4B	131.0	X1 S1 P1	166.4	X1 A13 S1 P1
4B1	131.9	X1 S1 P1	167.3	X1 A13 S1 P1
4B2	131.9	X1 S1 P1	166.6	X1 A12 S1 P1

[1] Xi Sj Pkk. i is element number. j is azimuthal stripe in plate, numbered 1-9 moving clockwise. kk is plate, numbered 1-24 moving from inner pressure vessel to outer pressure vessel.

[2] Xi Azz Sj Pkk. i is element number. zz is axial level, numbered 1-24 from top of fuel meat. j is azimuthal stripe in plate, numbered 1-9 moving clockwise. kk is plate, numbered 1-24 moving from inner pressure vessel to outer pressure vessel.

Table 4.5. Summary of Key Hot-Stripe and Local Heat Fluxes Evaluated for LEU Cores.

	Hot Stripe Heat Flux (W/cm^2)		Local Heat Flux (W/cm^2)	
Case	Peak	Location[1]	Peak	Location[2]
5A	125.3	X5 S1 P4	222.2	X8 A18 S9 P23
5A1	129.6	X8 S1 P4	233.3	X6 A17 S9 P23
5A2	129.8	X1 S9 P4	229.5	X8 A17 S9 P23
6A	125.8	X7 S1 P23	211.9	X6 A16 S9 P23
6A1	143.2	X6 S9 P23	222.2	X6 A15 S9 P23
6A2	141.0	X8 S9 P23	216.4	X7 A15 S9 P23
7A	130.6	X1 S1 P23	210.8	X1 A16 S1 P23
7A1	142.0	X1 S1 P23	228.1	X1 A16 S1 P23
7A2	148.1	X1 S1 P23	218.1	X1 A16 S1 P23
8A	149.0	X1 S1 P23	193.0	X1 A12 S1 P23
8A1	155.0	X1 S1 P23	201.9	X1 A13 S1 P23
8A2	**156.8**	X1 S1 P23	196.7	X1 A12 S1 P23
5B	126.9	X5 S9 P4	220.3	X6 A17 S1 P23
5B1	133.8	X7 S1 P4	**234.0**	X6 A17 S9 P23
5B2	132.2	X8 S9 P4	229.9	X8 A17 S9 P23
6B	127.3	X6 S9 P23	210.2	X6 A15 S9 P23
6B1	144.0	X7 S1 P23	217.2	X6 A14 S9 P23
6B2	142.0	X8 S9 P23	213.5	X7 A15 S9 P23
7B	133.1	X1 S1 P23	208.9	X1 A15 S1 P23
7B1	144.1	X1 S1 P23	226.4	X1 A15 S1 P23
7B2	150.0	X1 S1 P23	217.0	X1 A14 S1 P23
8B	151.3	X1 S1 P23	190.7	X1 A12 S1 P23
8B1	152.5	X1 S1 P23	191.3	X1 A13 S1 P23
8B2	154.6	X1 S1 P23	191.6	X1 A12 S1 P23

[1] Xi Sj Pkk. i is element number. j is azimuthal stripe in plate, numbered 1-9 moving clockwise. kk is plate, numbered 1-23 moving from inner pressure vessel to outer pressure vessel.
[2] Xi Azz Sj Pkk. i is element number. zz is axial level, numbered 1-24 from top of fuel meat. j is azimuthal stripe in plate, numbered 1-9 moving clockwise. kk is plate, numbered 1-23 moving from inner pressure vessel to outer pressure vessel.

The margin to OFI is primarily dependent upon total heat transferred to a coolant channel rather than the axial shape of the heat flux. The largest hot-stripe heat flux calculated for the HEU cores is 141.3 W/cm^2 in Case 3B2, while the largest hot-stripe heat flux for the LEU cores is 156.8 W/cm^2 in Case 8A2.

Figure 4.4 plots the axial and azimuthal average heat flux for each plate of each element for Case 8A2. The peak axial average heat fluxes for this case is in plate 23 (outermost plate) of element in core position 1 (fresh element). The radial shape of the heat flux in the figure illustrates the important effect of moderation and fissile material self-shielding, as well as the choice of fuel foil thickness for reducing the heat flux peaking. The innermost and outermost plates in the MURR tend to have a much higher heat flux (i.e., fission rate) due to their proximity to the heavily-moderated flux trap (plate 1) and reflectors (plate 23 for the LEU design). The interior plates have a lower heat flux due to both less moderation from the coolant channels and the self-shielding effect of outboard plates consuming thermal neutrons coming from the flux trap and reflector. As indicated in the figure, the fuel foils in the innermost and outermost plates are thinned relative to the interior plates in order to prevent extremely high heat flux peaking which would reduce the margin to OFI (as well as the margin to CHF).

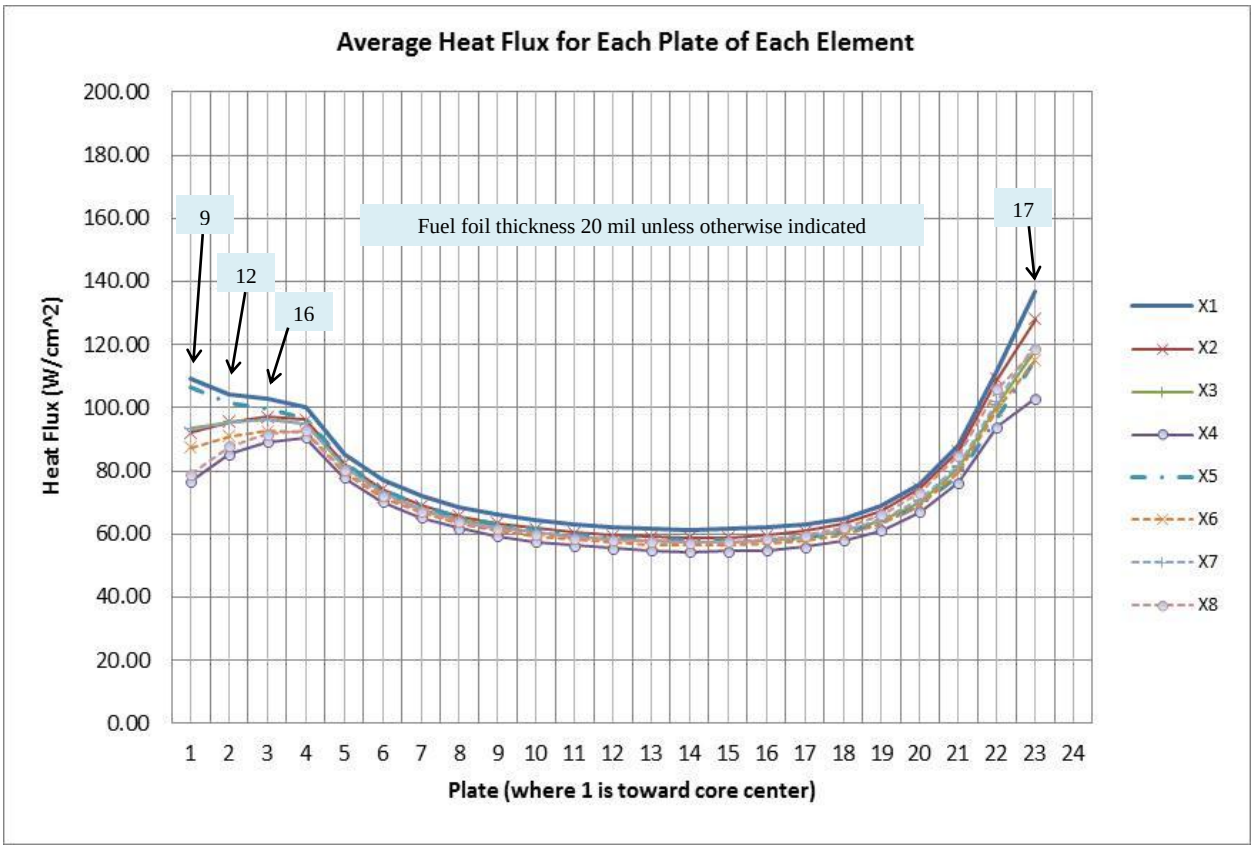

Figure 4.4. Average Heat Flux in Each Plate of Each Element in Case 8A2.
LEU Week 76 Day 2 with Loaded Flux Trap and Blades A and D at Depleted Composition.

The effects of moderation and self-shielding are also important in the azimuthal power profile of the MURR elements. There is a 70 mil wide unfueled region of the plates adjacent to the side plates. Consequently, the fuel near the side plates sees relatively more moderation and less self-shielding than the azimuthal interior region. As discussed in Section 2.2.5, the details of the MCNP fission power were tallied with azimuthal stripes of 5 mm width (~200 mil) along the edge of the fuelled region of each plate. The remainder of each plate in the azimuthal interior of the plate was subdivided into three tally regions of equal angle, so that the entire meat width was included in the detailed power distribution.

Figure 4.5 illustrates the azimuthal peaking factor for each plate of each element for Case 8A2. The moderation effect on the power peaking along the fueled edge is clearly pronounced for the interior plates, which have azimuthal peaking factors of 1.15 to 1.35. The effect is most pronounced for the elements in positions 1, 3, and 7 in this reference core due to uneven burnup and positioning of the shim blades assumed in this case. As can be seen in the inset chart for Case 8A with the blades at their fresh composition and banked, the azimuthal power peaking is less skewed in these elements. The azimuthal effect is somewhat smaller for the outboard plates since there is significant moderator and little self-shielding already, as discussed above. For plate 1, the azimuthal peaking factor is < 1.05, while for plate 23 the peaking factor is < 1.20 (< 1.15 when the blades are uniform and banked).

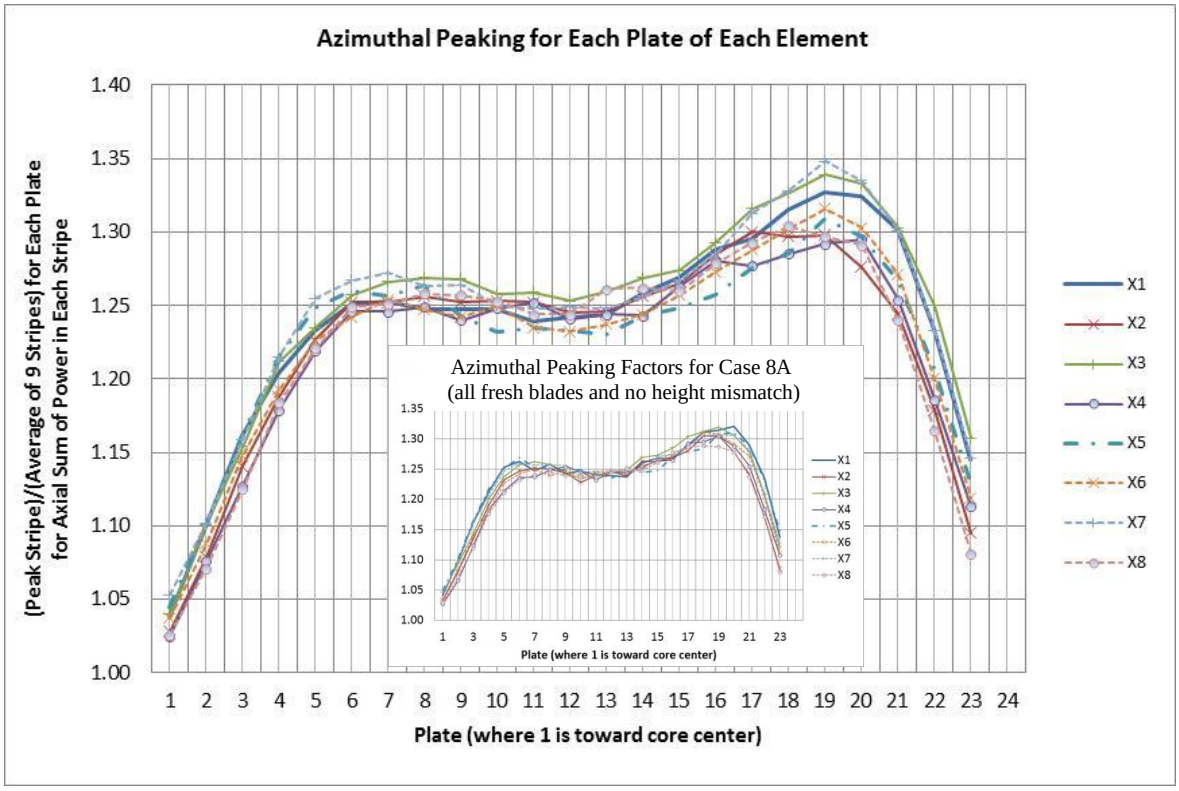

Figure 4.5. Azimuthal Peaking Factors for Each Plate of Each Element in Case 8A2.
LEU Week 76 Day 2 with Loaded Flux Trap and Blades A and D at Depleted Composition.

Another trend in the azimuthal peaking factor is illustrated in Figure 4.6, which plots the average azimuthal peaking factor for all elements in a given core by fuel plate. For the all fresh core (Case 5A), the shim blades are more deeply inserted, which pushes the power more towards the innermost plates. Consequently, the azimuthal peaking factor which tends to be greatest for plate 20 is smaller than in the mixed burnup reference cores. Cases 7A and 7B are for the same mixed burnup state of the fuel, but with and without samples loaded in the flux trap region, respectively. Since the blades are slightly more withdrawn in Case 7B, the azimuthal peaking factor in plate 20 is slightly greater. As xenon builds to equilibrium (Cases 8A and 8B), the critical position for the control blades moves upward to nearly fully withdrawn, which shifts the power radially outward, increasing the importance of the edge effect for those plates that are closer to the reflector.

The average heat flux in the interior plates is lower than in the outboard plates, so the largest azimuthal peaking factors do not correspond to a "hot stripe" for the entire element. Figure 4.7 illustrates the hot-stripe heat flux for each plate of each element in Case 8A2. The hot-stripe heat flux can be thought of as the multiplication of the plate average heat flux (Figure 4.4) by the azimuthal peaking factor (Figure 4.5).

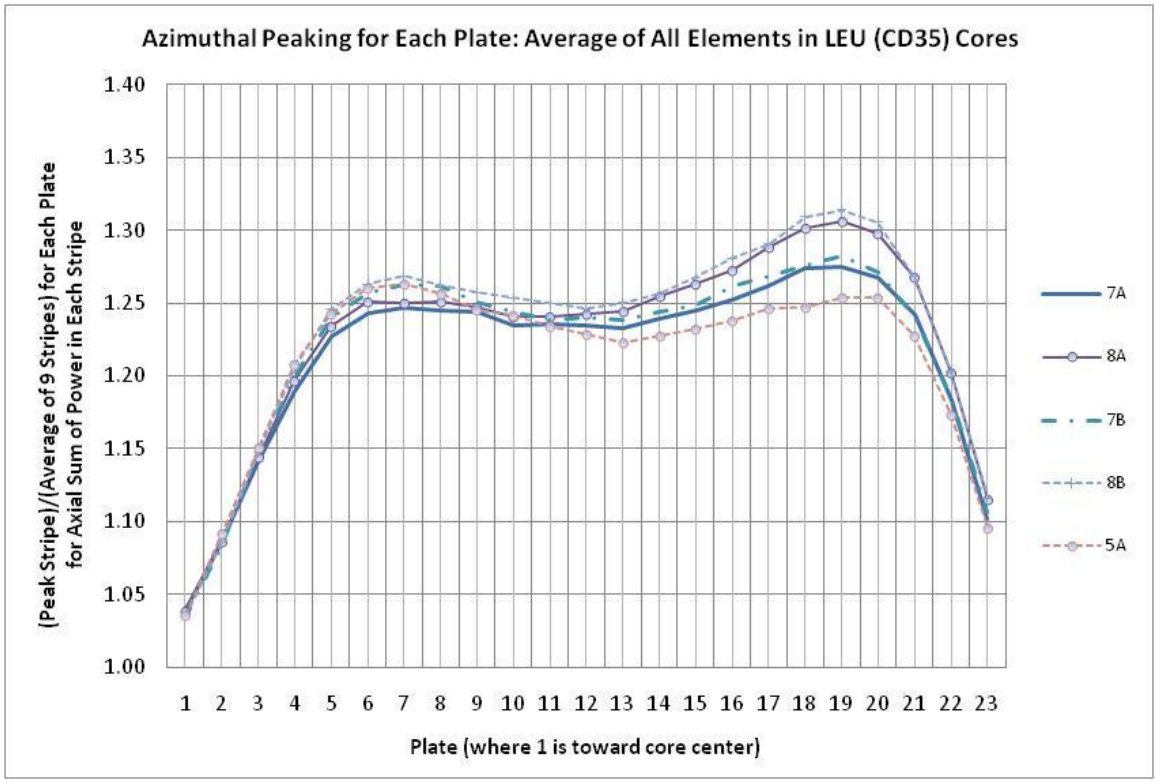

Figure 4.6. Azimuthal Peaking Factors by Plate Averaged for All Elements in Core.

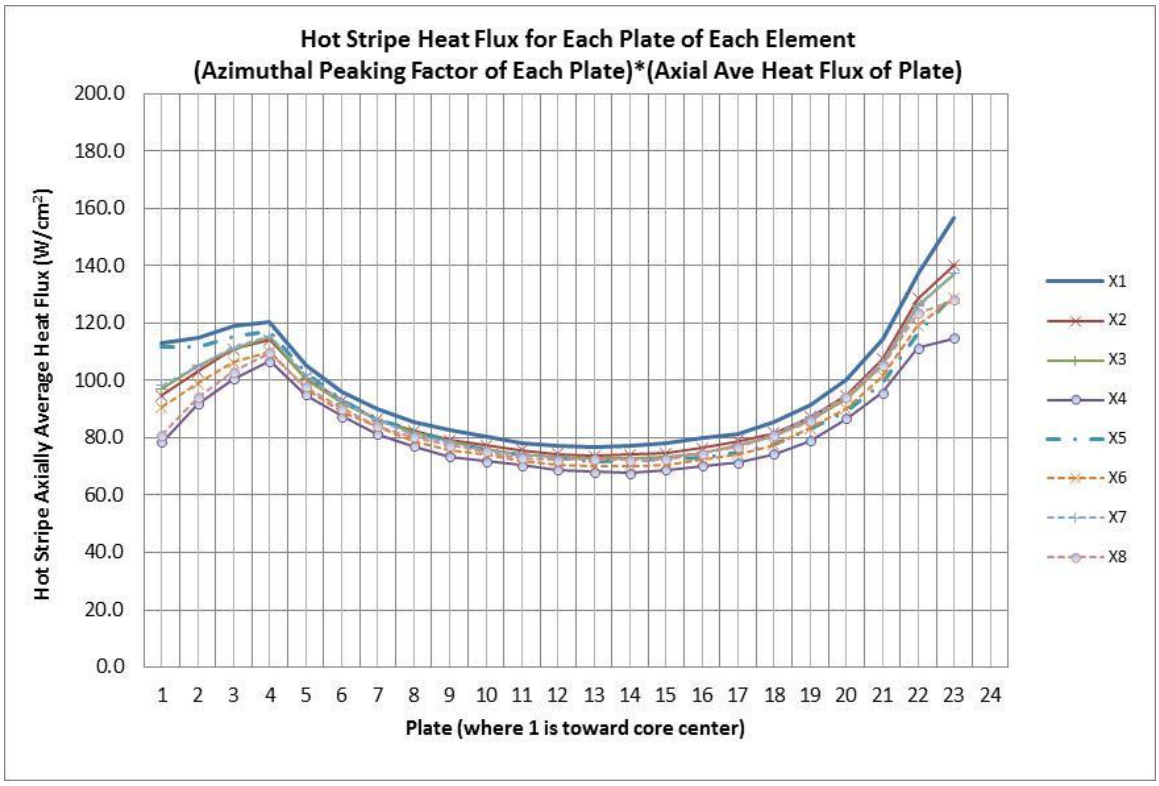

Figure 4.7. Hot-Stripe Heat Flux for Each Plate of Each Element in Case 8A2.
LEU Week 76 Day 2 with Loaded Flux Trap and Blades A and D at Depleted Composition.

The hot-stripe heat flux in the first 4 plates is relatively flat (~5% variation); achieving as flat a power distribution as possible was a design goal. Also, as the elements reach the end of their lifetime, the outboard plates deplete more than the interior plates, so that the power profile becomes less peaked.

The hot stripe heat flux and local heat flux tend to be highest in plate 23 of the fresh elements for the LEU cores. Figure 4.8 illustrates how the heat flux profile in plate 23 evolves axially and azimuthally over the life of the fuel. The three figures show the plate 23 heat flux in a) a fresh element at BOC with no xenon, b) for the same plate with equilibrium xenon, and c) at near the end of life for the outermost plate of an element that is about to be discharged. The heat flux profiles used for this illustration are for a loaded flux trap and the control blades all fresh and banked together (Cases 7A and 8A). At BOC the control blades are inserted at around 17.6" withdrawn (axially down to 8.4" from the top of the fuel), which pushes the heat flux profile axially down the plate. At 2 days in the cycle, the blades are withdrawn to compensate for the reactivity loss from equilibrium xenon; the axial profile becomes more cosine-shaped and the peak heat flux decreases. By the end of life, the peak heat flux in the plate has decreased significantly, from 210.8 to 153.5 W/cm^2, or nearly 30%. The hot stripe heat flux in plate 23 decreases less significantly, but still reduces about 6.4% (from 130.6 to 122.0 W/cm^2) over the life of the fuel.

In previous analyses of the margin to OFI performed for the Feasibility Study, only the fresh elements in the core were considered in the PLTEMP calculations because, as seen above, the heat flux is greatest for plates in the fresh elements of the core. However, fuel swelling and oxide growth during the life of the fuel contribute to restriction in the coolant channel, so that OFI possibly could occur first in burned elements that have a lower heat flux than a fresh element and a reduced channel size. In order to do a full assessment of the cases to determine the limiting margin to OFI, all cases in Tables 4.4 and 4.5 will be evaluated by PLTEMP with the detailed power distributions calculated by MCNP and a robust PLTEMP model with all eight elements represented. Likewise, all 24 cases for each fuel type will be evaluated to calculate the critical heat flux ratio (CHFR), and ensure CHFR > 2.

4.3 Fuel Cycle Performance

The MURR operates at a utilization factor of 90%, with reactor shutdown, refueling, and restart occurring on a weekly basis. The typical targeted discharge burnup for the elements is 150 MWd. About 22 elements are consumed every year.

The HEU fuel cycle simulation was set up to model the typical weekly fuel shuffling and operating cycle of the MURR, and predicted a discharge burnup of 149 MWd, compared with 150 MWd target burnup in the actual MURR fuel cycle. At 10 MW core power, this corresponds to the consumption of 22.1 elements/year. The LEU fuel cycle developed in Section 2.2.3 results in an average discharge burnup of 180 MWd. It was assumed that the reactor power level will be uprated to 12 MW in the conversion order. The results in Section 4.6 will show that the power increase is necessary to maintain the current experimental performance with HEU fuel. Consequently, the proposed LEU fuel cycle results in the consumption of about the same number of fuel elements/year as the HEU fuel cycle, 21.9. Table 4.6 summarizes the fuel operating characteristics of the HEU and proposed LEU fuel cycle.

The peak fission density burnup of the HEU fuel is limited by Technical Specification at 2.3×10^{21} fissions/cm^3. The peak local HEU burnup estimated from the fuel cycle simulation is 1.54×10^{21} fissions/cm^3, well below the limit. Table 4.7 provides the plate by plate burnup for the HEU discharged fuel. In the REBUS-DIF3D depletion modeling, the fuel was depleted plate-by-plate in 12 axial segments. The fuel was not subdivided azimuthally for the depletion calculations. In order to account for the influence of the azimuthal power shape on the burnup, the azimuthal peaking factors by plate calculated by the detailed MCNP power distribution calculations were applied to the fission density. The azimuthal peaking factors for the mixed burnup core at equilibrium xenon conditions (Case 4A) were

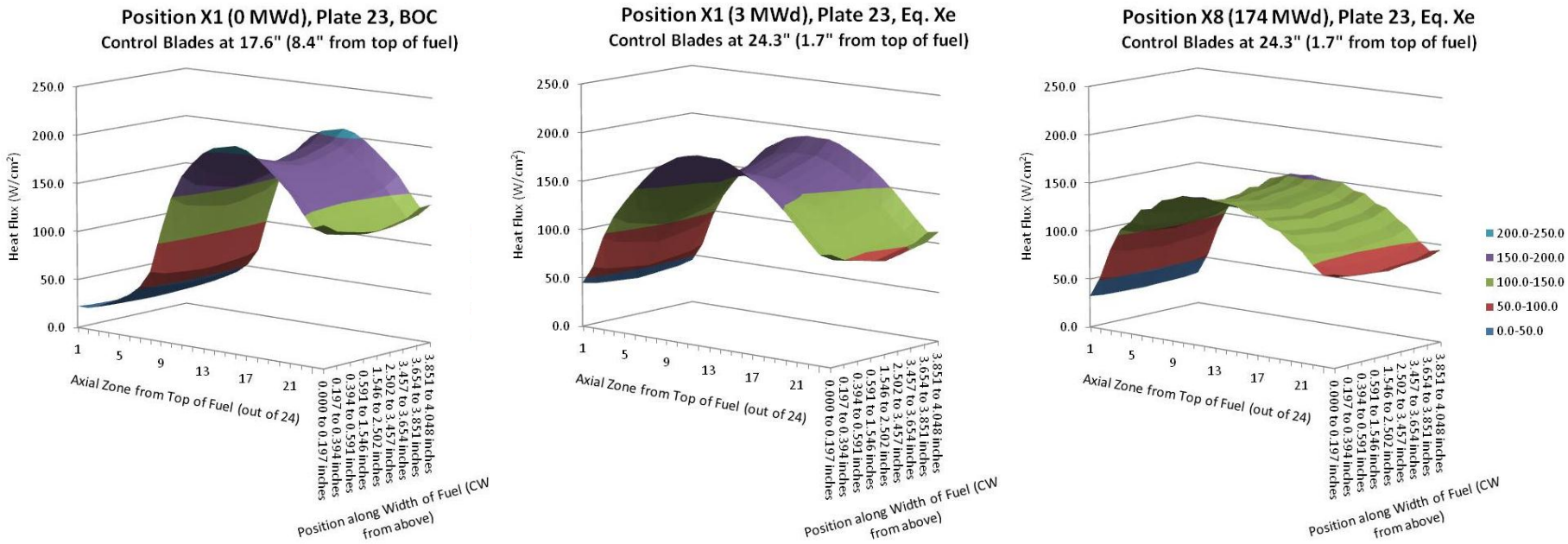

a)Fresh element, BOC (no xenon) b)Fresh element, Day 2 (eq. xenon) c)Depleted element, Day 2 (eq. xenon)

Figure 4.8. Heat Flux Profile in Plate 23 in LEU Reference Mixed Burnup Core.

Table 4.6. Current and Proposed MURR Fuel Cycle Operating Characteristics.

Parameter	Current HEU Fuel	Proposed LEU Fuel (CD35)
Maximum burnup:	150 MWd/element due to insufficient excess reactivity < 1.6E+21 peak fissions/cc burnup (i.e., < 43 at% U5 peak burnup) HEU Technical Specification limit is 2.3E+21 peak fissions/cc	180 MWd/element due to insufficient excess reactivity < 3.4E+21peak fissions/cc burnup (i.e., < 44 at% U5 peak burnup)
EOC Core MWds (control blades full out):	~640 MWd core with equilibrium xenon	~765 MWd core with equilibrium xenon
Refuelings:	Weekly – replace all eight fuel elements; fuel elements are used in 18-20 core loadings to achieve 145 to 150 MWd burnup at 10 MW	Weekly – replace all eight fuel elements; fuel elements are used in about 18-20 core loadings to achieve ~180 MWd burnup at 12 MW
Fuel Cycle:	22 elements used per year at 10 MW 32 fuel elements in active fuel cycle	22 elements used per year at 12 MW 32 fuel elements in active fuel cycle

utilized, because a) these were considered most realistic since the bulk of the fuel residence in the core is under those conditions and b) the plate-by-plate azimuthal peaking factors become larger as the equilibrium xenon builds in and the blades are withdrawn. Figure 4.9 plots the average and peak fission density by plate in the discharged HEU fuel.

For the U-10Mo fuel form that will be utilized for the LEU fuel elements, the calculated peak fission density in the MURR fuel cycle is 3.37×10^{21} fissions/cm^3, corresponding to 43.5 atom-percent burnup relative to the initial U-235 in the fuel. The calculated fission density includes fissions from all fissionable species. Table 4.8 provides the plate-by-plate burnup in the discharged LEU fuel. The local burnup was calculated in the same fashion as for the HEU fuel. The azimuthal peaking factors for Case 8A, which corresponds to the equilibrium xenon condition in the mixed burnup core, were utilized to account for the azimuthal shape of the fuel burnup. Figure 4.10 plots the average and peak fission density burnup by plate in the discharged LEU element.

4.4 Control System Reactivity Worth

Table 4.9 shows the excess reactivity and shutdown margins for fresh and mixed core states of both HEU and LEU. The mixed core states do not represent the most reactive states possible within the fuel cycle, but the cores are representative of typical operation. The reactivity of all possible mixed core states is bounded by an all-fresh core. The total control bank worth is reduced for the LEU core because of the harder spectrum of the LEU fuel.

Each core analyzed meets the Technical Specification requirement of shutdown margin > 2% $\Delta k/k$ with the most reactive blade and the regulating blade fully withdrawn. The calculations were performed for fresh Boral meat in every control blade. The ECP comparisons discussed in Section 3.3.4 indicate that

Table 4.7. Plate Discharge Fission Density for HEU Fuel.

Plate	Plate Average Fission Density ($x10^{20}$ fiss/cm^3)	Axial Burnup Peaking Factor	Azimuthal Peaking factor (Case 4A)	Peak Local Burnup	
				Fission Density ($x10^{20}$ fiss/cm^3)	Atom % Burnup
1	12.32	1.189	1.048	15.35	42.1%
2	10.54	1.205	1.084	13.77	37.7%
3	9.29	1.215	1.118	12.63	34.6%
4	8.39	1.222	1.145	11.75	32.2%
5	7.73	1.227	1.163	11.02	30.2%
6	7.27	1.230	1.171	10.47	28.7%
7	6.88	1.232	1.173	9.95	27.3%
8	6.59	1.234	1.179	9.58	26.3%
9	6.36	1.236	1.180	9.28	25.4%
10	6.19	1.238	1.181	9.05	24.8%
11	6.06	1.240	1.179	8.86	24.3%
12	5.97	1.242	1.182	8.77	24.0%
13	5.97	1.244	1.189	8.83	24.2%
14	5.94	1.247	1.190	8.81	24.1%
15	5.94	1.250	1.196	8.88	24.3%
16	5.98	1.253	1.201	9.00	24.7%
17	6.07	1.258	1.206	9.20	25.2%
18	6.21	1.262	1.209	9.49	26.0%
19	6.45	1.267	1.214	9.91	27.1%
20	6.83	1.271	1.209	10.50	28.7%
21	7.36	1.274	1.197	11.23	30.8%
22	8.08	1.276	1.172	12.08	33.1%
23	9.19	1.273	1.139	13.32	36.5%
24	10.74	1.265	1.093	14.85	40.7%

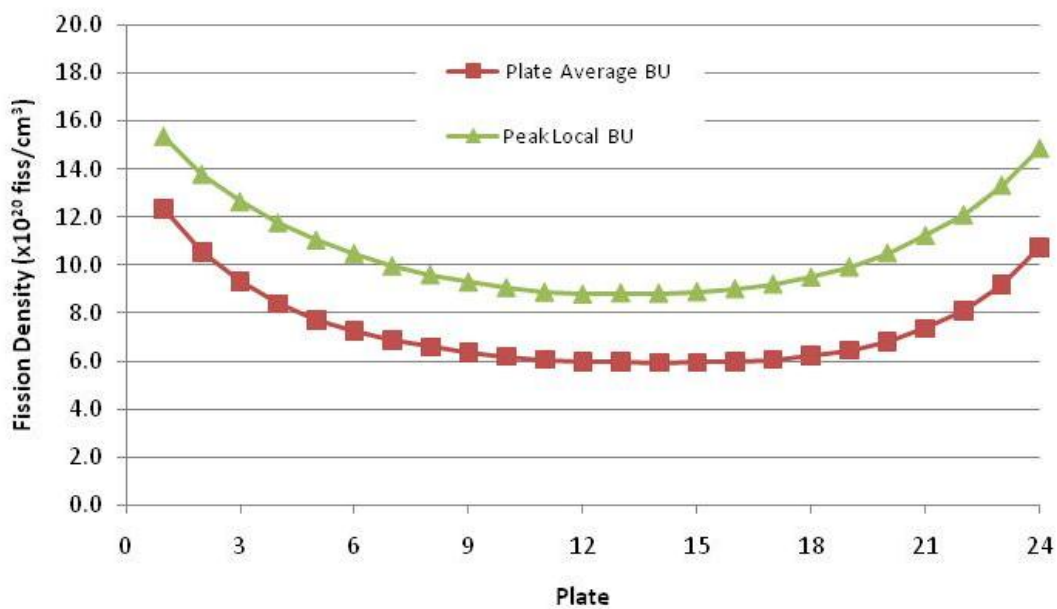

Figure 4.9. Fission Density by Plate in Discharged HEU Fuel.

Table 4.8. Plate Discharge Fission Density for LEU Fuel.

Plate	Plate Average Fission Density ($x10^{20}$ fiss/cm^3)	Axial Burnup Peaking Factor	Azimuthal Peaking factor (Case 8A)	Peak Local Burnup	
				Fission Density ($x10^{20}$ fiss/cm^3)	Atom % Burnup
1	26.56	1.223	1.038	33.72	43.5%
2	20.60	1.245	1.087	27.86	35.9%
3	15.68	1.254	1.144	22.50	29.0%
4	12.25	1.262	1.196	18.49	23.9%
5	10.36	1.264	1.234	16.17	20.9%
6	9.34	1.263	1.251	14.76	19.0%
7	8.58	1.263	1.250	13.54	17.5%
8	8.07	1.263	1.251	12.75	16.4%
9	7.72	1.263	1.247	12.16	15.7%
10	7.46	1.264	1.241	11.71	15.1%
11	7.28	1.265	1.240	11.43	14.7%
12	7.15	1.266	1.243	11.26	14.5%
13	7.18	1.267	1.245	11.33	14.6%
14	7.13	1.269	1.255	11.35	14.6%
15	7.11	1.271	1.264	11.42	14.7%
16	7.15	1.274	1.273	11.60	15.0%
17	7.28	1.278	1.288	11.98	15.5%
18	7.52	1.282	1.302	12.55	16.2%
19	8.05	1.287	1.307	13.53	17.5%
20	8.84	1.293	1.297	14.83	19.1%
21	10.34	1.297	1.268	17.01	22.0%
22	13.22	1.300	1.202	20.66	26.7%
23	18.01	1.289	1.115	25.89	33.4%

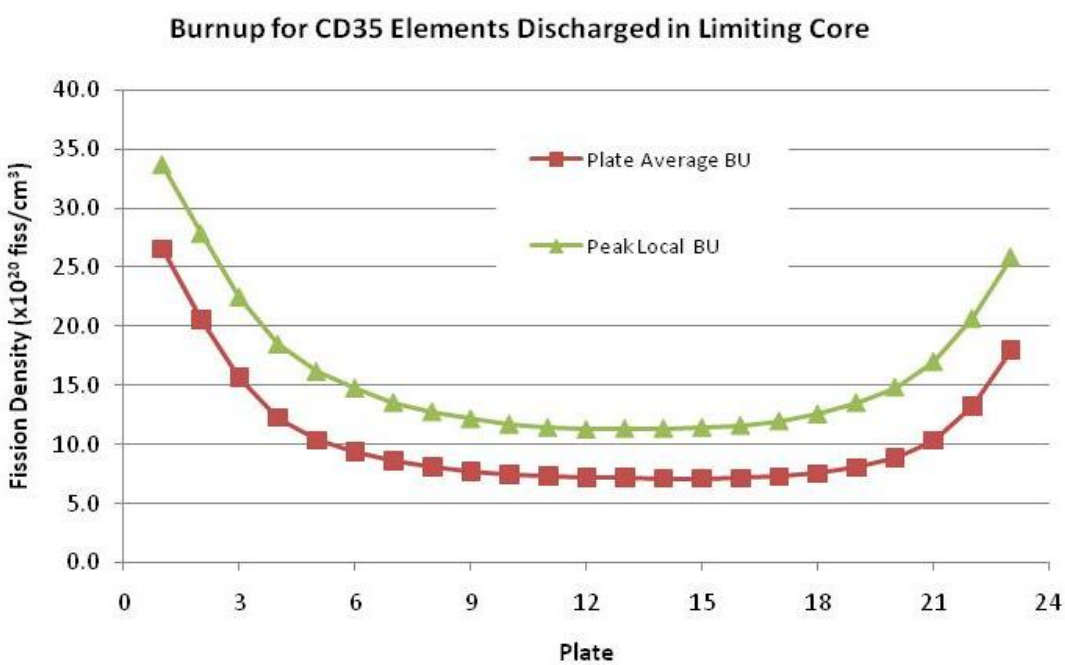

Figure 4.10. Fission Density by Plate in Discharged LEU Fuel.

Table 4.9. Control System Worth Calculations.

Simulated Core:	HEU		LEU	
	Fresh	Week58 Day 0	Fresh	Week 76 Day 0
Hot[1] Excess Reactivity (% Δk/k)	8.5	4.0	7.0	3.6
Cold[2] Excess Reactivity (% Δk/k)	8.6	4.1	7.0	3.6
Cold Reactivity with All Blades In[3] (% Δk/k)	-11.6	-17.2	-10.0	-14.0
Total Bank Worth at Cold Conditions[4] (% Δk/k)	-20.2	-21.3	-17.0	-17.7
Cold Minimum Shutdown Margin[5] (% Δk/k)	4.3	9.7	3.9	7.6

1 Hot conditions are for 10 MW operation with HEU, 12 MW operation with LEU.
2 Cold conditions are isothermal after forced convection pumps are running (increased pressure in coolant channels increases moderator density relative to stagnant state).
3 All Blades In is defined as Boral control blades A-D fully inserted, but steel Regulating Blade parked at 10" withdrawn
4 Total Worth of Blades A-D with the regulating rod fixed at 10" withdrawn.
5 Minimum Shutdown Margin case is Most Reactive Blade and Regulating Blade fully withdrawn, others fully inserted.

All cases have no Xe or I; no Sm for fresh cores, Sm per prior depletion history for mixed cores.
k-effectives from MCNP calculations had σ <12 pcm, so reactivities reported have σ <0.02% Δk/k.

control blade depletion is significant in MURR due to the combination of high fluxes and relatively long blade use. A case with two of the shim blades (blades A and D) having the composition corresponding to 8 years irradiation history and the remaining blades at fresh Boral composition yielded an LEU fresh fuel core shutdown margin of 3.4% Δk/k, versus 3.9% Δk/k shutdown margin with all fresh blades.

Further studies are needed to evaluate the various options available to address shutdown margin for an all fresh LEU transition core (borated side plates for fresh LEU to reduce excess reactivity, use of all fresh blades for an all fresh core, redesign of the control blades, etc.). This analysis shows, however, that on the basis of calculated shutdown margins, the conversion of MURR using the proposed LEU fuel element meets the Technical Specification requirements.

4.5 Reactivity Coefficients

Kinetics parameters and reactivity coefficients are needed to perform reactivity induced transient analyses. MCNP was used to calculate the kinetics parameters β_{eff} (effective delayed neutron fraction) and Λ (neutron lifetime) using the kinetics option in MCNP5. The coolant void, coolant temperature, and fuel temperature reactivity coefficients were calculated by making small perturbations to the appropriate reactor conditions from the nominal (hot operating) conditions in MCNP.

To verify this method for calculating the coolant void coefficient, an MCNP calculation was used to model the experimental measurement of the void coefficient performed during the low-power startup testing of the all fresh HEU core performed in 1971 [10]. The void coefficient was measured at low power isothermal conditions by inserting aluminum shims in the coolant channels between fuel plates in the element in position 8 to simulate the presence of a coolant void. Experiments with 23 shims (all coolant channels between the 24 HEU fuel plates) and 12 shims (odd numbered channels only) were conducted. After inserting the shims, the new critical blade position was measured, and the reactivity difference based on the blade worth curves was calculated. Table 4.10 summarizes the results of this

Table 4.10. Coolant Void Coefficient Experiment Performed During Low-Power Testing.

1971 Startup Testing (Reference 10) Blades move to new critical configuration (Table 1); reactivity worth evaluated from startup s-curves (Tables 7-8, Figures 21-22)			
Experiment	Change in critical blade configuration	Coolant void coefficient (% Δk/k/%-void)	
23 shims in element 8, 0.547%-void in total core coolant	Step 7 to Step 3 D: 11.8" to 12.415" R: Fixed 26.4"	-0.297%	-0.288%[1] (Average of experiments)
	Step 8 to Step 4 D: 12.08" to 12.848" R: 10.78" to 6.0"	-0.319%	
12 shims in element 8 (odd-numbered channels), 0.285%-void in total core coolant	Step 8 to Step 6 D: Fixed 12.08" R: 10.78" to 23.23"	-0.277%[1]	
	Step 7 to Step 6 D: 11.8" to 12.08" R: 26.4" to 23.23"	-0.260%[1]	

[1] Table 2 of reference reports values of -0.306% and -0.287% Δk/k. However, those values appear to have been calculated using a void fraction of 0.258%, transposing the last two digits of the correct void fraction. This also affects the average value for the coolant void coefficient reported on p. 21 of the report.

experiment taken from Reference 10. The average value of four different experiments for the void coefficient gives a measured coolant void coefficient of -0.288% Δk/k/%void.

Next, the experiment was modeled in MCNP by placing aluminum shims in the fuel assembly in position 8 that matched the number and size of the shims in the experiment. An impurity content equivalent to 10 ppm boron was assumed for the shims. The void coefficient was calculated in two ways from the MCNP models, with the results presented in Table 4.11. In the first approach, a method similar to the experimental procedure was used; a critical state was determined with the shims in place, and the change in reactivity from the "void" was computed based on the worth of the blade motion that compensated for the shims. The void coefficient calculated this way was -0.280% Δk/k/%-void, which is agrees very well with the experimental measurement of -0.288% Δ/k/%-void.

In the second method of modeling the experiment, the blades were fixed in place at a critical position reported in the reference, and the change in reactivity calculated by MCNP was used for determining the void coefficient. Additionally, a case with 20 ppm boron impurity content in the aluminum was modeled to assess the effect of aluminum purity on the experiment. The results of this experiment simulation show a calculated void coefficient close to the experiment; about 7% lower than the measured void coefficient with 10 ppm boron impurity modeled in the shims, and about 6% lower than the experiment with 20 ppm boron in the shim.

Lastly, the coolant void coefficient was calculated using the methodology typically used in MCNP, which is to model voids in the coolant by an isothermal reduction of the coolant density. The results of this set of calculations are presented in Table 4.12. In the first calculation, the coolant density only in the element position 8 was reduced by 3.969%, which is the equivalent amount of voiding from 23 of the aluminum shims in just that element. In the second calculation, the coolant density in the entire core was reduced by 0.547%. The coolant void coefficients calculated by this typical method are close to the experimentally measured value, differing from the experiment by 3.5% and 8.0%, respectively.

Table 4.11. Simulation of Coolant Void Coefficient Experiment in MCNP.

New critical blade positions found by critrods (σ = 8 pcm); reactivity worth evaluated from control blade s-curves			
Experiment	Change in critical blade configuration	Coolant void coefficient (% Δk/k/%-void)	
23 shims in element 8 (Al with 10 ppm boron), 0.547%-void in total core coolant	Step 7 to Step 3' D: 11.8" to 12.317" R: Fixed 26.4"	-0.276%	-0.280% (Average of experiments)
	Step 8 to Step 4' D: 12.08"to13.005" R: 10.78" to 6.0"	-0.270%	
12 shims in element 8 (Al with 10 ppm boron in odd-numbered channels), 0.285%-void in total core coolant	Step 7 to Step 6' D: 11.8" to 12.08" R: 26.4" to 26.0"	-0.287%	

Blades fixed at Critical Position 3, Table 5 of Reference 10 (A=11.93", B=11.92", C=11.92", D=10.50", R=11.24")		
Experiment	Shim material	Calculated Void Reactivity Coefficient (% Δk/k/%-void)
23 shims in element 8, 0.547%-void in total core coolant	Al with 10 ppm B	-0.259% ± 0.021%
	Al with 20 ppm B	-0.270% ± 0.021%
12 shims in element 8 (odd-numbered channels), 0.285%-void in total core coolant	Al with 10 ppm B	-0.276% ± 0.040%

Table 4.12. Coolant Void Coefficient Calculated by Density Reduction Method.

Reduced Water Density Modeling, 1971 Startup Core Blades fixed at Critical Position 3, Table 5 of Reference 10 (A=11.93", B=11.92", C=11.92", D=10.50", R=11.24")	
3.969% coolant density reduction in element F8 only; equivalent to 0.547% coolant density reduction in total core coolant	-0.298% ± 0.023%
0.547% coolant density reduction in all elements in core	-0.311% ± 0.021%

The primary coolant temperature coefficient for an all fresh HEU core was also experimentally measured and reported in Reference 10. Values were reported for several experiments, ranging from -4.4×10^{-5} to -77.5×10^{-5} $\Delta k/k/^{o}F$, depending on the range over which the coolant temperature was adjusted in the experiment. In the current work (see Table 4.13 below), the primary coolant temperature coefficient was calculated as -2.68×10^{-5} $\Delta k/k/^{o}F$ (-4.83×10^{-5} $\Delta k/k/^{o}K$). Although the fuel design in the experiment (which was performed in 1971) was the same as in MCNP calculation, there are differences in the flux trap contents, reflector conditions, and control blade design and compositions. However, the main reason for the difference between the results of the current calculations and the former experimental measurements is that the experiment included both temperature and density changes for the primary coolant water. In the calculation, only the effect of temperature change was modeled, by adjusting the coolant cell temperature and using $S(\alpha,\beta)$ data that corresponded to the nominal and perturbed temperatures in the MCNP model. With the coolant temperature and density changes modeled, as well as 1971 conditions for the flux trap, reflector, and control blades, the calculated coolant temperature coefficient is -13.4×10^{-5} $\Delta k/k/^{o}F$, which is within the range of the experimentally measured values.

The previous exercises were performed to demonstrate the method for calculating reactivity coefficients based on small perturbations in material properties in MCNP compared with experimental results. Using the same methodology as utilized in calculating the results in Table 4.12 with a global change to the material property being evaluated, reactivity coefficients were calculated for all-fresh cores of HEU and LEU, as well as mixed burnup cores. The results of those evaluations are provided in Table 4.13.

The delayed neutron fraction is slightly smaller for the LEU fueled core relative to HEU. The neutron lifetime is shorter by about 25% in the harder spectrum of LEU fuel. The coolant void coefficient is roughly the same for both HEU and LEU cores. The coolant temperature coefficient, however, is much less negative (about 60% smaller) for LEU fuel. For HEU, it is assumed that the fuel temperature coefficient is negligible. For LEU, fuel temperature increases provide a negative reactivity effect due to Doppler broadening of the U-238 resonances.

4.6 Experimental Performance

The conversion of the MURR from HEU to LEU fuel will affect experimental fluxes. The effects were examined by calculating flux and reaction rate predictions in a number of important experimental locations for several core states.

Based on current and projected MURR utilization, the following three experimental locations were selected for comparing the effect of an HEU to LEU fuel conversion. The tally runs were performed with 600M histories, resulting in the RMS relative error noted in the tables of results.

- Center Test Hole (Flux Trap) Irradiation Positions:
  One of MURR's primary missions is to produce high specific activity isotopes for various applications including medical use. While the majority of isotopes are produced through thermal neutron reactions, a few require fast neutron threshold reactions. The current unperturbed peak thermal flux in the flux trap region is 6E+14 n/cm^2-s, whereas the peak fast flux (> 1.0 MeV) is 6E+13 n/cm^2-s.

  Detailed 2 group and 69 group tallies in MCNP were used to compare HEU and LEU values of:
  - Flux in Flux Trap (FT) tube B, 18-21" above bottom of holder, where a sulfur bearing sample can was modeled for P-33 production;
  - Flux and S-32(n,p)P-32 reaction rate in FT tube B, 13-15" above bottom of holder, where a sulfur bearing sample can was modeled for P32 production via the fast threshold reaction;

Table 4.13. Kinetics Parameters and Reactivity Coefficients.

	HEU All Fresh	HEU "Week 58"	
		Day 0	Day 2 (Eq. Xe)
β_{eff}	0.800% ± 0.004%	0.790% ± 0.003%	0.783% ± 0.003%
Λ (μs)	49.5 ± 0.1	57.8 ± 0.1	62.1 ± 0.1
Coolant Void (Δk/k/% void)			
0 to 0.5% void	-3.38E-03 ± 1.71E-04	-2.76E-03 ± 8.47E-05	-2.36E-03 ± 8.48E-05
0.5 to 1.0% void	-3.23E-03 ± 8.51E-05	-2.88E-03 ± 8.50E-05	-2.42E-03 ± 8.50E-05
1.0 to 5.0% void	-3.33E-03 ± 1.08E-05	-2.91E-03 ± 1.08E-05	-2.58E-03 ± 1.07E-05
Coolant Temperature (Δk/k/deg-K)			
293.6 to 400K	-4.83E-05 ± 4.00E-07	-6.52E-05 ± 4.00E-07	-6.69E-05 ± 4.01E-07
Fuel Temperature (Δk/k/deg-K)			
400 to 500K	-	-	-
500 to 600K	-	-	-

	LEU All Fresh	LEU "Week 76"	
		Day 0	Day 2 (Eq. Xe)
β_{eff}	0.789% ± 0.002%	0.772% ± 0.002%	0.765% ± 0.002%
Λ (μs)	38.7 ± 0.030	43.8 ± 0.033	47.9 ± 0.036
Coolant Void (Δk/k/% void)			
0 to 0.5% void	-3.04E-03 ± 7.21E-05	-2.76E-03 ± 7.21E-05	-2.42E-03 ± 7.21E-05
0.5 to 1.0% void	-2.93E-03 ± 8.67E-05	-2.65E-03 ± 8.69E-05	-2.33E-03 ± 8.68E-05
1.0 to 5.0% void	-3.04E-03 ± 1.08E-05	-2.77E-03 ± 1.08E-05	-2.41E-03 ± 1.07E-05
Coolant Temperature (Δk/k/deg-K)			
293.6 to 400K	-1.85E-05 ± 3.99E-07	-2.64E-05 ± 3.99E-07	-2.82E-05 ± 3.99E-07
Fuel Temperature (Δk/k/deg-K)			
400 to 500K	-2.07E-05 ± 4.24E-07	-2.04E-05 ± 4.24E-07	-1.93E-05 ± 4.25E-07
500 to 600K	-1.99E-05 ± 4.26E-07	-1.93E-05 ± 4.26E-07	-1.89E-05 ± 4.26E-07

- Flux and reaction rates of Ir191(n,γ) and Ir193(n,γ) in FT tube C, 17-20" above bottom of holder, where Ir wires were explicitly modeled in an aluminum holder; and
- Flux in FT tube B, 6-8" above bottom of holder, where a BaCO sample was modeled for Cs production.

❖ Graphite Reflector Region Irradiation Positions:
The graphite reflector region has a number of sample positions that are used to irradiate various sample materials. The average measured value of thermal flux can vary from approximately 1E+13 n/cm^2-s to 1E+14 n/cm^2-s.

Detailed 2 group and 69 group tallies in MCNP were used to compare HEU and LEU values of:

- Flux in the bottom three inches of the Wedge 3 Row 1 Pneumatic Tube (P-tube); and
- Flux and Si-30(n, γ) reaction rate in the Green 5 location, where a 5" diameter silicon sample was modeled.

❖ Beamports:
There are four (4) radial and two (2) radial-tangential beamports. The measured thermal and epithermal beams emerging from the beam tubes are approximately 9.0E+9 n/cm^2-s and 2.7E+8 n/cm^2-s, respectively.

Detailed tallies in MCNP were used to compare HEU and LEU values of:

- The 47 group outbound current at a plane bisecting beam tube E at the radius of the inner wall of the reflector tank (i.e., beyond the outer edge of the graphite reflector). Outbound current was defined as current in a direction within the outbound half-space.

The 69 group tallies were made for the energy group structure of the WIMS-ANL libraries. The 47 group spectrum of the Beam Tube E currents was specified by a key experimentalist.

The fluxes and reaction rates were calculated for reference cores described in Section 4.1. The cores were Week 58 of the HEU simulation and Week 76 of the LEU simulation. Both the beginning-of-week core at Day 0 (i.e., no Xe, lower control blades) and the same core depleted to Day 2 (equilibrium Xe, higher control blades) were examined.

All tallies were normalized by post-processing to allow different power levels to be compared. While the LEU depletions were performed at 12MW, it would be possible to define an LEU fuel cycle for 10MW operation. Since the fresh and most depleted elements would not have significantly different burnup for a 10MW LEU fuel cycle, it is assumed that the overall power sharing and associated flux profile would not be significantly different.

Table 4.14 summarizes the ratio of LEU fluxes and reaction rates at 10 MW and 12MW to HEU at 10 MW for the critical state at the beginning of the week, labeled Day 0. Table 4.15 presents the same comparisons after equilibrium Xe, at Day 2 of the key week.

Figures 4.11 and 4.12 illustrate the ratio of LEU 47 group outbound currents in Beam Tube E at 10 MW and 12MW to HEU at 10 MW for Day 0 and Day 2. Figures 4.13-4.16 show the 69 group comparison of fluxes and reaction rates.

It is clear from the tables and figures that the flux and reaction rate losses would exceed 10% if the power level of 10 MW is maintained for LEU operation. However, an uprate to 12 MW would provide modest benefit for all of the fluxes and reaction rates tallied. In a companion technical basis report [3] the thermal safety margins of the LEU core at 12 MW are evaluated.

On the basis of experimental performance, the conversion of MURR using the proposed LEU fuel element is feasible at 12 MW.

Table 4.14. Comparison of Day 0 LEU Fluxes and Reaction Rates to HEU.
HEU is 10 MW Week 58 Day 0 (no Xe), Critical Bank 17.809" withdrawn, Reg Blade 10" withdrawn.

Metric	Neutron Energy Range		
	<= 1 eV	> 1 eV	Sum
LEU 10 MW Week 76 Day 0 (no Xe), Critical Bank 17.567" withdrawn, Reg Blade 10" withdrawn			
Flux[1] in FT Tube B[2] 18-21"	87% ±0.1%	93% ± 0.1%	90% ± 0.1%
S-32(n,p) Reactions[3] in FT Tube B 13-15"	N/A	94% ± 0.2%	94% ± 0.2%
Flux in FT Tube B 13-15"	88% ± 0.1%	94% ± 0.1%	91% ±0.1%
Ir-191(n,γ) Reactions in FT Tube C 17-20"	88% ± 0.3%	93% ± 1.5%	88% ± 0.3%
Ir-193(n,γ) Reactions in FT Tube C 17-20"	88% ± 0.3%	98% ± 2.1%	90% ± 0.6%
Flux in Ir Wires of FT Tube C 17-20"	88% ± 0.3%	94% ± 0.4%	92% ± 0.3%
Flux in FT Tube B 6-8"	88% ± 0.1%	93% ± 0.1%	90% ± 0.1%
Flux in Wedge 3 Row 1 P-Tube Bottom 3 inches	87% ± 0.1%	93% ± 0.2%	89% ± 0.1%
Si-30(n,γ) Reactions in Green 5 Position	89% ± 0.0%	93% ± 1.5%	89% ± 0.2%
Flux in Green 5 Sample Position	89% ± 0.0%	92% ± 0.1%	90% ± 0.0%
LEU 12 MW Week 76 Day 0 (no Xe), Critical Bank 17.567" withdrawn, Reg Blade 10" withdrawn			
Flux[1] in FT Tube B[2] 18-21"	105% ± 0.1%	110% ± 0.1%	106% ± 0.1%
S-32(n,p) Reactions[3] in FT Tube B 13-15"	N/A	114% ± 0.3%	114% ± 0.3%
Flux in FT Tube B 13-15"	105% ± 0.1%	113% ± 0.1%	109% ± 0.1%
Ir-191(n,γ) Reactions in FT Tube C 17-20"	106% ± 0.4%	111% ± 1.8%	105% ± 0.4%
Ir-193(n,γ) Reactions in FT Tube C 17-20"	106% ± 0.4%	112% ± 2.4%	106% ± 0.7%
Flux in Ir Wires of FT Tube C 17-20"	106% ± 0.4%	111% ± 0.5%	108% ± 0.3%
Flux in FT Tube B 6-8"	106% ± 0.1%	113% ± 0.1%	110% ± 0.1%
Flux in Wedge 3 Row 1 P-Tube Bottom 3 inches	105% ± 0.1%	109% ± 0.2%	104% ± 0.1%
Si-30(n,γ) Reactions in Green 5 Position	106% ± 0.1%	110% ± 1.7%	105% ± 0.2%
Flux in Green 5 Sample Position	107% ± 0.0%	109% ± 0.1%	106% ± 0.0%

[1] Fluxes were compared as n/s/cm^2.
[2] Axial positions noted as inches above bottom of flux trap sample holder.
[3] Reaction rates were compared as Reactions/s.

Table 4.15. Comparison of Day 2 LEU Fluxes and Reaction Rates to HEU.
HEU is 10 MW Week 58 Day 2 (eq. Xe), Critical Bank 24.031" withdrawn, Reg Blade 15" withdrawn.

Metric	Neutron Energy Range		
	<= 1 eV	> 1 eV	Sum
LEU 10 MW Week 76 Day 2 (eq. Xe), Critical Bank 24.314" withdrawn, Reg Blade 15" withdrawn			
Flux[1] in FT Tube B[2] 18-21"	87% ± 0.1%	93% ±0.1%	90% ± 0.1%
S-32(n,p) Reactions[3] in FT Tube B 13-15"	N/A	93% ± 0.3%	93% ± 0.3%
Flux in FT Tube B 13-15"	86% ± 0.1%	93% ± 0.1%	90% ± 0.1%
Ir-191(n,γ) Reactions in FT Tube C 17-20"	87% ± 0.3%	94% ± 1.5%	87% ± 0.3%
Ir-193(n,γ) Reactions in FT Tube C 17-20"	87% ± 0.3%	94% ±2.0%	89% ± 0.6%
Flux in Ir Wires of FT Tube C 17-20"	87% ± 0.3%	92% ± 0.4%	91% ± 0.3%
Flux in FT Tube B 6-8"	87% ± 0.1%	91% ± 0.1%	88% ± 0.1%
Flux in Wedge 3 Row 1 P-Tube Bottom 3 inches	88% ± 0.1%	93% ± 0.2%	89% ± 0.1%
Si-30(n,γ) Reactions in Green 5 Position	89% ± 0.0%	92% ± 1.4%	89% ± 0.1%
Flux in Green 5 Sample Position	89% ± 0.0%	92% ± 0.1%	90% ± 0.0%
LEU 12 MW Week 76 Day 2 (eq. Xe), Critical Bank 24.314" withdrawn, Reg Blade 15" withdrawn			
Flux[1] in FT Tube B[2] 18-21"	105% ± 0.1%	112% ± 0.1%	108% ± 0.1%
S-32(n,p) Reactions[3] in FT Tube B 13-15"	N/A	112% ± 0.3%	112% ± 0.3%
Flux in FT Tube B 13-15"	104% ± 0.1%	111% ± 0.1%	107% ± 0.1%
Ir-191(n,γ) Reactions in FT Tube C 17-20"	105% ± 0.4%	112% ± 1.8%	105% ± 0.4%
Ir-193(n,γ) Reactions in FT Tube C 17-20"	105% ± 0.4%	113% ± 2.4%	107% ± 0.7%
Flux in Ir Wires of FT Tube C 17-20"	105% ± 0.4%	111% ± 0.5%	109% ± 0.3%
Flux in FT Tube B 6-8"	104% ± 0.1%	110% ± 0.1%	106% ± 0.1%
Flux in Wedge 3 Row 1 P-Tube Bottom 3 inches	105% ± 0.1%	111% ± 0.2%	107% ± 0.1%
Si-30(n,γ) Reactions in Green 5 Position	107% ± 0.0%	111% ± 1.7%	107% ± 0.2%
Flux in Green 5 Sample Position	107% ± 0.0%	111% ± 0.1%	108% ± 0.0%

[1] Fluxes were compared as n/s/cm^2.
[2] Axial positions noted as inches above bottom of flux trap sample holder.
[3] Reaction rates were compared as Reactions/s.

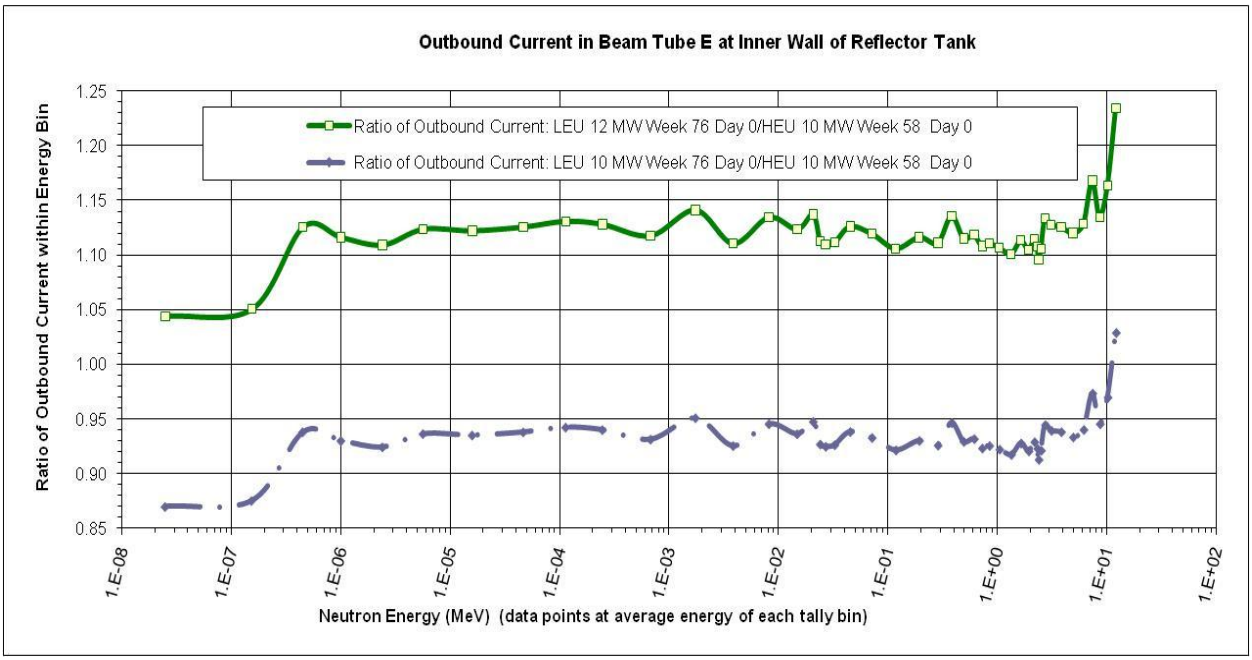

Figure 4.11. Comparison of LEU and HEU Beam Tube E Outbound Current at Day 0.

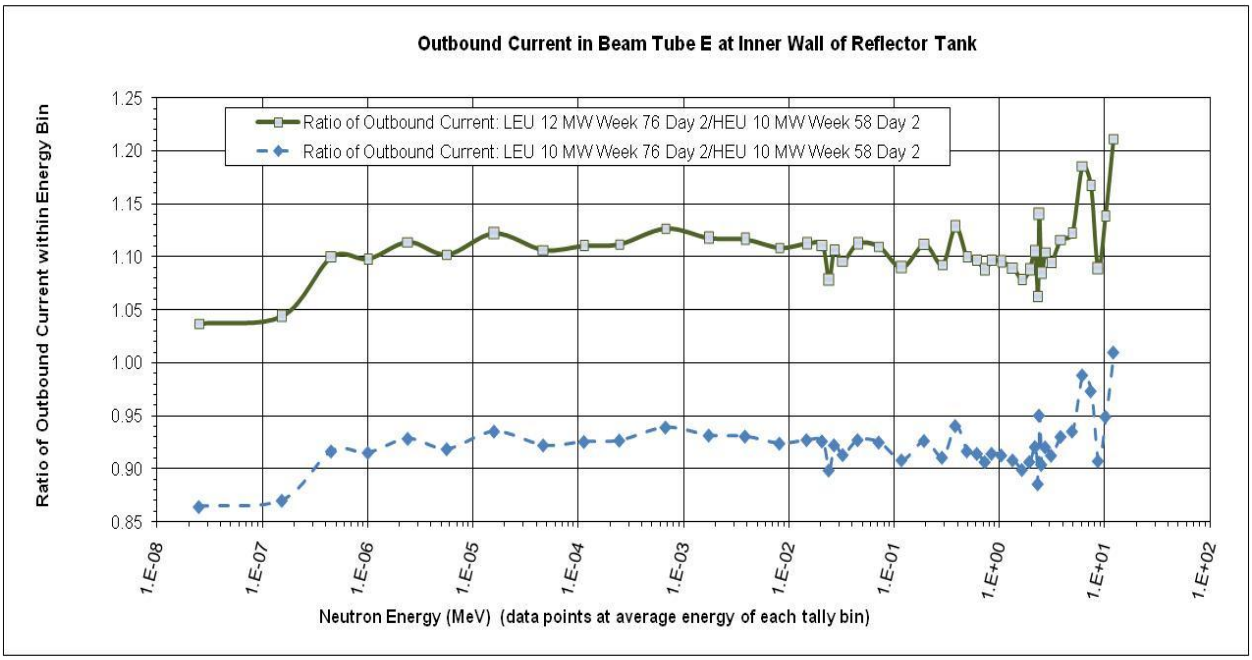

Figure 4.12. Comparison of LEU and HEU Beam Tube E Outbound Current at Day 2.

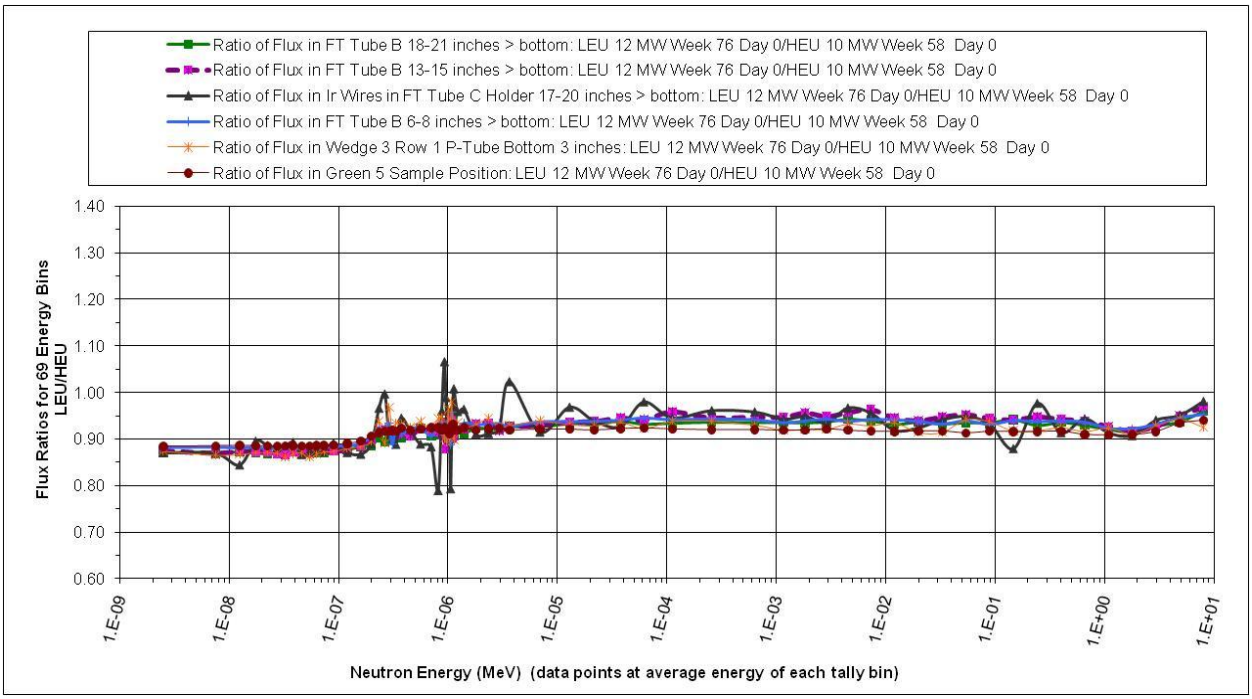

Figure 4.13. Comparisons of LEU 10 MW to HEU 10 MW at Day 0.

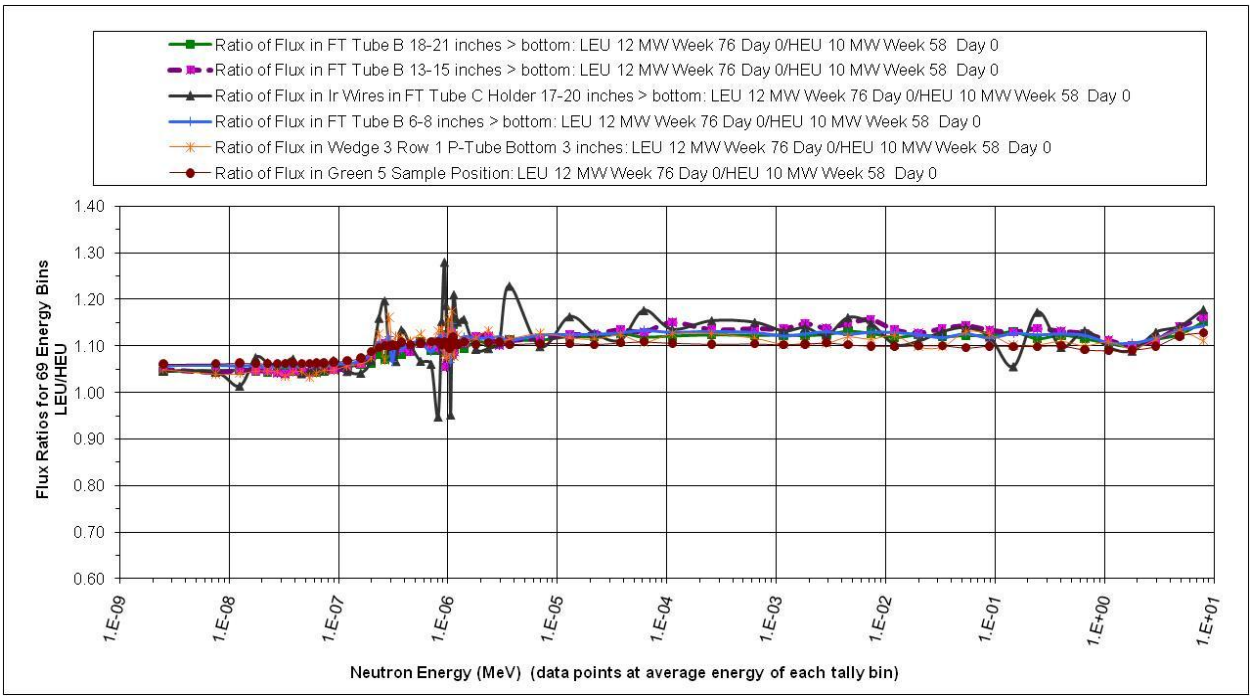

Figure 4.14. Comparisons of LEU 12 MW to HEU 10 MW at Day 0.

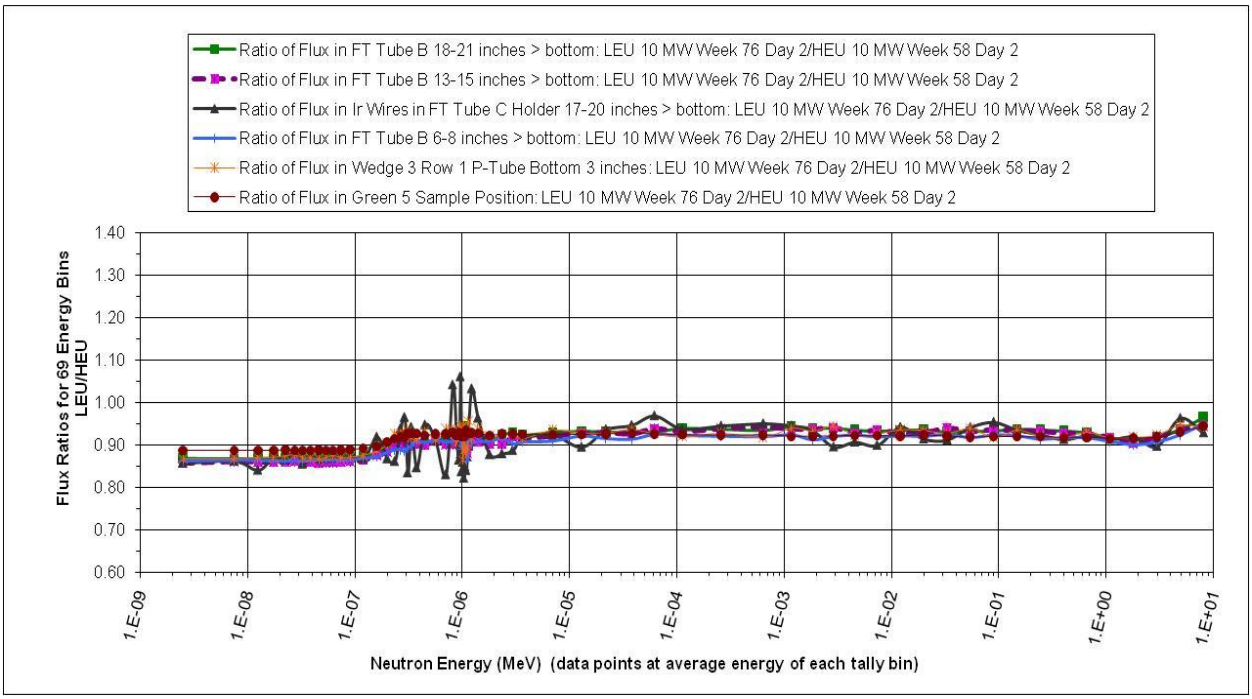

Figure 4.15. Comparisons of LEU 10 MW to HEU 10 MW at Day 2.

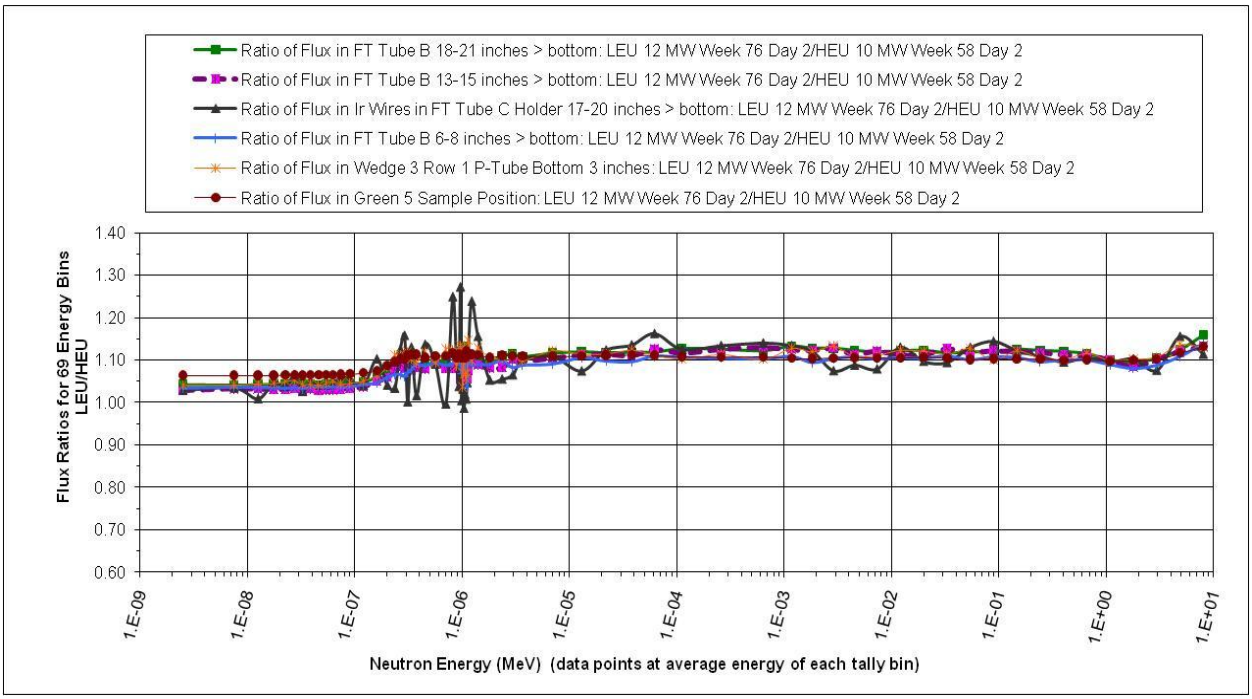

Figure 4.16. Comparisons of LEU 12 MW to HEU 10 MW at Day 2.

5.0 CONCLUSIONS

The analyses performed in this report provide a technical basis for the neutron physics characteristics of the MURR operating with LEU fuel. The analyses are based on the assumption that the U-10Mo monolithic fuel form can be qualified and manufactured. Additionally, as has always been true for reactor conversion projects, full safety analyses need to be performed and regulatory approvals received before the reactor will be able to convert.

It is important to note that the U-10Mo Monolithic Fuel is not yet qualified or commercially available. The Fuel Development (FD) and Fuel Fabrication Capability (FFC) efforts within the GTRI Reactor Conversion Program are both working to clarify the fuel specifications that will be supported for the new LEU fuel. The positive results reported here are predicated on the best information available to date, as communicated through the US High Performance Research Reactor Working Group (USHPWG).

The LEU fuel element design was developed based on constraints for reliable fuel element and fuel plate fabrication communicated by FD and FFC. In particular, the fuel element was redesigned from the previous Feasibility Study Design developed in Reference 1 to comply with a constraint of a thinnest nominal clad of 12 mil. The design selected here came from an extensive optimization study, considering both fuel reactivity (which affects the fuel lifetime in the MURR) and power peaking (which affects the margin to onset of flow instability and critical heat flux).

Reactivity to maintain operating lifetime with LEU has been obtained by increasing the water to metal ratio in the core by removing one fuel plate (resulting in 23 plates versus 24 plates in the HEU and FSD designs), and thinning the fuel plates, which increased the coolant channel widths. Plates 1 through 22 were decreased from 50 mil thick to 44 mil, while plate 23 is 49 mil thick. Experiments and analyses to prove the hydrodynamic stability of the thinner 44 mil fuel plates must still be performed.

Most of the plates are designed with a 20 mil U-10Mo foil and a 12 mil clad (including any interlayer to control fuel swelling behavior). Reduced foil thicknesses were designed in four of the fuel plates in order to control power peaking and assure safety margins. Detailed power distributions were obtained for a number of core states that bound the power peaking expected in steady-state operations. Steady-state thermal hydraulic safety analyses are being performed to assess the safety margins [3].

Fuel cycle simulations have shown that the LEU fuel design will allow for the kind of weekly operations that are currently practiced at MURR. Furthermore, the number of fuel elements consumed per year will be the same for LEU as for the current HEU fuel.

Acceptable experimental fluxes will only be maintained if the reactor power can be increased from 10 MW in order to offset the inherent penalty of introducing additional U-238 into the core. A power uprate to 12 MW with the LEU fuel will provide modest benefit for all of the fluxes and reaction rates evaluated in this report. This analysis also justifies an in depth look into the thermal safety margins of the LEU core at 12 MW, which is the topic of a companion technical basis report [3]. Regulatory issues of the uprate are being addressed to assure successful conversion.

In conclusion, an LEU fuel element design that meets the goals of conversion has been developed. The goal is to safely replace the current MURR HEU fuel element with LEU fuel and maintain performance while requiring minimal, if any, changes to the control blades and control blade drive mechanisms, as well as the instrumentation and control system. Furthermore, the element design satisfies a set of manufacturing assumptions specified by the FD and FFC pillars of the GTRI RERTR program.

REFERENCES

1. McKibben, J. C., et al., *Feasibility Analyses for HEU to LEU Fuel Conversion of the University of Missouri Research Reactor (MURR)*, MURR Technical Data Report No. 0125, September 2009.

2. Foyto L., et al., *Preliminary Safety Analysis Report Methodologies and Scenarios for LEU Fuel Conversion of the University of Missouri Research Reactor (MURR)*, MURR Technical Data Report No. 0128, August 2011.

3. Feldman, E. E., et al., *Technical Basis in Support of the Conversion of the University of Missouri Research Reactor (MURR) Core from Highly-Enriched to Low-Enriched Uranium – Steady-State Thermal-Hydraulic Analysis*, ANL/RERTR/TM-37, Argonne National Laboratory, 2012.

4. X-5 Monte Carlo Team, "MCNP-A General Monte Carlo N-Particle Transport Code, Version 5 Volume I, II and III," LA-UR-03-1987/LA-CP-03-0245/LA-CP-03-0284, Los Alamos National Laboratory (2003).

5. Deen, J. R., et al., "WIMS-ANL User Manual, Rev. 5," ANL/TD/TM99-07, Argonne National Laboratory, 2003.

6. Olson, A. P., A User's Guide for the REBUS-PC Code, Version 1.4, ANL/RERTR/TM-32, Argonne National Laboratory, 2001.

7. Stevens, J.G., *The REBUS-MCNP Linkage*, ANL/RERTR/TM-08-04, Argonne National Laboratory, 2008.

8. Dionne, B., Stillman, J, and Stevens, J., "Applicability of WIMS-ANL to Generate Cross Sections for Very High Density UMo Fuel in Proposed LEU Fuel Assembly," Proc. 2008 International Meeting on Reduced Enrichment for Research and Test Reactors, Washington, D.C., Oct. 5-9, 2008.

9. Hanan, N.A., et al., "The Use of WIMS-ANL Lumped Fission Product Cross Sections for Burned Core Analysis with the MCNP Monte Carlo Code," Proc. 1998 International Meeting on Reduced Enrichment for Research and Test Reactors, São Paulo, Brazil, Oct. 18-23, 1998.

10. Julian, C., "Low power testing," MURR internal report, 1971.

11. McKibben, J.C., Kutikkad, K., and Foyto, L.P., "Current Status of the Missouri University Research Reactor HEU to LEU Conversion Feasibility Study," Proc. 2007 International Meeting on Reduced Enrichment for Research and Test Reactors, Prague, Czech Republic, Sep. 23-27, 2007.

12. McKibben, J.C., Kutikkad, K., and Foyto, L.P., "Progress Made on the University of Missouri Research Reactor HEU to LEU Fuel Conversion Feasibility Study," Proc. 2008 International Meeting on Reduced Enrichment for Research and Test Reactors, Washington, D.C., Oct. 5-9, 2008.

13. Peters, N. and Kutikkad, K., "MURR Control Blade Depletion Study Report," MURR Technical Data Report No. 134, June 2012.

14. Olson, A. P. and Kalimullah, *A User's Guide to the PLTEMP/ANL Code*, Version 4.1, ANL/RERTR/TM-11-22, Nuclear Engineering Division, Argonne National Laboratory, April 9, 2011.

15. STAR-CD Version 3.20, CD-adapco, New York (2004).

16. Tzanos, C. and Stillman, J., *Effect of Lateral Conduction on the Azimuthal Distribution of Heat Flux in the Hot Plate of a Research Reactor*, ANS Summer Meeting, June 2012.

Appendix A: Material Properties and Composition Data in MURR Core Models

Table A.1. Water Properties.

Component	Conditions	Fuel	Temperature (^oF)	Pressure (psia)	Density (g/cm^3)
Primary Coolant	Cold conditions (comparisons to 1971 low-power startup tests)	HEU	100.0[1]	25	0.9932
	Hot Operating Conditions	HEU	128.0[2]	60	0.9866
		LEU	129.6[3]	60	0.9862
Flux Trap and Pool	Cold conditions (comparisons to 1971 low-power startup tests)	HEU & LEU	100.0	25	0.9932
	Hot Operating Conditions	HEU & LEU	103.0	25	0.9925

[1] Core power level = 500 W
[2] Core power level = 10 MW
[3] Core power level = 12 MW

Table A.2. Fuel Properties.

Conditions	Fuel	Temperature	
		^oF	MeV
Cold conditions	HEU & LEU	100.0	2.6794E-08
Hot Operating Conditions	HEU	158.0[1]	2.9570E-08
	LEU	176.0[2]	3.0432E-08

[1] Core power level = 10 MW
[2] Core power level = 12 MW

Table A.3. Fresh HEU Fuel Meat Composition in 1971 Criticals Models.

	MCNP		DIF3D	
	Atoms/b-cm	*Wt. Fraction in U*	Atoms/b-cm	*Wt. Fraction in U*
U-235	3.641E-03	*93.3%*	3.623E-03	*93.1%*
U-238	2.597E-04	*6.7%*	2.648E-04	*6.9%*
Al	4.923E-02		4.992E-02	

Table A.4. Fresh HEU Fuel Meat Composition (U-Al_x) in Fuel Cycle Simulation Models.

	MCNP		DIF3D	
	Atoms/b-cm	*Wt. Fraction in U*	Atoms/b-cm	*Wt. Fraction in U*
U-234	4.030E-05	*1.0%*	4.026E-05	*1.0%*
U-235	3.656E-03	*93.1%*	3.651E-03	*93.1%*
U-236	1.307E-05	*0.3%*	1.306E-05	*0.3%*
U-238	2.134E-04	*5.5%*	2.132E-04	*5.5%*
Al	4.986E-02		4.987E-02	

Table A.5. Fresh LEU Fuel Meat Composition (U-10Mo) in Fuel Cycle Simulation Models.

	MCNP	
	Atoms/b-cm	*Wt. Fraction in U*
U-234	1.025E-04	*0.26%*
U-235	7.751E-03	*19.75%*
U-236	1.798E-04	*0.46%*
U-238	3.082E-02	*79.53%*
Mo	1.068E-02	

Table A.6. Al-6061 Aluminum Composition: MCNP Model.

Isotope	Weight Fraction
Al	9.761E-01
B-10[1]	2.030E-06
B-11[1]	8.170E-06
C	9.240E-03
Si-28	4.610E-03
Si-29	2.340E-04
Si-30	1.540E-04
Ti	1.260E-04
V	1.020E-04
Cr-50	5.883E-05
Cr-52	1.135E-03
Cr-53	1.290E-04
Cr-54	3.202E-05
Mn-55	7.000E-04
Fe-54	2.070E-04
Fe-56	3.248E-03
Fe-57	7.501E-05
Fe-58	9.980E-06
Cu-63	2.033E-03
Cu-65	9.060E-04
Zi	8.920E-04
Zr	2.600E-05

[1] A total of 10.2 ppm boron is added to the Al-6061 material composition to account for impurities and constituents for which cross section data not available.

Table A.7. Al-6061 Aluminum Composition: DIF3D Model.

Isotope	Weight Fraction
Al	1.0
B-10[1]	3.686E-06
B-11[1]	1.632E-05

[1] 20 ppm natural boron is added to the Al-6061 material composition to account for constituents not explicitly represented, and for impurities.

Table A.8. Fresh Shim Blade Dimensions and Compositions.

Nominal data for 1971 blades used in core models related to 1971 core. As-built data used for models related to 2008 core.

	1971		2008 (Current)		
Control Blade[1]	Minimum[2]	Nominal[3]	Minimum[2]	Nominal[3]	As-Built[4-6]
Blade thickness (inches)	0.2		0.175		
Clad thickness (inches)	0.032		0.037		
Core thickness (inches)	0.136		0.101		
Wt. % B_xC in Core (range)	50±10		52±2		
B_4C Grit size (mesh #)	20-200		60-200		
Wt. % B_xC in Core	40%	50%	50%	52%	
B_xC surface density (g/cm^2)	0.328	0.398	0.305	0.316	0.323206
B_xC smear density in meat (g/cm^3)	0.950	1.152	1.189	1.231	1.29616
Straight B_xC density (g/cm^3)	2.010	2.010	2.124	2.124	
B-10 density in meat (g/cm^3)					0.1813
B density in meat (g/cm^3)					0.9916
Meat density (g/cm^3)					
Al density in meat (g/cm^3)					1.2757
(Min.) Wt. % B in B_xC	70.0%	70.0%	76.0%	76.0%	
Fe in Al powder					0.091%
Boron to Carbon atoms					4.1051
B surface density (g/cm^2)	0.230	0.2785853	0.232	0.2399267	0.2543
B-10 surface density (g/cm^2)	0.0414	0.05135	0.0418	0.04422	
C surface density (g/cm^2)	0.09840	0.119	0.0732	0.076	
Core Al surface density (g/cm^2)	0.492	0.398	0.305	0.291	
Boral Atom Densities (atoms/b-cm)					
Al (at/b-cm)	3.179E-02	2.571E-02	2.654E-02	2.535E-02	2.8474E-02
C (at/b-cm)	1.428E-02	1.733E-02	1.431E-02	1.481E-02	1.3453E-02
B-10 (at/b-cm)	7.208E-03	8.940E-03	9.800E-03	1.037E-02	1.0902E-02
B-11 (at/b-cm)	2.901E-02	3.598E-02	3.944E-02	4.173E-02	4.4324E-02
O (at/b-cm)					5.7850E-04
Fe (includes Fe in B_xC and in Al powder)					2.1604E-05

[1]Thickness and minimum surface density data from letter, Les Molen (Brooks and Perkins) to Chester Edwards (MURR), June 8, 1978.
[2]Loadings based on minimum B4C surface density.
[3]Loadings based on nominal B4C surface density.
[4]E-mail from Charlie McKibben, "2008 Control Blades B4C," 11/6/2008.
[5]ESK Test Report for boron carbide, 399/2005, 6/16/2006, faxed by C. McKibben 1/5/2009.
[6]Certificate of analysis by The Aluminium Powder Company, #34307, 3/7/2005, faxed by C. McKibben 1/5/2009.

Table A.9. Graphite Reflector Composition.
Based on Data from SGL Carbon Material Assay, Dated 1/18/2002.

Element	Detection Limit (ppm)	Assay		Average; for elements not detected (ND) use detection limit	B equivalent[1] (ppm)
		Lot 7108	Lot 7109		
B	0.005	0.16	0.44	0.30	3.000E-01
Na	0.005	0.04	0.04	0.04	1.300E-05
Mg	0.005	ND[2]	ND	0.0025	9.134E-08
Al	0.01	0.05	0.04	0.045	5.430E-06
Si	0.01	0.51	0.67	0.59	5.063E-05
P	0.01	ND	ND	0.005	3.914E-07
K	0.05	ND	ND	0.025	1.893E-05
Ca	0.05	ND	ND	0.025	3.781E-06
Ti	0.005	0.04	0.05	0.045	8.070E-05
V	0.001	0.005	ND	0.005	7.028E-06
Cr	0.1	ND	ND	0.05	4.134E-05
Mn	0.005	ND	ND	0.0025	8.531E-06
Fe	0.01	0.02	0.01	0.015	9.692E-06
Ni	0.005	0.05	0.05	0.05	5.391E-05
Cu	0.01	ND	ND	0.005	4.192E-06
Zn	0.05	ND	ND	0.025	5.982E-06
As	0.005	ND	ND	0.0025	2.116E-06
Zr	0.05	0.04	0.03	0.035	1.000E-06
Mo	0.01	ND	ND	0.005	1.822E-06
Sn	0.01	ND	ND	0.005	3.716E-07
Sb	0.01	ND	ND	0.005	2.842E-06
W	0.01	0.06	0.05	0.055	7.717E-05
Pb	0.01	ND	ND	0.005	5.816E-08
S	0.01	0.11	0.12	0.115	2.679E-05
Cl	0.01	0.14	0.42	0.28	3.729E-03
Total B Equivalent (ppm)					**0.304**

Density (g/cm^3)	1.725	1.72	**1.7225**	

[1] Boron equivalents calculated from 2200 m/s cross section of element relative to boron cross section (767 barns).
[2] ND = not detected.

Table A.10. Beryllium Reflector Composition.

Detailed material definition based on element weight percent fractions used in MCNP model. For DIF3D model, reflector material defined with beryllium and 3 ppm total boron equivalent to represent impurities.

	wt. %	B equivalent[1] (ppm)
Be	98.34	
O	1.2179	0.0020
C	0.08	0.0033
Fe	0.1060	0.6849
Al	0.05	0.0603
Ni	0.009997	0.1078
Si	0.05500	0.0472
Mg	0.01	0.0037
Ca	0.01	0.0151
Cr	0.006	0.0496
Mn	0.013	0.4436
Pb	0.0001479	0.0000
Mo	0.0005	0.0018
Ag	0.0005	0.0414
Co	0.00025	0.0222
Li	0.000025	0.0358
B	0.0001299	1.2990
Cd	0.00005006	0.1582
ppm B Equivalent for Impurities (DIF3D models)		**2.9760 (3)**

Density (g/cm^3)	**1.849**

[1] Boron equivalents calculated from 2200 m/s cross section of element relative to boron cross section (767 barns).

(This page intentionally left blank.)

Nuclear Engineering Division
Argonne National Laboratory
9700 South Cass Avenue, Bldg. 208
Argonne, IL 60439-4842

www.anl.gov

Argonne National Laboratory is a U.S. Department of Energy
laboratory managed by UChicago Argonne, LLC